Origin of Uranium Mineralization at Coles Hill Virginia (USA) and its Natural Attenuation within an Oxidizing Rock-Soil-Ground Water System

James L. Jerden Jr.

Dissertation submitted to the Faculty of the Virginia Polytechnic Institute and State University in partial fulfillment of the requirements for the degree of

Doctor of Philosophy
in
Geological Sciences

Committee:
A. K. Sinha, Chair
James Beard
William Henika
Donald Hickmott
J. Donald Rimstidt
Lucian W. Zelazny

September 21, 2001
Blacksburg, Virginia

Keywords: Uranium Transport, Natural Attenuation, Uranium Deposit, Autunite, Crandallite

Origin of Uranium Mineralization at Coles Hill Virginia (USA) and its Natural Attenuation within an Oxidizing Rock-Soil-Ground Water System

James L. Jerden Jr.

Abstract

Development of a scientific basis for management of uranium bearing wastes and contaminants requires information from natural geologic systems. The following study of the Coles Hill uranium deposit and associated weathered zone constrains processes leading to the natural attenuation of uranium within an oxidizing, fluid rich environment typical of the eastern US.

At the Coles Hill deposit fracture hosted, primary U(IV) bearing mineral assemblages formed during hydrothermal activity associated with Mesozoic faulting. The most abundant ore assemblage consists of coffinite and apatite, but uraninite-zeolite and uraninite-calcite assemblages are also present. Within the shallow bedrock there is a uranium redox transition where alteration of U(IV) minerals has produced secondary uranium minerals. Geochemical data suggests that the volume of rock containing this U(IV)/U(VI) transition is acting as a closed system with respect to uranium mass transport during oxidation. The dominant mechanism of uranium fixation within the oxidizing zone is the precipitation of Ba-U(VI) phosphates (meta-autunite group). Speciation and mineral stability calculations indicate that ground waters from the Coles Hill weathered zone are saturated with respect to Ba-meta-autunite and that this mineral is capable of buffering dissolved uranium concentrations to values lower than 20 parts per billion.

U(VI) phosphates of the meta-autunite group are not stable in the vadose zone (soil pH ~ 4.5) at the Coles Hill site. In this zone uranium is associated with (Ba, Ca, Sr) aluminum phosphate of the crandallite group as well as with phosphate sorbed to iron oxy-hydroxide mineral coatings. Uranium leached from the vadose zone is reprecipitated as new meta-autunite minerals below the water table due to higher pH conditions of ~6.0 and relatively high activity ratios of dissolved phosphate to carbonate (e.g. $\log [H_2PO_4^-/HCO_3^-] > -3$).

It is estimated that the U(VI) phosphates responsible for the natural attenuation of uranium at this site persist within the weathering zone for hundreds of thousands of years. Thus, the Coles Hill deposit represents an excellent natural laboratory for the study of uranium attenuation with potential applications for the design and implementation of cost effective remediation and containment strategies, such as soil amendments techniques and in-situ reactive barriers technologies.

Funding for Research

Byron N. Cooper Geoscience Fellowship
(Virginia Tech, Department of Geological Sciences)

Virginia Museum of Natural History Graduate Fellowship

Virginia Department of Health Research Grant

Virginia Division of Mineral Resources

Society of Economic Geologists Research Fellowship

Acknowledgements

I would like to thank the following people for their help throughout my dissertation research:

Mr. Walter Coles and Mrs. Sarah Coles-McBrayer for allowing me to work on their property and for logistical support throughout the project.

Dr. A. K. Sinha (committee chair) who introduced me to the topic of my research and whose guidance has been instrumental in keeping me on the right track.

All members of my committee for four years worth of discussions and debates about the geology and geochemistry of the Coles Hill deposit.

Each committee member provided essential and timely guidance allowing me to develop the tools required for tackling this type of research project. In this regard I would specifically like to thank **Dr. Sinha** for preparing me to deal with complex geologic problems using tools from the fields of petrology, mineralogy and isotope geochemistry; **Dr. Beard** for helping me refine my knowledge of petrology and geochemistry; **Mr. Henika** for exposing me to the complexities of Virginia geology and helping me put my project in a regional geologic context; **Dr. Hickmott** for introducing me to aspects of geochemical modeling and low temperature metal stabilization techniques; **Dr. Rimstidt** for solidifying my background in thermodynamics, kinetics and aqueous geochemistry; **Dr. Zelazny** for preparing me to deal with the complexities of soil chemistry and soil mineralogy.

Dr. Gretchen Benedix and Dr. Todd Solberg for training and assistance with micobeam analyses.

Mr. Hal Pendrak for training and assistance with thermal ionization mass spectrometry techniques.

Fellow graduate student Jay Thomas for helping me with mass spectrometry and illustrating.

Mr. John Wilson and Mr. Scott Lucas the help in the field.

Dr. Lee Daniels for help with soil sampling techniques.

Dr. Robert Finch for X-ray diffraction analyses and thoughtful discussions about uranium mineralogy.

Dr. Norman Reynolds (past President of Marling Uranium Corporation) and Dr. Chris Halladay (Marline Uranium Corporation Geologist) for sharing information gathered during the exploration of the Coles Hill deposit

Dr. Robert Ayuso (US Geological Survey, Reston) for sharing whole rock geochemical data from the Coles Hill deposit.

Dr. Paul Bertch and Dr. Andrew Sowder (University of Georgia, Savannah River Ecology Laboratory) for thoughtful discussions about the natural attenuation of uranium.

The Virginia Division of Mineral Resources (particularly Dr. Rick Berquist and Mr. William Henika) for auger drilling at the Coles Hill site.

The Virginia Museum of Natural History (particularly Dr. James Beard) for access to their collection of rock core from the Coles Hill deposit.

I would also like to thank Hal and John for intellectually stimulating doughnut meetings, the fourth floor staff: Connie, Carolyn, Mary and Linda for all sorts of advice and support as well as fellow graduate students for providing an always-interesting work (and out of work) environment.

Table of Contents

Table of Tables

Table of Figures

Chapter 1: Geology and Geochemistry of the Coles Hill Uranium Deposit, Virginia

Abstract

The Coles Hill uranium deposit consists of two structurally controlled, hydrothermal orebodies hosted in cataclastic zones along the northwest margin of the Danville Triassic Basin in Pittsylvania County, Virginia. The host lithologies consist of a sequence of quartzo-feldspathic augen gneisses and interlayered amphibolites. The deposit was discovered by the Marline Uranium Corporation, which conducted extensive exploratory work, however, due to economic and regulatory reasons the deposit was not mined. The exploratory data base indicates that the Coles Hill deposit contains over 22,000 metric tons U_3O_8 at an average grade of 0.113 weight percent (Halladay, 1989), thus making it the largest uranium deposit in the eastern United States. The Coles Hill ore zones also contain high concentrations of phosphorous relative to the unmineralized host rocks, with most ore grade samples ranging from 1-9 weight percent P_2O_5.

The mineralizing process is associated with cataclasis and syn-tectonic sodium metasomatism, chloritization and hematization. The deposit contains three distinct ore bearing mineral assemblages. The oldest consist of subhedral and cryptocrystalline coffinite intimately associated with fine-grained, uranium rich fluor-apatite, chlorite and Ti oxides. This assemblage is cross-cut by two ore bearing vein sets: one containing uraninite, calcite and minor sulfides, and a later set containing uraninite, sulfides and Ba zeolite (harmotome). Analyses of whole rock data indicate that the alteration processes preceding mineralization resulted in approximately 18% loss in volume for the system and were associated with an enrichment in Na and depletions in K, Ba, Rb and Si. The mineralization events resulted in approximately 7% volume gain associated with significant enrichments in U, P, F, Sr, Th, Ca, Nb and the light rare earth elements. The highest grade ore zones occur within or near pervasively hematized amphibolite layers. Textural observations suggest that the oxidation of reduced iron in the deposit host rock played an important role in the precipitation of the ore assemblages. The age of the deposit is constrained by the fact that Norian (208-225 Ma) age sediments adjacent to the deposit are affected by the deformation and alteration events associated with uranium mineralization. However, no uranium bearing assemblages have been recognized within these Triassic sediments within the study area.

The unique ore mineralogy and geologic context of the Coles Hill deposit suggest that it may represent a new sub-type of U deposit that forms in phosphate rich hydrothermal systems within cataclastic zones associated with extensional tectonics.

Introduction

Since the 1960's, exploration for uranium in the eastern United States has led to the discovery of several significant occurrences of both fracture hosted, hydrothermal ores as well as sedimentary roll-front and strata-bound type deposits. Important examples of the hydrothermal types include the sets of uraninite rich veinlets that cross cut the Wilson Creek gneiss in the Grandfather Mountain window of North Carolina (Crandall et. al., 1982) and the uranium-thorium rich cataclastic zones of the Lovingston Formation in central Virginia (Baaillieul and Daddazio, 1982). Sedimentary types are typified by sandstone hosted uraninite-coffinite roll-type and stratabound deposits that occur within the Upper Devonian Catskill deltaic strata of Pennsylvania and Virginia (Klemic, 1962; Klemic, 1963; Lesure et. al., 1977; Smith and Hoff, 1984). Several significant uranium occurrences have also been discovered within or adjacent to Triassic sedimentary basins (Glaeser, 1979; Turner-Peterson, 1985). Of particular importance is the Danville-Dan River Triassic basin in south-central, Virginia (Dribus, 1978). The exploration of this region by the Marline Uranium Corporation in the late 1970's led to the discovery of nine significant radiometric anomalies, one of which was shown to be of potential economic significance (Marline Uranium Corporation, 1983). Further characterization of this anomaly revealed an extensive uranium deposit underlying a local topographic high known as Coles Hill, in Pittsylvania County, Virginia.

The Coles Hill deposit is hosted in a zone of sheared quartzo-feldspathic gneiss and interlayered amphibolite that form the foot wall of the Danville Triassic basin border fault. Ground-based gamma ray spectrometer surveying and assays of drill core from the site indicate that the Coles Hill deposit subcrops as two discrete ore bodies with a combined foot print of approximately 230,000 m^2. Exploration of the deposit by the Marline Corporation involved the drilling of 182 rotary percussion holes, 74 diamond bit core holes (most of which were cored to approximately 300 m), and geophysical surveying that produced detailed (1:4800 scale) radiometric, magnetic and gravity maps of the of the deposit area (Marline Uranium Corporation, 1983). Bore holes were logged with gamma and neutron probes to produce ore grade maps for 53

different depth levels thus constraining the ore body dimensions. Data from these studies suggest that two discrete ore bodies present at the surface connect at depth.

Ore reserves calculations using polygonal and kriged block model methods were based on a cutoff grade of 0.05 weight percent U_3O_8. These estimates indicate the southern most orebody of the Coles Hill deposit contains approximately 22,000 metric tons of U_3O_8 with an average grade of 0.113 weight percent (Halladay, 1989). The north orebody contains similar total reserves with a lower average grade (Halladay, 1989). Thus, in terms of total reserves the Coles Hill deposit is larger than the Koongara deposit in northern Australia and the Rabbit Lake deposit in northern Saskatchewan, Canada which contain 15,600 tons and 18,200 tons U_3O_8 respectively (Dahlkamp, 1991).

Although the Coles Hill deposit was not mined, the exploration database including approximately 20,000 meters of core and percussion cuttings were retained by the Virginia Museum of Natural History (VMNH) and the Department of Geological Sciences at Virginia Tech. In 1986, these exploratory studies were augmented by a geochemical investigation of 47 core samples by the US. Geological Survey (Ayuso personal communication, 2001). For this paper, the geochemical database and non- proprietary exploration data (made available to the authors by VMNH and USGS) have been synthesized and interpreted in light of new geologic and mineralogic data being collected as part of a natural analogue project focusing on uranium transport and natural attenuation at this site.

Regional Geologic Setting

The Coles Hill uranium deposit occurs along the northwestern margin of the Chatham fault zone, which separates the Danville Triassic basin from polydeformed, polymetamorphosed crystalline rocks of the Piedmont Geologic Province (Figure 1-1). Near the study area the Chatham fault is defined by a zone of silicified breccia and cataclasite that overprints ductile mylonitic fabrics. These sheared (protomylonitic) quartzo-feldspathic gneisses are the host rocks of the Coles Hill uranium deposit. The mylonitic fabric of the deposit host rock is interpreted to have formed during displacement along the Brookneal shear zone, which separates the Western Piedmont Belt from the Central Virginia Volcanic-Plutonic Belt (CVVPB) (Figure 1-1).

Within the study area the CVVPB consists of a sequence of quartzo-feldspathic gneisses and interlayered amphibolites. Although affected by later deformation, exposures of CVVPB

lithologies present on the southeast side of the Danville basin retain evidence for primary volcanic features (e.g. eutaxic structure, pumice lapilli and feldspar phenocrysts) (Henika and Thayer, 1983). The most common rock types in this sequence are meta-rhyolite, meta-dacite, and porphyroblastic quartzo-feldspathic biotite gneiss interlayered with amphibolite. Northwest of the Brookneal shear zone the CVVPB gives way to the Western Piedmont belt (WPB) (Virginia Division of Mineral Resources, 1993).

Rocks of the WPB located within the study area are mapped as part of the Smith River Allochthon (Conley and Henika, 1973). This litho-tectonic unit has been interpreted as a rootless crystalline thrust sheet that has been transported westward over late Precambrian-Cambrian metasediments (Lynchburg Group) during Paleozoic tectonism (Conley and Henika, 1973). The allochthon is bounded on the northwest by the southeast dipping Bowens Creek Fault, and on the southeast by the Ridgeway Fault. The geology of the allochthon near the study area is dominated by the biotite gneiss and mica schist units of the Fork Mountain Formation, and the Martinsville Igneous Complex (MIC). The MIC consists of the gabbroic Rich Acres Suite and the Leatherwood granite which has U-Pb zircon ion probe age of 441 +/-8 Ma (unpublished data of authors measured at UCLA ion probe laboratory). Other igneous rocks mapped in the vicinity of study area include tholeitic metabasalts in the Precambrian(?) Bassett Formation and regional sets of north and northwest trending Mesozoic diabase dikes (Henika and Thayer, 1983; Ragland et. al., 1983). The diabase intrusions cross-cut both Piedmont and Triassic lithologies and are of particular interest due to their potential role as a heat source in the formation of the Coles Hill deposit. The Danville basin consists of sediments of the Chatham Group of the Newark Super-group (Henika, 1997; Weems and Olsen, 1997). Within the study area these formations are the fluvial, Stoneville Formation and lacustrian Cow Branch Formation, both of which were deposited within a half-graben during the late Triassic (Manspeizer et al., 1989). The thickness of the clastic wedge is estimated to be 1,100 meters in the narrowest portions of the basin to more than 4,000 meters in its widest regions (Henika, 1981).

Host Rock Geology

The study area is underlain by a heterogeneous volume of rock consisting of six distinct lithologic units (Figures 1-1 and 1-2). These include (from west to east): (1) the Leatherwood granite, of the Martinsville Igneous Complex, (2) biotite gneiss and mica schist of the Fork

Mountain Formation, (3) quartzo-feldspathic augen gneisses and interlayered amphibolites correlated with the Central Virginia Volcanic-Plutonic belt, (4) silicified breccia and cataclasite of the Chatham fault zone, (5) noncohesive clay-rich fault gouge and breccia that marks the trace of Triassic border fault and (6) Triassic conglomerates and sandstones of the Stoneville Formation interlayered with siltstones and shales of the Cow Branch Formation. All of these lithologies were important in developing the physico-chemical environment in which the Coles Hill deposit formed. The following discussion, however, will focus on the augen gneisses, interlayered amphibolites, cataclasitc zone, Triassic sediments and diabase intrusions as they appear to have played the most critical roles in ore genesis.

Augen gneiss units and interlayered amphibolites

Based on variations in texture, modal mineral proportions (e.g. Table 1-1) and geochemistry the augen gneiss host rocks are differentiated into three members (Marline Uranium Corporation, 1983): the upper, middle and lower augen gneiss units (Figure 1-3). Uranium rich mineral assemblages have been noted in all three units, however, most of the ore is concentrated within the upper augen gneiss. The penetrative, northeast striking, southeast dipping protomylonitic (augen) fabric that forms the primary structural grain in the study area is defined by preferentially oriented feldspar porphyroclasts, biotite (altered to chlorite), muscovite and ribbons of stretched quartz. These rocks also contain coarse grained, euhedral-subhedral apatite and euhedral titanite; both of which are preferentially oriented within the gneissic foliation. This fabric parallels both local and regional lithologic trends and is pervasive in all augen gneiss units but is obscured within the overlying cataclastic zone. Modal mineralogical data for unaltered and altered augen gneiss and amphibolites are shown in Table 1-1.

The lower augen gneiss unit is approximately 120 - 180 meters thick and consists of potassium feldspar and oligoclase porphyroclasts surrounded by a dark schistose matrix consisting of feldspar, quartz, biotite (altered to chlorite) +/-muscovite. In the southern part of the study area the lower augen gneiss can be delineated by a positive magnetic anomaly (Marline Uranium Corporation, 1983). The anomaly, which is believed to reflect magnetite content, is relatively continuous except in the immediate vicinity of the ore zones where magnetite has been altered to hematite (Marline Uranium Corporation, 1983). This lower unit is structurally overlain by the approximately 60 - 75 meters thick middle augen gneiss unit. This lithology is

distinguished from the other augen gneisses as it contains less quartz, and has larger and more abundant feldspar porphyroclasts (Table 1-1). The augen grains in this unit consist of potassium feldspar, oligoclase and polycrystalline feldspathic aggregates enclosed within a medium- to coarse-grained matrix containing feldspar, biotite (altered to chlorite) +/-quartz, +/-muscovite. The middle augen gneiss is overlain by the approximately 150 - 180 meters thick upper augen gneiss unit which hosts most of the uranium ore. This unit contains approximately 20 modal percent feldspar augen that range in size from 5 to 10 millimeters in length. These feldspar augens are surrounded by a sheared matrix consisting of plagioclase (altered to albite), quartz and biotite (altered to chlorite) +/-muscovite. All unaltered samples of augen gneiss contain minor amounts of magnetite, titanite, apatite and zircon. In altered samples, however, hematite, titanium oxides (e.g. anatase), and chlorite are the dominant minerals. Electron microprobe analyses of phases involved in the alteration reactions associated with mineralization are presented in a later section.

The amphibolite layers that occur within the augen gneiss units are generally 1 to 5 meters thick and composed of medium- to coarse-grained, equigranular hornblende and plagioclase (+/-quartz, +/-biotite). The least altered amphibolites contain 30 to 40 volume percent hornblende, 40 to 50 volume percent plagioclase, 10 to 15 volume percent biotite, 0 to 5 volume percent quartz and trace amounts of apatite, magnetite/ilmenite, titanite and zircon (Table 1-1). Hornblende crystals are 1 to 1.5 millimeters in length and contain inclusions of apatite, quartz and feldspar. Hydrothermally altered amphibolites contain variable amounts of calcite, chlorite, hematite, titanium oxide and riebeckite (mineral chemistry of hornblende → riebeckite reaction is presented below). The extent of ductile shearing and later cataclastic deformation make it difficult to identify the protolith of the augen gneiss host rocks. These gneisses do however, yield U-Pb zircon ages similar to those of the 441 +/- 8 Ma Leatherwood granite suggesting that these lithologies may be related (ages are unpublished data of authors measured at the UCLA ion probe laboratory).

Cataclastic zone

This unit is a continuous, approximately 40 meter thick zone of intense brittle fracture and silicification that separates the upper augen gneiss unit from fault gouge of the Triassic basin border fault (Figure 1-3). Petrographic observations of core segments from this zone show

gradients in the extent of cataclasis. These gradients occur over meters to centimeters scale distances where regions of moderate intergranular fracturing (micorbreccia, protocataclasite) grade into discrete zones of intense grain size reduction (ultracataclasite) (fault rock terminology from Sibson, 1977). In nearly all cases brecciation and alteration have obliterated pre-existing fabrics. Most samples from this unit contain tectonically rounded to subrounded clasts and aggregate grains within a fine-grained matrix consisting of quartz, feldspar, white mica and trace amounts of pyrite. Some aggregate clasts contain previously formed cataclastic fabrics indicating that these cataclastic zones have accommodated repeated brittle shearing events.

The extent of cataclasis becomes progressively more pervasive as the Triassic border fault is approached. However, individual centimeter to meters scale zones of cataclasite and breccia also occur within the augen gneiss units where they are likely to have acted as conduits for hydrothermal fluids during mineralization. The upper (southeast) boundary of the cataclastic zone is marked by a 1 - 5 meters thick continuous zone of noncohesive fault gouge. This material consists of 2 to 3 centimeters wide, angular fragments of feldspar and quartz surrounded by unconsolidated matrix of green and gray clay. This gouge zone represents the trace of the Danville Triassic Basin (Chatham) border fault.

Triassic sediments and diabase of the Danville Basin

The Danville Basin clastic sequence and associated diabase dikes do not host uranium mineralization within the study area (Marline Uranium Corporation, 1983). However, they are considered key lithologic units due to their potential role in the formation of the deposit. The most abundant Triassic sedimentary unit within the study area is an arkosic conglomerate with a siltstone matrix. Clasts are subrounded to angular and consist of 1-2 centimeters long feldspar grains, 1-2 centimeters diameter quartz pebbles and 1-5 centimeters diameter quatzo-feldspathic aggregates. Many of these clasts are derived from augen gneiss units that were exposed by Triassic normal displacement along the border fault. These conglomerates are part of the Stoneville formation (Thayer, 1970) which has been shown to be Norian in age (208-225 Ma) based on fossil assemblages (Olsen et. al., 1991). Within the study area the Stoneville formation locally interfingers with gray siltstones, shales and carbonaceous black mudstones of the Cow Branch formation (Thayer, 1970). Throughout the Danville Basin the Cow Branch shales and mudstones show high background radioactivity and locally contain phosphate rich beds

consisting of articulated fish and reptile fossils within a black shale matrix. These phosphate rich layers are also carbonaceous locally containing up to 4 weight percent organic carbon (Olsen, et. al., 1991).

All Triassic lithologies near the border fault are cross-cut by numerous veins of quartz and calcite. Many of these veins are mineralogically sealed, however, some occur as open fractures with 1-10 millimeters wide apertures that are lined with drusy crystals of quartz or calcite +/- barite, +/-zeolite. The quartz and calcite veins locally cross-cut 1-10 millimeters wide graphite filled fractures, some of which accommodated displacement as indicated by well developed slickensides on exposed graphite surfaces. The presence of these vein sets, along with the fact that Triassic rocks are locally brecciated along the border fault indicates that the hydrothermal/cataclastic event that is associated with the deposit, also affected the Danville basin sediments.

Approximately 1 kilometer southwest of the Coles Hill deposit the Triassic sediments and Piedmont lithologies are intruded by a set of north trending, 100 - 200 meters wide, vertical diabase dikes (Henika and Thayer, 1983). These intrusions are clearly delineated on magnetic maps of the area around the deposit and their presence has been confirmed by geologic drill hole logs and surface exposures (Marline Uranium Corporation, 1983).

Structural Geology

The augen gneiss units, cataclastic zone and Triassic sediments are all cross cut and displaced by a set of steeply dipping, northwest striking faults (Figure 1-2). This fault set is evidenced by: (1) measurable meter scale off-sets of lithologic units in cores, (2) topographic lineaments and (3) abrupt truncations of magnetic signatures near the orebodies (Marline Uranium Corporation, 1983). Similar northwest trending faults have been noted elsewhere along the margins of the Danville and other Triassic basins (Meyertons, 1963; Ratcliffe, 1971). Within the study area these cross-faults are of particular importance because of their potential role in the formation of the Coles Hill deposit as well as their present-day role as preferential transport pathways for uranium and daughter elements (Jerden and Sinha, 1998, 1999).

Most fractures within the mineralized zones are sealed or coated with hydrothermal mineral assemblages, and the mineralogy of individual fracture sets depends on when they formed during the hydrothermal event. Textural relations suggest that fractures containing

uranium ore assemblages formed early in the brittle deformation event and were subsequently cross-cut by multiple unmineralized fracture sets. In some core sections (e.g. 41-113, depths 180-200 meters, and 57-23, depths 280-300 meters) the network of mineralized fractures form 1-2 meters thick breccia-like stockworks that cross cut the protomylonitic foliation of the augen gneisses. Apertures for individual mineralized fractures in these zones range from 5 microns to 5 millimeters.

The correlation between fracture development and uranium mineralization shows that the formation of the Coles Hill deposit involved a multiphase cataclastic/hydrothermal event. Petrographic evidence (discussed below) indicates that both alteration and uranium mineralization were episodic in nature, suggesting that mineralized cataclastic zones acted as channel-ways within which hydrothermal fluids flowed cyclically during deformation. The cyclical nature of this processes may reflect the action of a "suction-pumping" mechanism (e.g. Sibson, 1987) triggered by abrupt drops in elastic strain following brittle rupture events. This mechanism has been suggested as an important process in the formation of many other epithermal, fault hosted ore bodies including the vein hosted Schwartzwalder deposit in Colorado and breccia-hosted uranium deposits of Salamanca Spain (Wallace and Karlson, 1985; Wallace and Whelan, 1986, and Both et, al., 1994).

Petrography and Chemistry of Hydrothermal Mineral Assemblages: Uranium Ore and Associated Alteration Phases

There are three mineralogically and structurally distinct uranium ore assemblages within the Coles Hill deposit. The most common assemblage consists of coffinite and uranium rich apatite that occur in millimeters to centimeters scale zones of mineralized cataclasite and fault breccia. These zones are cross cut by two sets of uraninite bearing veins. One set contains both cubic and botryoidal uraninite in association with coffinite, calcite and sulfides, where as the other set contains botryoidal uraninite in association with coffinite, zeolites and sulfides. The uraninite and coffinite within these later assemblages are intimately intergrown. Both cataclastic and vein type ore assemblages are surrounded by centimeters thick hematite rich zones. The extent of both hematite staining and uranium mineralization (ore grade) increase abruptly where ore bearing fractures intersect amphibolite layers. This observation suggests a potential genetic relationship between alteration of the amphibolites and the precipitation of the uranium ore

assemblages. In order to better understand their relationship, the alteration reactions occurring in the amphibolites and adjacent augen gneisses were studied using electron microprobe data.

Mineral chemical expression of hydrothermal alteration

Mineralogic studies indicate that in addition to hematization the two most pervasive forms of alteration associated with uranium mineralization are: (1) sodium metasomatism and (2) chloritization. Textural evidence suggest that these alteration events occurred as cyclical pulses associated with brittle deformation. However, in some samples (e.g. core 41-127, 256 meters depth and 41-127, 105 meters depth) textural evidence suggests that both sodium metasomatism and chloritization processes were occurring simultaneously. Evidence for these alteration events within amphibolites adjacent to high grade ore zones is reflected by the development of reaction textures that document the following assemblage transformation:

hornblende – biotite – plagioclase (An_{16}) – titanite – quartz → riebeckite – chlorite – albite – anatase – quartz + Ca^{2+} + K^{+}

These alteration phases usually occur as rims around relict primary minerals however, in some instances complete pseudomorphic replacement is observed (e.g. core 41-127, 256 meters depth). Samples containing the alteration assemblage found nearest the coffinite/uraninite ore zones also contain trace to minor amounts of hematite giving these zones a red-stained appearance.

Sodium metasomatism

The most pervasive reaction texture observed in both amphibolites and augen gneiss units is the alteration of primary microcline and oligoclase to albite. A typical microprobe transect from relict plagioclase core to an alteration rim shows the following transition: $An_{16}Ab_{84}$ → An_2Ab_{98} → An_0Ab_{100} (Table 1-2), A similar pattern is observed across alteration rims on the primary potassium feldspars. The wide spread nature of this sodic alteration event is demonstrated by the observation that most feldspar grains within the altered zone have rims of optically clear albite.

This pervasive sodium metasomatic episode also resulted in the alteration of primary amphibole to secondary riebeckite within the amphibolite units. Electron microprobe analyses indicate that the primary amphiboles have compositions between edenite

($NaCa_2(Mg,Fe)_5[Si_7AlO_{22}](OH)_2$) and pargasite ($NaCa_2(Mg,Fe)_4Al[Si_6Al_2O_{22}](OH)_2$) (Table 1-3). They have (100Mg/Mn+Mg+Fe) values that range from 54 – 55 and estimated Fe^{2+}/Fe^{3+} ratios ranging from 3.0 – 4.3. These iron ratios were estimated by assuming that the sum of (Al^{VI}+Ti+Fe^{3+}+Fe^{2+}+Mg+Mn) = 5.0 per formula unit. These estimates are similar to measured ferric/ferrous ratios reported for amphiboles of similar composition (Deer, et. al., 1993). In altered amphibolite layers the primary calcic amphiboles are rimmed or completely replaced by sodic amphibole. Microprobe analyses indicates that the sodic amphibole is a low aluminum riebeckite with (100Mg/Mn+Mg+Fe) values that range from 30 – 48. The ferrous/ferric iron ratios of the riebeckites, which were estimated by assuming that all tetrahedral sites (Si_T) were filled by silica and that Si_T = 8.0, range from 1.2 – 1.8. These estimates are similar to ferrous/ferric ratios for sodic amphiboles of similar composition reported by Deer, Howie and Zussman (1993). Thus, using the calcic amphiboles to riebekite transition as a monitor of fluid composition during hydrothermal activity suggests that alteration of the amphibolite layers not only involved an influx of sodium, but also resulted in the production of an alteration assemblage typified by low ferrous/ferric iron ratios.

Chloritization

Another pervasive alteration texture observed in the host rocks (both amphibolite and augen gneiss units) is the transition of primary biotite to chlorite. Chlorite occurs as a fracture filling mineral, and in association with coffinite, uraninite and apatite within the primary ore zones. Electron microprobe analyses indicates that the primary biotites from the upper augen gneiss unit have compositions typified by $K_{1.6}(Mg_3,Fe_2)(Al_{0.5},Ti_{0.2})[Si_{5.7}Al_{2.3}O_{20}](OH,F)_4$ (Table 1-4). The low potassium contents of these biotites is probably due to incipient alteration to chlorite (e.g. potassium loss). These biotites have (100Mg/Mn+Mg+Fe) values ranging from 58 – 59 while the chlorites that replace these grains have values ranging from 48 – 49. Microprobe results also suggest that chlorites show more compositional variation than the primary biotites. For example, chlorite alteration layers observed along (001) cleavage surfaces of relict biotite are typified by the composition: $(Mg_{4.6},Fe_{4.8},Al_{2.4})[(Si_6,Al_2)O_{20}](OH)_{16}$ and, commonly contain over 1000 ppm K_2O and TiO_2. Chlorites that have completely replaced primary biotite within the foliation of the augen gneisses have nearly identical formulas as that given above except that levels of K_2O and TiO_2 are below detection limits (e.g. < 1,000 ppm). The fracture filling

generation of chlorite is distinct in composition and is represented by the formula: $(Mg_{4.8},Fe_{4.9},Al_{1.9})[(Si_{6.6},Al_{1.4})O_{20}](OH)_{16}$. Thus, as shown on Table 1-4, the two generations of chlorite (biotite replacement and fracture fill) share similar Mg/Fe ratios but are distinct in their Si/Al ratios (Table 1-4).

The chlorite-riebeckite assemblage also contains hematite which forms haloes around uranium ore-grade fracture zones. The three major sources of iron released during alteration were: (1) primary iron bearing silicates (e.g. biotite, hornblende), (2) magnetite, which is an important accessory phase in both augen gneiss and amphibolite units, and (3) titanite, which is shown by microprobe analyses (present study) to contain up to 7,000 ppm FeO_{total}. The observation that hematite is a common alteration phase and that the riebeckites have low ferrous/ferric ratios suggest that during early stages of alteration fluids were oxidizing. If advection was slow relative to reaction rates the oxidation of ferrous iron could locally lead to fluids depleted in oxygen (oxygen used up in hematite precipitation). This process may have resulted in the development of a geochemical environment conducive to the precipitation of U(IV) minerals (coffinite, uraninite).

Apatite-coffinite assemblage

Modal abundances within the apatite-coffinite zones are heterogeneous on the millimeter scale. In general, however, these zones contain 75 to 90 volume percent apatite, 5 to 10 volume percent chlorite, 5 to 10 volume percent albite, 1 to 5 volume percent coffinite, and accessory amounts of hematite, anatase, calcite, and aggregate clasts of the pre-cataclasis host assemblage. Within these ore grade fracture zones apatite occurs as felty, randomly-oriented, uniformly small (generally 0.2 mm long) prismatic crystals (Figure 1-4). The ore stage apatite also occurs locally as rims around coarse (generally 0.5 - 1 mm diameter) pre-ore stage apatite crystals that occur as accessory minerals within the host augen gneiss and amphibolites. Electron microprobe analyses reveal that pre-ore stage apatite have relatively high concentrations of fluorine (2.12 - 3.39 wt. %) and negligible concentrations of UO_2 (Table 1-5). The felty, ore stage apatites are also fluorine rich (2.35 - 3.62 wt. %), but contain high concentrations of UO_2 (0.25 - 3.06 wt. %) (Halladay, 1983) (Table 1-5). It is thus estimated that 10 to 15% of the total uranium content of the deposit is associated with this ore stage apatite. Within the primary ore assemblage coffinite commonly occurs as 1 micron to 500 nanometer thick cryptocrystalline rims on uranium rich

apatite laths (Figure 1-4c). Within the same assemblage coffinite also occurs as subhedral, 1 to 10 microns in grains locally intergrown with minor amounts of uraninite. The spatial distribution of the coffinites is nonuniform. In some samples (e.g. 41-127, 105 meters depth) they are disseminated throughout the apatite-chlorite matrix, while in others they are concentrated around the borders of feldspathic breccia clasts. Both subhedral and cryptocrystalline coffinite locally contain 0.5-1 micron diameter galena cubes (radiogenic Pb?) (Figure 1-4d). Another important mineral association in the cataclastic ore assemblage is the apparent affinity of uranium for titanium oxides. Uranium minerals are commonly concentrated around anatase grains within the apatite-chlorite matrix, and in some cases coffinite and trace amounts of uraninite are intimately intergrown with anatase in dense concentrations.

The coffinite-apatite assemblage occurs within cataclastic zones that are locally themselves cross-cut by later brittle fractures. This demonstrates that the hydrothermal/cataclastic event associated with ore deposition had multiple stages and that the coffinnite-apatite assemblage formed early during the deformation episode. The sequence of mineral growth within these zones is: (1) precipitation of hematite at fracture margins, (2) precipitation of felty apatite, followed by coffinite and chlorite in fracture interiors, (3) precipitation of trace amounts of sulfides (mainly pyrite) throughout the apatite-chlorite matrix. Although this mineral paragenesis is rare for uranium deposits, similar assemblages have been noted within the apatite bearing uranium orebodies of Espinharas and Ceara Brazil (Silveira et. al., 1991; Netto, et. al., 1991).

Uraninite - calcite and uraninite - zeolite veins

The uraninite bearing calcite veins cross-cut the apatite-coffinite assemblage (Figure 1-5a). This relationship, however, is locally difficult to resolve as many of these veins are commonly parallel to the apatite-coffinite filled fractures. The calcite-uraninite veins themselves are rimmed by hematite, and contain botryoidal colloform uraninite intergrown with coffinite and fine-grained anatase. The anatase commonly occurs in diamond shaped clusters suggesting that it formed directly from the alteration of primary titanite. The calcite-uraninite assemblage occurs mostly as 10 to 100 micron thick zones along the margins of calcite +pyrite veins that containing accessory chalcopyrite, sphalerite and trace amounts of galena. The sequence of mineral growth within these veins is: (1) hematite and trace amounts of uraninite along vein

walls, (2) calcite and uraninite in vein interiors, (3) sulfides (pyrite, sphalerite, galena) along calcite grain boundaries. Cubic crystals of uraninite occur locally as inclusions in calcite within vein interiors. This texture is indicative of higher temperature, uraninite-type mineralization (Rich et al., 1977) and, suggests that uranium was originally deposited as crystalline uraninite and later altered to uraninite aggregates. The uranium-mineralized calcite veins are cross cut by non-ore bearing quartz and calcite filled fractures.

The zeolite - uraninite veins are up to several millimeters wide (Figure 1-5b) and occur both concordant and oblique to the gneissic layering of the host rocks. The main uranium phase in these veins is a colloidal uraninite, which is concentrated primarily along the fracture walls. Energy dispersive x-ray (EDS) analyses of these uranium oxide aggregates show localized silica peaks suggesting the presence of fine-grained coffinite (Figure 1-6). Other areas within the aggregates are rich in iron and/or titanium suggesting intergrowths of uranium oxide with, hematite and/or anatase. Galena (radiogenic lead?) is present as 0.5-10 micron inclusions within uranium oxide aggregates (Figure 1-5d). Some uranium bearing, mineralized fractures locally contain coarse, drusy, euhedral quartz crystals and large pyrite octahedra that have grown inward from the vein walls (Figure 1-5b). The centers of these veins are filled with coarse harmatome (barium zeolite) containing numerous inclusions of iron/titanium oxides and coarse pyrite crystals. Minor amounts of uraninite intergrown with coffinite also occur as rims around pyrite crystals within the vein interiors (Figure 1-6c). Thus, the paragenesis of these veins is: (1) hematite, anatase and uraninite at vein walls, (2) quartz and sulfides +/- uraninite/coffinite, (3) harmotome-phillipsite zeolite. Textural observations from these cross-cutting, structurally and mineralogically distinct uranium bearing assemblages demonstrate the cyclical nature of the cataclastic/hydrothermal process recorded within and around the ore zones.

Whole Rock Geochemistry

The geochemical database provided by the US Geological Survey was used to assess chemical mass transfer associated with mineralization and host rock alteration. Based on petrographic and geochemical criteria whole rock samples from the deposit and host rocks are divided into three major categories: (1) unaltered augen gneiss and amphibolite, (2) altered but unmineralized (non-ore bearing) augen gneiss, amphibolite and cataclasite, (3) altered and mineralized (ore bearing) augen gneiss, amphibolite and cataclasite. Mineralized samples are

defined as those containing uranium bearing assemblages and greater than 40 ppm uranium. The unaltered augen gneiss samples are characterized by SiO_2 contents ranging from 62-68 weight percent for the lower and middle augen gneiss units, and 70-75 weight percent for the upper augen gneiss unit. All of the unaltered gneiss samples plot within the calc-alkaline field on the AFM diagram of Irvine and Baragar (1971) and within the rhyolite to trachydacite fields on the total alkalis versus silica diagram of LeBas et. al., (1986). Unaltered amphibolites have SiO_2 concentrations ranging from 50-57 weight percent and plot within the calc-alkaline field of the AFM diagram of Irvine and Baragar (1971). Furthermore, these samples are shown to have basaltic to trachy-andesite compositions based on the total alkalis versus silica plot of LeBas et. al., (1986).

The transition from the unaltered to altered samples is marked by a geochemical decoupling of the alkalis and a decrease in silica content (Figure 1-7a and b). This involves a depletion in potassium from an average value of 3 weight percent in unaltered augen gneiss samples to less than 1 weight percent in altered samples, and a corresponding enrichment in sodium from an average of 5 weight percent in unaltered augen gneiss samples to an average of 9 weight percent in altered varieties. This alteration signature is associated with the destabilization of potassium feldspars and biotites, and growth of albite and chlorite. Reaction textures further indicate that this sodium metasomatic event precedes uranium mineralization and is pervasive throughout the ore-hosting augen gneiss units.

Other important major element correlations are evident in plots of CaO versus SiO_2 and P_2O_5 versus SiO_2 (Figure 1-7c and d). These data show that both non-mineralized and mineralized sample sets have negative correlations between CaO versus SiO_2 and P_2O_5 versus SiO_2, but that these correlations have different slopes for the different sample groups. For example, linear regression lines fit to data for non-minerailized samples have slopes of -0.194 for CaO versus SiO_2 and -0.013 for P_2O_5 versus SiO_2; while, linear trend lines for mineralized samples have slopes of -0.668 for CaO versus SiO_2 and -0.457 for P_2O_5 (Figure 1-7c and d). The data also shows that altered but unmineralized samples fall along the same trends as unaltered samples. These observations suggest that the trends in the unmineralized samples reflect mineralogical differences in protolith lithologies (e.g. apatite and plagioclase content), whereas the trends for the mineralized sample group are controlled by the extensive precipitation of apatite during the formation of the primary ore bodies.

Minor and trace elements

The whole rock database was also used to assess correlations between trace elements and uranium within the Coles Hill deposit. Positive correlations were noted for Nb, Pb and P_2O_5 versus uranium (Figure 1-8). Samples containing large volumes of the apatite-coffinite assemblage show a direct correlation between P_2O_5 versus uranium, while mineralized samples dominated by the non-apatite bearing uranium assemblages show no apparent correlation between these elements. Although there is no well defined positive correlation between Ce versus uranium and La versus uranium, the data suggests that the most uranium-rich samples have the highest light rare earth element (LREE) concentrations. For example, two mineralized samples (41-127, depth 721 feet and 41-127, depth 722 feet) containing > 5 weight percent P_2O_5 and over 3000 ppm F also contain > 260 ppm La and > 340 ppm Ce. Thus, the presence of the apatite-coffinite assemblage is marked by elevated concentrations of the light rare earth elements.

Chondrite normalized rare earth element (REE) patterns for individual rock types were also assessed (normalizing values from Nakamura, 1974) (Figure 1-9). Plots of these data show that the slopes for unaltered (Figure 1-9a) and altered (Figure 1-9b) samples are similar, suggesting that the alteration process did not cause marked fractionation of the rare earth elements. The data from mineralized samples (Figure 1-9c) shares this general trend, but also contains a small number of samples (three out of eleven mineralized augen gneiss) that are significantly enriched in LREE relative to other samples. All of these LREE enriched samples also have P_2O_5 concentrations greater than 3 weight percent; again suggesting that there is an association between the coffinite-apatite assemblage and LREE enrichment. Rare earth element trends in the amphibolites (Figure 1-9d) do not vary significantly from those noted in the augen gneisses.

Composition-volume relationships and element mobility during alteration and mineralization

Gains and losses of individual elements and changes in the bulk volume of the system during alteration and mineralization provide information regarding element mobility, and can be assessed using the "isocon" method of Grant (1986). This method involves comparing the whole rock composition and density of an altered or mineralized sample to its "least altered equivalent"

or unaltered protolith. Thus, the determination of the proper protolith sample for a given altered sample is a key step in this type of analysis. For this study unaltered host rock samples and their altered and mineralized equivalents were paired using field relations, reaction textures and whole rock compositions. Unaltered examples of the gneissic host rocks of the Coles Hill deposit are distinguished by the fact that they contain unaltered titanite, potassium feldspar and plagioclase, and generally contain consistent whole rock concentrations ranging from 65 - 73 weight percent SiO_2, 0.2 - 0.4 weight percent TiO_2, 14 - 16 weight percent Al_2O_3, less that 1 weight percent P_2O_5 and less than 10 ppm uranium. While, altered, but unmineralized samples have lower concentrations of 60 – 65 weight percent SiO_2, greater concentrations of TiO_2 and Al_2O_3 (0.5 - 0.6 wt. % and 16.5 - 18 wt. % respectively) as well as concentrations of $P_2O_5 < 1$ weight percent and uranium < 40 ppm. Mineralized augen gneiss samples have more variable major element signatures but are clearly distinguished by concentrations of uranium > 40 ppm and generally $P_2O_5 > 1$ weight percent. Unaltered amphibolites contain 50 - 55 weight percent SiO_2; 1.14 - 1.60 weight percent TiO_2; 15 - 16 weight percent Al_2O_3, 0.3 - 0.4 weight percent P_2O_5 and < 10 ppm uranium. The geochemical data base does not contain any altered but unmineralized amphibolite samples; however, mineralized amphibolites also show clear signs of pervasive Na-metasomatism (e.g. riebeckite/crocidolite alteration rims on hornblende and albite rims on plagioclase) again indicating that mineralization was preceded by alteration. These mineralized amphibolites contain 40 - 55 weight percent SiO_2; 1.0 - 1.1 weight percent TiO_2; 11-15 weight percent Al_2O_3; 3 - 10 weight percent P_2O_5 and > 200 ppm uranium.

Although, relative concentrations of Al_2O_3 and TiO_2 are different in altered versus unaltered augen gneiss samples the ratio of Al_2O_3/TiO_2 can be used to match altered samples with their unaltered equivalents. This criteria is based on the assumption that aluminum and titanium represent the least mobile major and minor elements during alteration. The low mobility of aluminum and titanium has been demonstrated in a number of previous studies (i.e. Gresens, 1967; Correns, 1978, Ferry, 1979; Grant, 1986; Condie and Sinha, 1996). The usefulness of this ratio for matching altered samples with their unaltered equivalents is further supported by the observation that when various sets of altered and unaltered samples were compared using the isocon method, those samples with similar Al_2O_3/TiO_2 ratios gave the most internally consistent results (i.e. consistent values for gains and losses of elements and volume change of the system during alteration). Thus the Al_2O_3/TiO_2 criteria was used along with textural evidence to choose

altered and mineralized samples that formed from the same protolith. Examples of typical isocon diagrams for the Coles Hill samples are shown in Figure 1-10.

Using the isocon method (Grant, 1986) relative mobility (gain or loss) of an individual element is calculated from the slope of a line that pass from the origin through the data point of interest. Each mobile element will thus form a line with an equation of the general form: $C_A = (M_A/M_O)(C_O + \Delta C)$; where M_O and M_A are the equivalent masses of the unaltered and altered samples respectively, C_O and C_A are the concentrations of a given element in the unaltered (original) and altered samples respectively and $\Delta C = (C_A\text{-}C_O)/C_O$ (see Grant, 1986 for derivations). It follows that for a system that experienced no change in mass during alteration ($M_O = M_A$) the relative gain or loss of an element is given by: $(C_A\text{-}C_O)/C_O$. However, it has been demonstrated that it is commonly justified to assume that alteration processes involve changes in mass (and correspondingly, a change in volume) but that Al_2O_3 remains essentially immobile at the thin section scale (i.e. the constant alumina reference frame of Carmichael, 1969; Ferry, 1979). When this constant alumina assumption is applied it is possible to calculate the relative change in mass or volume ($V_A/V_O = M_A/M_O * \rho_O/\rho_A$) experienced by the system relative to the Al_2O_3 isocon (given the density ratio ρ_O/ρ_A).

Assuming aluminum immobility plots shown in Figures 1-10a and 1-10b (and similar isocon plots not shown) imply that the rock system experienced a 20 percent mass loss during alteration. This corresponds to an 18.5 percent volume loss based on the density ratio ρ_O/ρ_A = 2.67/2.64 for the two samples (41-162-213.3 and 41-162-400) used in this analyses (density measurements from Marline Uranium Corporation (1983). These data emphasize that the alteration process was dominated by sodium metasomatism involving significant enrichments in Na_2O, CO_2, P_2O_5 and uranium. Although the comparison of these two samples (41-162-213.3 and 41-162-400) indicates enrichment in uranium during alteration, the absolute increase is small (from 2.5 ppm in the unaltered sample to 11.7 ppm in the altered sample). The minor increases in P_2O_5 and uranium noted in some altered samples may represent a pre-ore stage enrichment of the deposit area in these elements. Alteration also involved significant depletions in K_2O and Rb, and moderate depletions in Sr, and Ba. These data further indicate that silica was removed from the ore zones during alteration but was reprecipitated within the cataclastic rocks surrounding the deposit. This process appears to be responsible for the formation of the silicified zone associated

with the Chatham fault within the study area. These changes are believed to correspond to the replacement of potassium-feldspars and plagioclase (An_{16}) by albite.

Petrographic and geochemical evidence indicate that the alteration event preceded mineralization. Thus, for assessing element mobility during mineralization the altered sample is treated as the "protolith" of the mineralized samples (Figs. 1-10c and 1-10d). The mineralized sample chosen for this mass transport assessment represents an average ore grade sample in terms of the concentrations of the key elements involved (U: 3340 ppm, F: 2300 ppm; Nb: 406 ppm; P_2O_5; 3.3 wt. %). It should be noted, however, that due to variations in the extent of mineralization for different samples, concentrations of these key elements show significant ranges (U: 50-3300 ppm; F: 300-10,000; Nb; 25-400 ppm; P_2O_5: 0.5-26 wt. %).

Assuming constant alumina, it is calculated that the mineralization event involved a mass gain of 6.4 percent for the ore-bearing augen gneiss rock system. This corresponds to a 7.2 percent gain in volume based on the density ratio $\rho_O/\rho_A = 2.64/2.59$ for the two samples (41-162-400 and 41-162-253) used in this analyses (density measurements from Marline Uranium Corporation, 1983). The volume loss/gain results for both alteration and mineralization are supported petrographically by the observation that altered samples contain numerous vugs and voids formed during the dissolution of quartz (volume loss) while in mineralized samples most of the open spaces as well as newly formed fracture zones have been filled and sealed with the mineralizing assemblages (volume gain).

The elements that are significantly enriched in the mineralized samples include (in order of enrichment): uranium, P_2O_5, Nb, F, Sr, Ba, CaO, and Th. This event did not result in significant element depletions, but is associated with moderate losses of K_2O and Y. The element gains and losses recorded in most mineralized samples are caused by precipitation of the apatite-coffinite assemblage. The mineralogical controls on Nb distribution is less well understood. However, the correlation between uranium and Nb coupled with the textural association between uranium minerals and fine-grained Ti oxides suggests that the Nb may be substituting for Ti within the ore-stage Ti phases.

Isocon analyses of the mineralized amphibolites indicates that these samples experienced a gain in mass of approximately 47 percent (assuming constant alumina). This corresponds to a volume gain of 48.7 percent based on the density ratio $\rho_O/\rho_M = 2.75/2.69$ for the two samples (41-126-711 and 41-126-637) used in this analyses (density measurements from Marline

Corporation, 1983). This calculation is supported by the petrographic observation that amphibolites within the ore zones have experienced more extensive mineralization (e.g. contain larger modal amounts of the apatite-coffinite assemblage) than adjacent augen gneisses. The highest ore grade zones are associated with amphibolite layers; however, the general geochemical trends reflecting the mineralization event are evident in augen gneiss and amphibolite host rocks. The major differences are that P_2O_5, Th, Nb, and the REE are more significantly enriched in the amphibolite samples, while Ba is less enriched. These observations suggest that the amphibolites contain relatively large modal volumes of the apatite-coffinite assemblage, but insignificant amounts of the Ba-zeolite-uraninite assemblage.

Discussion: Nature and Sequence of Hydrothermal Alteration and Mineralization

Synthesis of the petrographic and geochemical data reveals the nature and sequence of alteration and mineralization leading to the formation of the Coles Hill deposit (Table 1-6). This sequence is geochemically and structurally complex, involving multiple overprinting mineral assemblages occupying structurally disturbed zones created by intense brittle deformation. Preserved reaction textures and overprinted structural fabrics suggest that the sequence of cataclasis/alteration/mineralization involved cyclical pumping (e.g. Sibson et. al., 1975; Sibson, 1989) of hydrothermal fluids through the ore zones. Similar mechanisms have been suggested for the formation of other vein and breccia hosted, multi-stage uranium deposits, such as the Front Range Schwartzwalder ore body (Wallace and Karlson, 1985; Wallace and Whelan, 1986) and the Fe' deposit in Salamanca, Spain (Both, et. al., 1994). Oxygen and carbon isotope studies of the Salamanca deposits indicate that mineralization involved infiltration of meteoric fluids along extensional fault zones that formed during the opening of the Ciudad Rodrigo Tertiary basin (Both et. al., 1994). Based on structural and geologic similarities with these ore bodies we suggest that the formation of the Coles Hill deposit is likely to have involved similar processes.

The oldest recorded tectono-thermal event to affect the study area was an episode of ductile shearing that produced the protomylonitic (augen) fabric that defines the structural grain of the crystalline host rocks. The age of this fabric is constrained by the fact that it occurs in boulders from neighboring Triassic conglomerates and is cross-cut by tourmaline pegmatites of Paleozoic age (Robinson, 1979). The pre-Mesozoic age and structural setting of the augen gneiss

fabric thus suggest that it formed during Paleozoic displacement, perhaps associated with the Brookneal shear zone.

The sequence of hydrothermal alteration recorded in the augen gneiss and amphibolite units appears to have been initiated contemporaneously with a major cataclastic event. This alteration and associated veining also affect Triassic sediments along the northwest margin of the Danville basin indicating that the age of the alteration sequence is younger than 220 Ma (upper age limit on the Danville basin sequence) (Manspeizer et al., 1989). This age constraint is supported by an Rb-Sr isochron age of 180 Ma for silicified cataclasite of a southwest splay of the Chatham fault in North Carolina (Stony Ridge fault) (Fullagar and Butler, 1980).

Petrographic, mineral chemical and bulk geochemical data indicate that the earliest hydrothermal alteration event involved pervasive sodium metasomatism. This event is marked mineralogically by the growth of albite at the expense of potassium feldspar and plagioclase, and the growth of riebeckite at the expense of hornblende. It is marked geochemically by significant depletions in potassium and corresponding enrichment in sodium. Sodium metasomatism appears to have continued (either as discrete pulses or as a continuous event) throughout cataclastic deformation along the Triassic border fault. Sodium metasomatism precedes or is coeval with another alteration episode that involved the removal of SiO_2 from the ore zones and enrichment in SiO_2 along the deposit periphery (silicification). It is likely that this event marks the formation of the silicified cataclastic zone associated with the Chatham Fault. Desilicification within the ore zones is marked by dissolution features such as vugs and open spaces between grains and is associated with an approximately 18 percent volume loss for the system. Simultaneous with, or just following sodium metasomatism the study area experienced a multi-stage episode of chloritization. This event produced two generations, the first formed from the direct replacement of biotite, while the second fills fractures and is associated with uranium ore assemblages.

Uranium mineralization involved three stages: (1) coffinite-apatite accounts for the majority of uranium in the deposit) (2) uraninite-calcite bearing fractures, (3) uraninite-zeolite bearing fractures. All three of these uranium ore generations are associated with hematite staining. Based on spatial and textural relationships it is suggested that the major sources of iron in the mineralized zones are the meter scale layers and lenses of amphibolite common throughout the deposit area. These mafic interlayers, which contain up to 40 volume percent amphibole and

15 volume percent biotite, have approximately twice as much iron as the more quartzo-feldspathic augen gneiss units.

Estimated ferrous/ferric iron ratios for alteration minerals that formed during sodium metasomatism and chloritization suggest that these alteration events involved oxidizing fluids that would be capable of transporting uranium. The oxygen fugacity within these fluids may have been locally reduced where the rate of oxidation of ferrous iron ($2FeO + 0.5O_2 \rightarrow Fe_2O_3$) was greater than the rate at which oxygen was replenished to the reaction site. This type of reduction process may have led to the precipitation of the Coles Hill ore. A similar process has been suggested as a mechanism for the formation of other hydrothermal uranium deposits (Rich et. al., 1977). For example, the mineralized zones that form the Golden Gate Canyon uranium deposits of Colorado are similarly associated with hornblende rich interlayers and also contain extensive hematite halos (Adams and Stugard, 1956; Rich et. al., 1977).

The formation temperatures of the ore assemblages have not yet been assessed, but the observation that both feldspar and quartz deformed by brittle mechanisms during the cataclastic event suggests temperatures less than 300^{o}C (Tullis and Yund, 1987; Twiss and Moores, 1992). This estimate is in agreement with fluid inclusion homogenization temperatures measured for other hydrothermal coffinite and uraninite bearing assemblages (Rich et. al., 1977). In most cases the fluid inclusion data indicates uraninite precipitation occurs below 190^{o}C; however, Poty et al. (1974) indicate that the temperature of formation of a hydrothermal coffinite assemblage in the Bois-Noirs-Limouzat deposit in Forez France may have been as high as 350^{o}C. Most of the measured formation pressures for the hydrothermal uranium deposits reviewed by Rich et. al. (1977) are below 1 kb. The Coles Hill deposit also appears to have formed under low pressure, epithermal conditions as suggested by the occurrence of numerous vugs and open fractures in the mineralized zone. Furthermore, the presence of harmotome-phillipsite zeolites within the later Coles Hill ore veins implies formation temperatures around 60-80^{o}C and less than 1 kb (hydrothermal crystallization conditions of phillipsite; Tschernich, 1992). It is thus postulated that the Coles Hill uranium mineralization occurred below 300^{o}C (possibly below 100^{o}C) and at pressures of less than 1 kb.

Conclusion: Ore-Genesis Model

The Coles Hill uranium deposit was formed by cyclical, syn-tectonic, epithermal processes. Synthesis of the geology, structure, geophysics, mineral chemistry and whole rock geochemistry suggest that the deposit formed through fault controlled hydrothermal circulation during post-Triassic faulting and diabase intrusion associated with regional Mesozoic extension. The hydrothermal system may have been initiated and maintained by a steep geothermal gradient associated with crustal thinning (opening of the Danville-Dan River Basin) and the intrusion of regional sets of diabase dikes. Given the Mesozoic age and geologic setting, the most likely source of uranium for the deposit is the Triassic sedimentary package, specifically the Cow Branch formation, exposed along the hanging wall of the Danville basin border fault, adjacent to the deposit. These rocks contain altered carbonaceous zones (graphite filled fracture networks) that may represent previously uranium rich regions that were leached during alteration and mineralization. This theory is supported by the observation that unaltered sediments in the hanging wall of the border fault, southwest of the study area locally contain carbonaceous zones with anomolously high concentrations of uranium (0.03-0.16 weight % U_3O_8; Marline Uranium Corporations, 1983). It is possible that a uranium concentration of this type existed in the Coles Hill study area but was remobilized during hydrothermal circulation of meteoric water through the Chatham Fault zone (Figure 1-11).

A possible explanation for why this remobilization took place in the Coles Hill area may be related to the occurrence of the northwest trending cross-faults. This is evidenced by the unusually thick zones of silicified cataclasite adjacent to the deposit and associated with the mapped cross-faults (Figure 1-2). The carbonaceous, uranium rich Cow Branch sediments have also been shown to locally contain phosphate rich zones containing abundant vertebrate fossils. It is thus possible that this formation not only provided a source of uranium for the Coles Hill deposit but also provided the source of phosphate required to precipitate the large volume of apatite associated with the primary ore assemblage.

It is thus proposed that intense cataclasis and brecciation associated with displacement on the border fault exposed a section of uranium and phosphate rich Triassic sediments to oxidizing (meteoric ?) fluids that were being cyclically circulated through the fault zone during epithermal processes (Figure 1-11). After leaching the source rocks the uranium-phosphate enriched fluids may have been channeled or into the zone of brecciated augen gneiss and intersected localized

Fe^{2+}/Fe^{3+} redox fronts formed by the alteration of iron rich amphibolite layers. Where fluid bearing fracture zones intersected these reducing iron rich lithologies, uranyl complexes in the fluid would react and lead to the precipitation of the ore assemblages.

The abundance of fluor-apatite in the primary uranium ore assemblage indicates that, early in the mineralization process uranium was probably transported primarily as phosphate and/or fluoride complexes depending on the pH of the solution. The abundance of coffinite rather than uraninite within this assemblage further suggests that the fluid must have also had a relatively high activity of silica. Mineralizing fluids associated with the later vein type assemblages may have been dominated by uranyl dicarbonate complexes as suggested by the intimate association of uraninite and calcite suggesting that the fluids involved in this uraninite-calcite precipitation event were more alkaline than those involved in coffinite-apatite mineralization. The final ore bearing assemblage contains zeolites in equilibrium with uraninite. The absence of calcite in these later ore veins suggests that the activity of CO_2 in the hydrothermal fluid decreased during the later stages of mineralization.

Based on the classification system of Dahlkamp (1991), the Coles Hill deposit most closely fits the criteria for the vein hosted, "not granite related" uranium ore type; however, its geologic context and unique ore assemblage (e.g. apatite-coffinite) distinguish it from other deposits of vein type origin. Thus, the Coles Hill deposit may best be classified as a new subtype represented by vein hosted uranium ore bodies formed during cataclasis and syn-tectonic hydrothermal activity associated with extensional tectonics.

References

Adams, J.W., and Stugard, F., Jr., 1956, Wall-rock control of certain uraninite deposits in Golden Gate Canyon, Jefferson County, Colorado: U.S. Geological Survey Bulletin, 1030-G, p. 187-209.

Baillieul, T.A., and Daddazio, P.L., 1982, A vein-type uranium environment in the Precambrian Lovingston formation, central Virgina: Virginia Division of Mineral Resources Publication 38, 11 p.

Both, R.A., Arribas, A. and DeSaint-Andre', B., 1994, The origin of breccia-hosted uranium deposits in carbonaceous metasediments of the Iberian Peninsula: U-Pb geochronology and stable isotope studies of the Fe' deposit, Salamanca Province, Spain: Economic Geology, v. 89, p. 584-601.

Butler, J. R., 1980, Review of potential host rocks for radioactive waste disposal in the Piedmont province of North Carolina: Savannah River Laboratory, E. I. Du Pont de Nemours and Company, Report DP-1562, 47 p.

Correns, C.W., 1978, Titanium: behavior in metamorphic reactions. In: K.H. Wedepohl (Editor), Handbook of Geochemistry, 2(II). Springer, Berlin, 67

Carmichael, D.M., 1969, On the mechanism of prograde metmorphic reactions in quartz-bearing pelitic rocks: : Contributions to Mineralogy and Petrology, v. 20, p. 244-267.

Condie, K.C., and Sinha, A.K., 1996, Rare earth and other trace element mobility during mylonitization: a comparison of the Brevard and Hope Valley shear zones in the Appalachian Mountains, USA: Journal of Metamorphic Geology, v. 14, p. 213-226.

Conley, J.F. and Henika, W.S., 1973, Field trip across the Blue Ridge anticlinorium, Smith River allochthon and Sauratown Mountains anticlinorium near Martinsville, Virginia: Virginia Minerals, v. 19, no. 4, 37 p.

Crandall, T.M., Ross, R.B., Jr., Whitlow, J.W., and Griffitts, W.R., 1982, Mineral resource potential map of the Lost Cove and Harper Creek Roadless Areas, Avery and Caldwell counties, North Carolina: U.S. Geological Survey, Miscellaneous Field Studies Map MF-1391-A, Scale 1:48,000

Dahlkamp, F. J., 1991, Uranium ore deposits, Springer-Verlag, Berlin-Heidelberg-New York.

Deer, W.A., Howie, R.A. and Zussman, J., 1975, Rock-Forming Minerals: Volume 5, Non-Silicates, Longman Group Ltd., London.

Dribus, J.R., 1978, Preliminary study of the uranium potential of the Dan River Triassic Basin system, North Carolina and Virginia, U.S. Department of Energy GJBX-131 (78) open file report

Ferry, J.M., 1979, Reaction mechanisms, physical conditions, and mass transfer during hydrothermal alteration of mica and felspar in granitic rocks from south-central Maine, USA: Contributions to Mineralogy and Petrology, v. 68, p. 125-139.

Fullagar, P.D. and Butler, J.R., 1980, Radiometric dating in the Sauratown Mountains area, North Carolina, in Geologial Investigations of Piedmont and Triassic Rocks, Central North Carolina and Virginia, V. Price, Jr., Thayer, P.A., and Ranson, W.A., eds.: Carolina Geological Society Field Trip Guidebook p. II-1-II-10.

Glaeser, J.D., 1979, Environments for sedimentary uranium in Triassic-Jurassic basins, eastern North America: American Association of Petroleum Geologists Bulletin, v. 63, p. 827.

Grant, J.A., 1986, The isocon diagram-a simple solution to Gresens' equation for metasomatic alteration: Economic Geology, v. 81, p. 1976-1982.

Gresens, R.L., 1967, Composition-volume relationships of metasomatism: Chemical Geology, v. 2, p. 47-65.

Halladay, C.R., 1983, Summary of microprobe analyses, Unpublished Report, Marline Uranium Corporation, 15 p.

Halladay, C.R., 1989, The Swanson uranium deposit, Virginia: a structurally controlled U-P albitite deposit [abs.], in Uranium resources and geology of North America: Saskatoon, Canada, Proceedings of a technical committee meeting organized by the International Atomic Energy Agency, September 1987, p. 519

Henika, W.S., 1981, Geology of the Spring Garden quadrangle, Virginia: Virginia Division of Mineral Resources Open-File Map and Report, scale 1:24,000.

Henika, W.S., 1997, Geologic map of the Roanoke 30x60 minute quadrangle: Virginia Division of Mineral Resources Publication 148, scale 1:100,000.

Henika, W.S., 1998, Digital geologic map of the Virginia portion of the Danville 30x60 minute quadrangle: Virginia Division of Mineral Resources Publication DP-43A, unedited draft, scale 1:100,000.

Henika, W.S. and Johnson, S.S., 1980, Aeroradiometric contour pattern and rock distribution in the Danville 15-minute quadrangle, in Geological Investigations of Piedmont and Triassic Rocks, Central North Carolina and Virginia, V. Price, Jr., Thayer, P.A., and Ranson, W.A., eds.: Carolina Geological Society Field Trip Guidebook p. B-VI-1-B-VI-8.

Henika, W.S. and Thayer, P.A., 1983, Geologic map of the Spring Garden quadrangle, Virginia: Virginia Division of Mineral Resources, Publication 48 (GM47D).

Irvine, T.N., and Baragar, W.R.A., 1971, A guide to the chemical classification of the common volcanic rocks: Canadian Jouranl of Earth Science, v. 8, p. 523-548

Klemic, H., 1962, Uranium occurrences in sedimentary rocks of Pennsylvania: U.S. Geological Survey Bulletin 1107-D, p. D243-D288.

Klemic, H., Warman, J.C., and Taylor, A.R., 1963, Geology and uranium occurrences of the northern half of the Leighton, Pennsylvania quadrangle and adjoining areas: U.S. Geological Survey Bulletin 1138, 97 p.

LeBas, M.J., LeMaitre, R.W., Streckeisen, A., and Zanettin, B., 1986, A chemical classification of volcanic rocks based on the total alkali silica diagram: Journal of Petrology, v. 27, p. 745-750.

Lesure, F.G., Motooka, J.M., and Weis, P.L., 1977, Exploration geochemical studies of some sandstone copper-uranium deposits, Bradford, Columbia, and Lycoming counties, Pennsylvania: U.S. Geological Survey Journal of Research. v. 5, p. 609-621.

Lineberger, D.H., Jr., 1983, Geology of the Chatham fault zone, Pittsylvania County, Virginia: Unpublished M.S. Thesis, University of North Carolina, Chapel Hill, 79 p.

Manspeizer, W., DeBoer, J., Costain, J.K., Froelich, A.J., Coruh, C., Olsen, P.E., McHone, G.J., Puffer, J.H. and Prowell, D.C., 1989, Post-Paleozoic activity: in Hatcher, R.D., Thomas, W.A. and Viele, G.W., eds., The Appalachian-Ouachita Orogen in the United States, Geology of North America Volume F-2, Geological Society of America.

Marline Uranium Corporation, 1983, An evaluation of uranium development in Pittsylvania County Virginia: report submitted jointly by Marline Uranium Corporation and Union Carbide Corporation to the Virginia Uranium Administrative Group to the Virginia Uranium Administrative Group Pursuant to Section 45.1-285.1et seq of the Code of Virginia (1983) (Senate Bill 155), October, 15, 1983,

Meyertons, C.T., 1963, Triassic formations of the Danville basin: Virginia Division of Mineral Resources Report, Investigation 6, 65 p.

Nakamura, N., 1974, Determination of REE, Ba, Fe, Mg, Na and K in carbonaceous and ordinary chondrites: Geochim. Cosmochim. Acta, v.38, p. 757-775.

Netto, A.M., Meyer, A., Cuney, M. and Poupeau, G., 1991, A thermo-geochronological study of the Itataia phospho-uraniferous deposit (Ceara', Brazil) by apatite fission track analyses: genetic implications: in Source Transport and Deposition of Metals, Pagel, M. and Leroy, J.L., eds., Proceedings of the 25 Years SGA Anniversary Meeting, 1991.

North Carolina Geological Survey, 1985, Geologic map of North Carolina: North Carolina Department of Natural Resources and Community Development, Geological Survey Section, scale 1:500,000.

O'Hara, K., 1988, Fluid flow and volume loss during mylonitization: an origin for phyllonite in an overthrust setting NC, USA: Tectonophysics, v. 156, p. 21-36.

Olsen, P.E., Froelich, A.J., Daniels, D.L., Smoot, J.P. and Gore, P.J.W., 1991, Rift basins of Early Mesozoic Age: in The Geology of the Carolinas, Carolina Geological Society Fiftieth Anniversary Volume, Horton, J.W., Jr., and Zullo, V.A., p. 142-171.

Porto da Silveira, C.L., Schorscher, H.D. and Miekely, N., 1991, The geochemistry of albitization and related uranium mineralization, Espinharas, Paraiba (PB), Brazil: Journal of Geochemical Exploration, v. 40, p. 329-347.

Poty, B.P., Leroy, J. and Cuney, M., 1974, Les inclususions fluides dans les minerais des gisements d'uranium intragranitiques du Limousin et du Forez (Massif Central, France): in Formaton of Uranium Deposits, p. 569-582, International Atomic Energy Agency, Vienna.

Ragland, P.C., and Whittington, D., 1983, Early Mesozoic diabase dikes of eastern North America: Magma Types: Geological Society of America Abstracts with Programs, v. 15, p. 666.

Ragland, P.C., Conley, J.F., Allison, D., Kish, S.A., and Odom, A.L., 1993, Petrology of the Martinsville Igneous Complex, Smith River Allochthon, Southwestern Virginia Piedmont: Unpublished.

Randazzo, A.F., Swe, W., and Wheeler, W.H., 1970, A study of tectonic influence on Triassic sedimentation-Wadsboro sub-basin, Central Piedmont: Journal of Sedimentary Petrology, v. 40, no. 3, p. 998-1006.

Ratcliffe, N.M., 1971, The Ramapo fault system in New York and adjacent northern New Jersey: A case of tectonic heredity: Geological Society of America Bulletin, v. 82, p. 125-142.

Rich, R.A., Holland, H.D. and Petersen, U., 1977, Hydrothermal uranium deposits, Elsevier Scientific Publishing Company, Amsterdam-Oxford-New York, 264 p.

Robinson, G.R., Jr., 1979, Pegmatite cutting mylonite-evidence supporting pre-Triassic faulting along the western border of the Danville Triassic Basin, southern Virginia, [abs.]: Geological Society of America, Abstracts with Programs, v. 11, no. 4, p. 210

Rogers, J.J.W., Ragland, P.C., Nishimori, R.K., Greenberg, J.K., and Hauck, S.A., 1978, Varieties of granitic uranium deposits and favorable exploration areas in the eastern United States: Economic Geology, v. 73, p. 1539-1555.

Romberger, S.B., Transport and deposition of uranium in hydrothermal systems at temperatures up to 300 degrees C: geological implications: in de Viro, B., Ippolito, F., Capaldi, G. and Simpson, P.R., eds., Uranium Geochemistry, Mineralogy, Geology, Exploration and Resources, Institute of Mining and Metallurgy, London.

Sanders, J.E., 1963, Late Triassic tectonic history of northeastern United States: American Journal of Science, v. 261, p. 501-524

Sibson, R.H., Moore, J.M., and Rankin, A.H., 1975, Seismic pumping-a hydrothermal fluid transport mechanism: Geologic Society of London Journal, v. 131, p. 653-659.

Sibson, R.H., 1977, Fault rocks and fault mechanisms: Journal of the Geological Society of London, v. 133, p. 191-213

Sibson, R.H., 1987, Earthquake rupturing as a hydrothermal mineralising agent: Geology, v. 15, p. 701-704.

Sibson, R.H., 1989, Earthquake faulting as a structural process: Journal of Structural Geology, v. 11, p. 1-14.

Smith, R.C., II, and Hoff, D. T., 1984, Geology and mineralogy of copper-uranium occurrences in the Picture Rocks and Stonestown quadrangles, Lycoming and Sullivan counties, Pennsylvania: Pennsylvania Geological Survey, Mineral Resources Report 80, 271 p.

Thayer, P.A., 1970, Stratigraphy and geology of Dan River Triassic basin, North Carolina: Sourtheastern Geology, v. 12, p. 1-31.

Tschernich, R.W., 1992, Zeolites of the World: Geoscience Press, Inc. Phoenix Arizona.

Tullis, J.A. and Yund, R.A., 1987, Transition from cataclastic flow to dislocation creep in feldspar: mechanisms and microstructures: Geology, v. 15, P. 606-609.

Twiss R.J. and Moores, E.M., 1992, Structural Geology: W.H. Freeman and Company, p. 53-56.

Turner-Peterson, C.E., Olsen, P.E. and Nuccio, V.F., 1985, Modes of uranium occurrence in black mudstones in the Newark Basin, New Jersey and Pennsylvania: in Robinson, G.R., Jr. and Froelich, A. J., Proceedings of the Second U.S. Geological Survey Workshop on the Early Mesozoic Basins of the Eastern United States, U.S. Geological Survey Circular 946, 147 p.

Virginia Division of Mineral Resources, 1993, Geologic map of Virginia: Virginia Division of Mineral Resources, scale 1:500,000.

Wallace, A.R., and Karlson, R.C., 1985, The Schwartzwalder uranium deposit. I: Geology and structural controls on mineralization: Economic Geology, v. 80, p. 1842-1857.

Wallace, A.R., and Whelan, J.F., 1986, The Schwartzwalder uranium deposit. III: Alteration, vein mineralization, light stable isotopes, and genesis of the deposit: Economic Geology, v. 81, p. 872-888.

Weems, R. E. and Olsen P. E., 1997, Synthesis and Revision of groups within the Newark Super Group, eastern North America, Geological Society of America Bulletin, V. 109, no. 2 p.199

Table 1-1. Average modal data for unaltered and altered host rocks.

	(1)	(2)	(3)	(4)	(5)	(6)
Quartz	26	18	20	2	23	1
K-feldspar	23	28	20	Tr	Tr	----
Plagioclase (An_{10-16})	35	38	31	41	8	10
Biotite	7	9	10	10	1	1
Muscovite	Tr	Tr	Tr	----	Tr	----
Hornblende	----	----	----	30	----	15
Titanite	1	1	1	2	Tr	Tr
Apatite	1	1	1	2	1	2
Anatase	Tr	Tr	Tr	Tr	Tr	2
Other opaques	1	1	1	1	1	1
Albite	Tr	Tr	Tr	Tr	53	30
Chlorite	4	4	2	5	11	14
Riebeckite	----	----	----	----	----	15
Matrix	2	Tr	14	7	2	9
Vol. % porphyroclasts	20	35	20	5	20	5

(1) unaltered upper augen gneiss, (2) unaltered middle augen gneiss, (3) unaltered lower augen gneiss, (4) unaltered amphibolite, (5) altered augen gneiss, (6) altered amphibolite. *Matrix denotes fine-grained mixture of feldspar, quartz, biotite/chlorite +/- white mica, +/- calcite **Data from petrographic analyses (this study) and bulk X-ray diffraction studies of Marline Corporation, 1983.

Table 1-2. Electron microprobe analyses and mineral formula calculations for selected feldspars from the Coles Hill uranium deposit and host rocks.

	(F1)	(F2)	(F3)	(F4)	(F5)
SiO_2	64.26	65.08	65.16	68.61	69.27
Al_2O_3	22.29	22.15	21.98	19.77	19.32
FeO	0.12	0.11	0.10	----	0.21
CaO	3.30	3.11	2.87	0.26	----
Na_2O	9.66	9.68	9.82	11.06	11.02
K_2O	----	----	----	----	----
Sum:	*99.63*	*100.13*	*99.93*	*99.70*	*99.82*
Si	2.84	2.86	2.87	3.00	3.02
Al	1.16	1.15	1.14	1.02	0.99
Sum:	*4.00*	*4.01*	*4.01*	*4.01*	*4.01*
Fe	----	----	----	----	----
Na	0.83	0.82	0.84	0.94	0.93
Ca	0.16	0.15	0.14	----	----
K	----	----	----	----	----
Total:	*4.99*	*4.98*	*4.98*	*4.96*	*4.95*
An	15.88	15.08	13.91	1.28	----
Ab	84.12	84.92	86.09	98.72	100.00

* Formula ions calculated based on 8 oxygen equivalent basis Analyses F4 and F5 are of a clear reaction rims formed on primary plagioclase grains F1 and F2 respectively.

Table 1-3. Electron microprobe analyses and mineral formula calculations for selected amphiboles from the Coles Hill uranium deposit and host rocks.

	(H1)	(H2)	(H3)	(H4)	(H5)	(R1)	(R2)	(R3)	(R4)	(R5)
SiO_2	42.83	42.65	42.67	42.86	42.54	52.11	52.76	52.17	53.12	52.86
TiO_2	0.65	0.70	0.63	0.63	0.70	3.17	3.34	3.34	3.44	3.19
Al_2O_3	12.04	11.77	11.57	11.41	11.98	0.10	0.09	0.43	0.09	0.10
(Fe_2O_3)*	3.90	3.60	3.30	3.10	3.20	11.70	10.00	10.00	8.70	7.20
FeO	11.62	11.94	11.71	11.60	12.44	12.63	11.06	13.72	12.59	11.63
MnO	0.34	0.35	0.31	0.34	0.29	0.53	0.48	0.66	0.50	0.50
MgO	10.65	10.76	10.56	10.78	10.24	5.68	8.01	5.66	8.09	9.75
CaO	11.44	11.68	11.31	11.41	11.36	0.17	0.33	0.19	0.31	0.57
Na_2O	1.54	1.50	1.42	1.34	1.46	7.62	7.51	7.72	7.72	7.41
K_2O	1.13	1.25	1.18	1.13	1.30	0.47	0.61	0.57	0.67	0.99
Sum:	*96.14*	*96.20*	*94.66*	*94.60*	*95.51*	*94.18*	*94.19*	*94.46*	*95.23*	*94.20*
Si	6.45	6.44	6.52	6.54	6.47	8.01	8.00	8.00	8.00	8.00
Al^{IV}	1.55	1.56	1.48	1.46	1.53	----	----	----	----	----
Sum:	*8.00*	*8.00*	*8.00*	*8.00*	*8.00*	*8.01*	*8.00*	*8.00*	*8.00*	*8.00*
Al^{VI}	0.59	0.53	0.60	0.60	0.62	0.02	0.02	0.01	0.02	0.02
Ti	0.07	0.08	0.07	0.07	0.08	0.37	0.38	0.39	0.39	0.36
Fe^{3+}	0.44	0.41	0.38	0.36	0.37	1.35	1.14	1.15	0.99	0.82
Fe^{2+}	1.46	1.51	1.50	1.48	1.58	1.62	1.40	1.76	1.59	1.47
Mg	2.39	2.42	2.41	2.45	2.32	1.30	1.81	1.29	1.82	2.20
Mn	0.04	0.04	0.04	0.04	0.04	0.07	0.06	0.09	0.06	0.06
Sum:	*5.00*	*5.00*	*5.00*	*5.00*	*5.00*	*4.73*	*4.81*	*4.69*	*4.86*	*4.94*
Na	0.45	0.44	0.42	0.40	0.43	2.27	2.21	2.30	2.26	2.17
Ca	1.85	1.89	1.85	1.87	1.85	0.03	0.05	0.03	0.05	0.09
K	0.22	0.24	0.23	0.22	0.25	0.09	0.12	0.11	0.13	0.19
Sum:	*2.51*	*2.57*	*2.50*	*2.48*	*2.53*	*2.39*	*2.38*	*2.44*	*2.43*	*2.46*
OH**	2.00	2.00	2.00	2.00	2.00	2.00	2.00	2.00	2.00	2.00
Total:	*17.52*	*17.57*	*17.50*	*17.49*	*17.54*	*17.12*	*17.20*	*17.13*	*17.30*	*17.40*
(Fe^{2+}/Fe^{3+})	3.31	3.69	3.94	4.16	4.32	1.20	1.23	1.52	1.61	1.80
Mg#	55.09	55.25	55.66	56.60	53.90	29.94	41.00	30.14	40.80	48.28

*Fe_2O_3 for H1-H5 was estimated by assuming (Al^{VI}+Ti+Fe^{3+}+Fe^{2+}+Mg+Mn) = 5.0, Fe_2O_3 for R1-R5 was estimated assuming SiO_2 (tetrahedral) = 8.0 **Formula ions calculated assuming ideal OH (23 oxygen equivalent basis). Analyses R2, R4 and R5 are of reaction rims on primary hornblede (H2, H3, H4 respectively) Analyses R1 and R3 are of fibrous (crocidolite) crystals found in vugs.

Table 1-4. Electron microprobe analyses and mineral formula calculations for selected biotites and chlorites from the Coles Hill uranium deposit and host rocks.

	(B1)	(B2)	(B3)	(B4)	(B5)	(C1)	(C2)	(C3)	(C4)	(C5)
SiO_2	37.04	37.25	37.11	37.28	37.47	28.65	28.11	28.67	31.28	30.74
TiO_2	1.93	2.07	1.77	1.79	2.21	0.14	----	----	----	----
Al_2O_3	15.93	15.67	15.96	16.28	16.12	17.17	17.74	18.36	13.31	14.06
FeO	16.65	16.38	16.75	16.25	16.48	26.88	26.81	27.31	28.61	27.59
MnO	0.21	0.18	0.11	0.17	0.23	0.20	0.20	0.21	0.12	0.13
MgO	12.92	13.57	13.29	13.35	13.14	14.50	14.94	14.79	15.51	14.97
CaO	----	----	0.12	----	----	----	----	----	----	0.22
Na_2O	0.15	0.13	0.15	0.10	0.13	----	----	----	----	----
K_2O	8.42	8.17	8.35	8.60	8.60	0.14	----	----	----	----
Sum:	*93.25*	*93.42*	*93.61*	*93.82*	*94.38*	*87.68*	*87.80*	*89.34*	*88.83*	*87.71*
Si	5.66	5.66	5.65	5.65	5.65	6.07	5.94	5.95	6.57	6.52
Al^{IV}	2.34	2.34	2.35	2.35	2.35	1.93	2.06	2.05	1.43	1.48
Sum:	*8.00*	*8.00*	*8.00*	*8.00*	*8.00*	*8.00*	*8.00*	*8.00*	*8.00*	*8.00*
Al^{VI}	0.53	0.47	0.51	0.55	0.51	2.35	2.36	2.44	1.87	2.03
Ti	0.22	0.24	0.20	0.20	0.25	0.02	----	----	----	----
Fe	2.13	2.08	2.13	2.06	2.08	4.76	4.74	4.74	5.03	4.89
Mg	2.94	3.08	3.01	3.01	2.95	4.58	4.71	4.58	4.86	4.73
Mn	0.03	0.02	0.01	0.02	0.03	0.04	0.04	0.04	0.02	0.02
Sum:	*5.84*	*5.89*	*5.87*	*5.85*	*5.82*	----	----	----	----	----
Na	0.04	0.04	0.04	0.03	0.04	----	----	----	----	----
Ca	----	----	0.02	----	----	----	----	----	----	----
K	1.64	1.58	1.62	1.66	1.65	0.04	----	----	----	----
Sum:	*1.69*	*1.62*	*1.68*	*1.69*	*1.69*	11.79	*11.85*	*11.80*	*11.78*	*11.73*
OH*	4.00	4.00	4.00	4.00	4.00	16.00	16.00	16.00	16.00	16.00
Total:	*19.53*	*19.51*	*19.55*	*19.54*	*19.51*	*35.79*	*35.85*	*35.80*	*35.78*	*35.73*
Mg#	57.73	59.36	58.42	59.17	58.36	48.83	49.65	48.93	49.04	49.05

*Formula ions calculated assuming ideal OH (22 (O) equivalent basis for B1-B5 and 28 (O) basis for C1-C5). Analyses C1 is of a chlorite alteration zone within a relict biotite grain, C2 and C3 are chlorites that have completely replaced biotite within the augen gneiss foliation, C4 and C5 are fracture fill (vien) chlorites.

Table 1-5. Electron microprobe analyses of pre-ore stage and ore stage apatites from the Coles Hill Uranium Deposit, Virginia (Halladay, 1983; analyses performed at Virginia Polytechnic Institute and State University, Department of Geological Sciences).

(wt.%)	**41-127-1006**	**41-127-841**	**41-125-312**	**41-162-1057**	**41-127-785**	**41-167-682**	**41-167-371**	**41-127-721**	**41-167-467**	**41-167-682a**	**41-167-682b**
CaO	57.33	58.12	55.82	54.68	54.6	58.6	56.02	54.59	58.03	56.84	50.58
P_2O_5	40.5	43.72	44.92	43.08	43.74	38.32	41.79	41.02	39.32	36.59	35.52
F	2.77	2.12	3.39	3.29	2.97	2.69	3.62	2.35	3.03	2.29	3.32
Cl	----	0.11	----	----	----	----	----	----	----	----	----
SiO_2	0.24	0.13	0.21	0.13	0.2	0.17	----	0.18	0.34	0.39	0.72
Al_2O_3	----	----	----	----	----	----	----	----	----	0.14	0.3
(ppm)	----	----	----	----	----	----	----	----	----	----	----
Mg	----	----	----	----	----	----	----	----	----	9650	13268
Mn	13167	7745	7745	9294	7745	10069	----	----	----	7745	11618
Fe	----	----	----	13214	----	----	----	14769	16323	13214	----
Na	----	----	----	----	----	----	----	45998	7419	27450	54901
Sr	----	----	----	----	----	----	52427	27904	----	43971	27059
Ba	1612	1343	----	----	----	----	----	----	896	----	----
La	----	----	----	----	----	----	640	512	938	----	----
Ce	598	----	640	----	683	----	----	----	----	----	----
Th	----	----	----	----	----	----	----	----	----	1142	----
U	----	----	----	----	----	----	2204	4760	7493	2821	26974

Table 1-6. Sequence of alteration and mineralization leading to the formation of the Coles Hill uranium deposit.

Alteration/Mineralization Event	Mineral Reactions and Observed Textures
I Formation of augen gneiss fabric	Euhedral apatite and titanite - preferentially oriented within protomylonitic foliation
II Intrusion of diabase dikes and pervasive cataclasis along the Chatham Fault zone (exposes augen gneisses and Triassic sediments to hydrothermal fluids)	Tectonic grain-size reduction and fracture induced increase in porosity and permeability of augen gneisses and interlayered amphibolites
III Na metasomatism	Growth of albite, destruction of quartz, plagioclase & K-feldspar (plag-An_{16}) $\longrightarrow$ albite) (Na + Al + K-feldspar $\longrightarrow$ albite) (primary amphiboles $\longrightarrow$ riebeckite/crocidolite)
IV Chloritization	Growth of coarse-grained, blue-green chlorite (biotite and amphiboles $\longrightarrow$ chlorite)
V Continued cataclasis along Chatham Fault zone	Tectonic grain-size reduction - cataclasis and brecciation of Stage II cataclastic zones
VI Hematization	Growth of hematitic "dust" around cataclastic zones that intersect amphibolites (these zones will host the Stage IX ore assemblage) (mafic minerals and magnetite $\longrightarrow$ hematite)
VII Coffinite-Apatite mineralization (associated with chloritizaiton)	Precipitation of apatite-coffinite assemblage in fractures; ore phases associated with chlorite, anatase and trace sulfides
VIII Hematization	Growth of thin hematite "films" along walls of veins that will host Stage XI ore assemblages - reddening of feldspars. Precipitation of calcite-pitchblende & zeolite-pitchblende assemblages in fractures; ore phases also associated with anatase & pyrite
IX Calcite-Pitchblende and Zeolite-Pitchblende mineralization	
XII Formation of fault gouge on border fault and minor veining throughout study area	Growth of clay and calcite rich fault gouge; non ore-bearing calcite and quartz veins cross-cut cataclastic zones
XIII Displacement of Triassic basin border fault by northwest striking cross faults	Formation of non mineralized, northwest and northeast striking joint sets

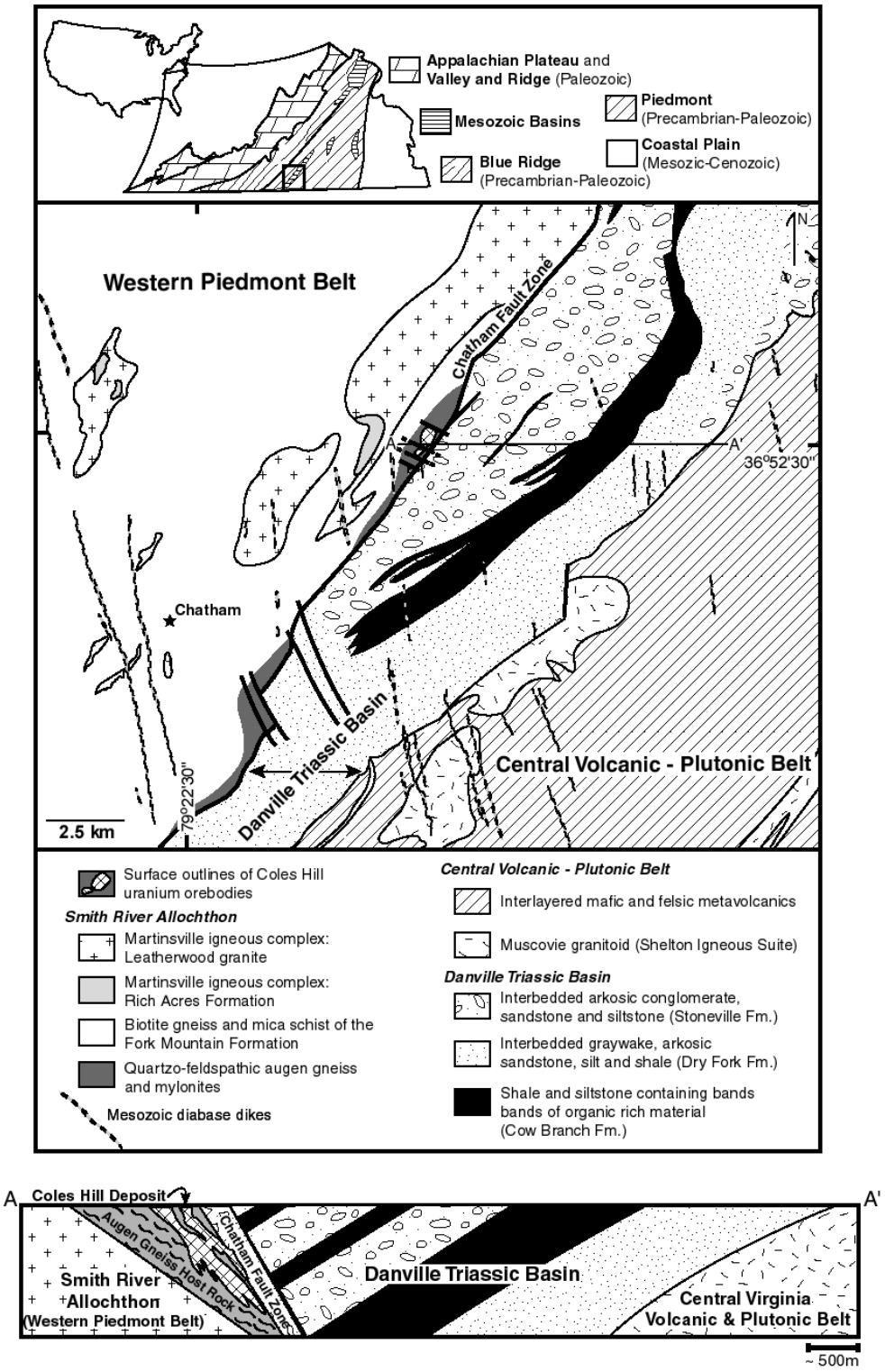

Figure 1-1. Location, regional geologic map and cross-section of the study area showing the geologic setting of the Coles Hill orebodies (adapted from Henika, W.S., 1998, Digital geologic map of the Virginia portion of the Danville 30x60 minute quadrangle: Virginia Division of Mineral Resources Publication DP-43A, unedited draft, scale 1:100,000).

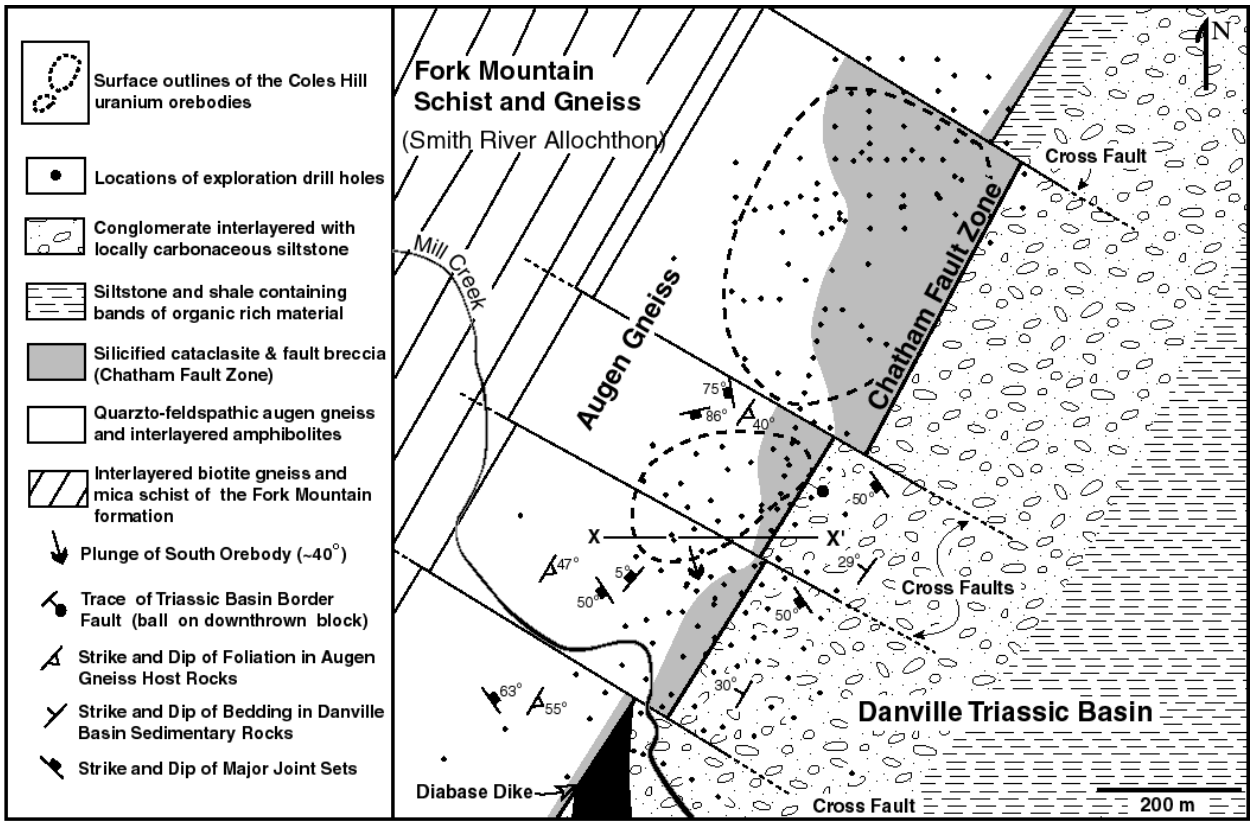

Figure 1-2. Geologic map of the Coles Hill site showing major lithologic units and the locations of exploration drill holes (Marline Corporation, 1983). The geology is based on surface mapping, and geologic logging of drill core. Additional geologic map data from Henika and Thayer (1981), Lineberger (1983) and this research.

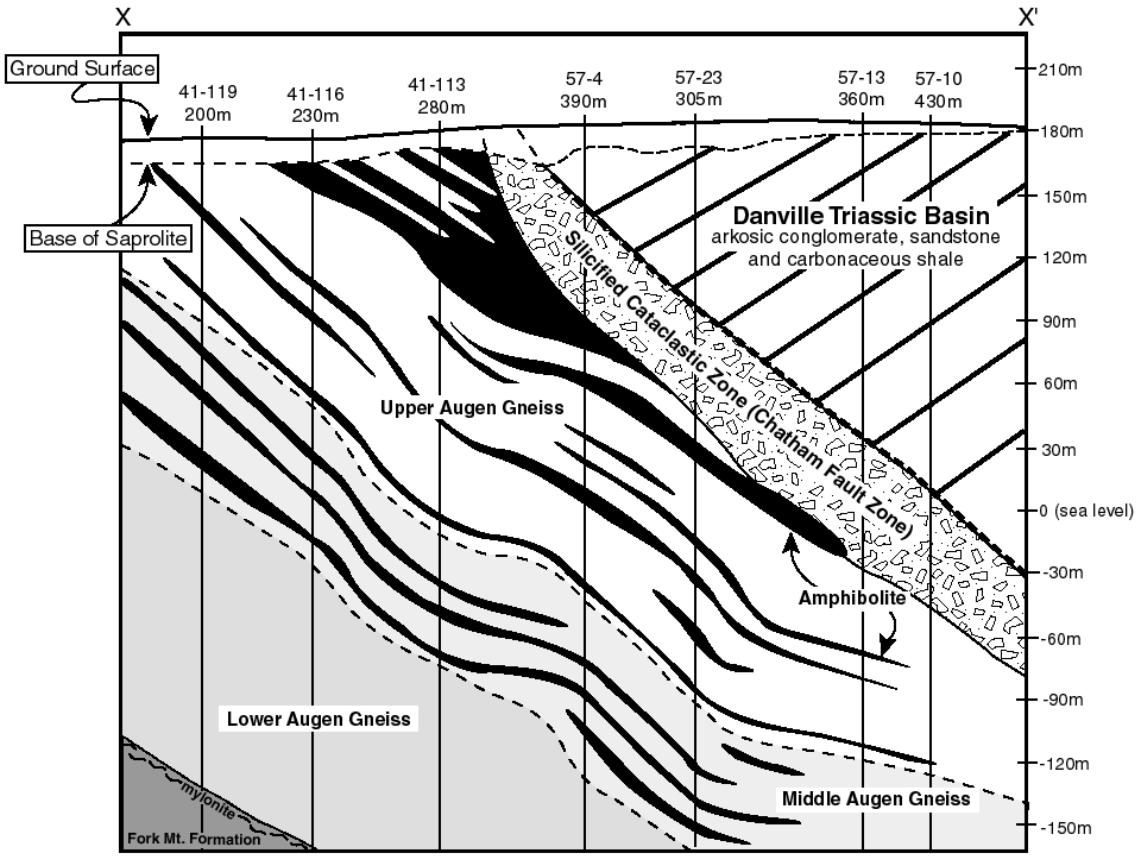

Figure 1-3. Geologic cross-section of the Coles Hill uranium deposit host rocks (X - X' on Fig. 2), constructed from Marline Corporation drill hole data (Marline Uranium Corporation, 1983). Vertical holes drilled within the plane of the cross-section are shown as solid lines and are identified by well number and total well depth (respectively).

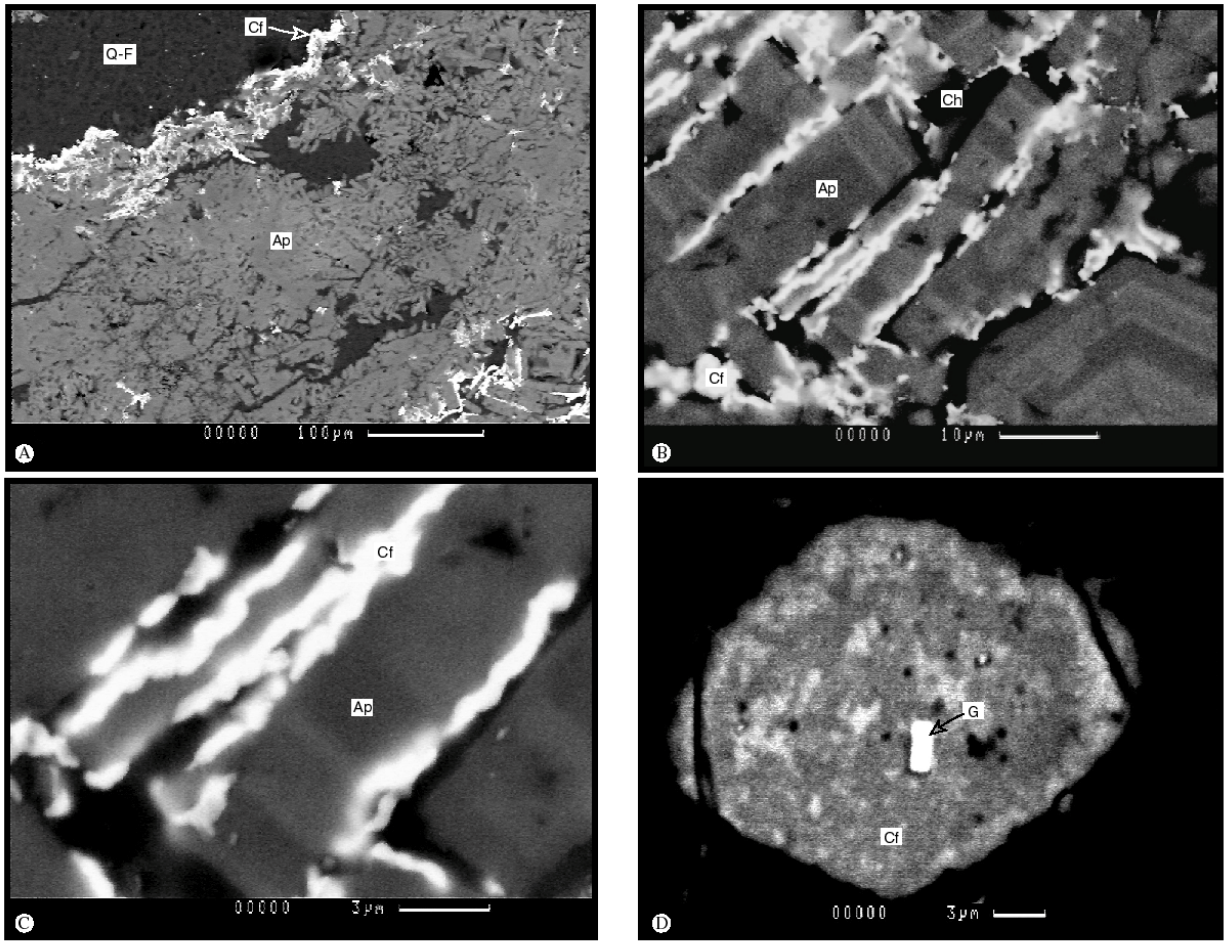

Figure 1-4. Backscatter electron images of the coffinite-apatite ore assemblage. Abbreviations are Q-F = quartzo-feldspathic host rock, Cf = coffinite, Ap = apatite, Ch = chlorite G = galena (all phases identified by energy dispersive x-ray spectra): (A) edge of coffinite apatite filled fracture showing cryptocrystalline coffinite (white) concentrated at fracture margin, (B) enlargement of coffinite-apatite assemblage showing that coffinite occurs as thin films surrounding ore-stage apatite laths, (C) enlargement of apatite laths surrounded by coffinite, (D) subhedral coffinite crystal with inclusion of galena (radiogenic lead?).

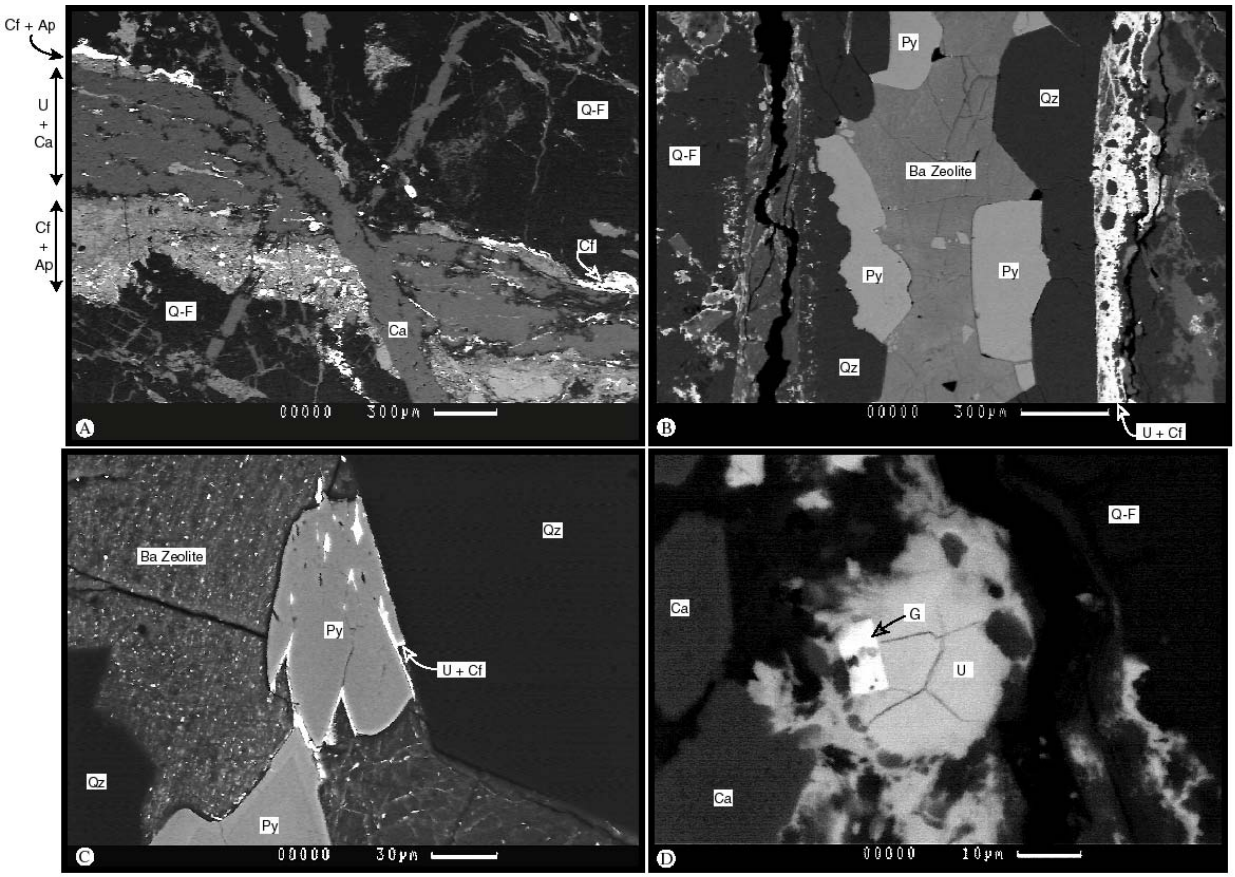

Figure 1-5. Backscatter electron images of the uraninite-calcite and uraninite-zeolite ore assemblages. Abbreviations are Q-F = quartzo-feldspathic host rock, Cf = coffinite, Ap = apatite, Qz = quartz, U = uraninite (intergrown with trace amounts of coffinite), Ca = calcite, Py = pyrite (all phases identified by energy dispersive x-ray spectra): (A) sub-parallel uraninite-calcite and apatite-coffinite filled fractures (U + Ca cross-cuts Cf + Ap) both off-set by barren calcite vein, (B) fine-grained, intergrown uraninite + coffinite precipitated along the margin of a vein filled with euhedral quartz, pyrite and Ba zeolite, (C) rim of intergrown uraninite + coffinite on pyrite within uraninite-zeolite vein, (D) fractured botryoidal uraninite with inclusion of galena (radiogenic lead?) surrounded by calcite.

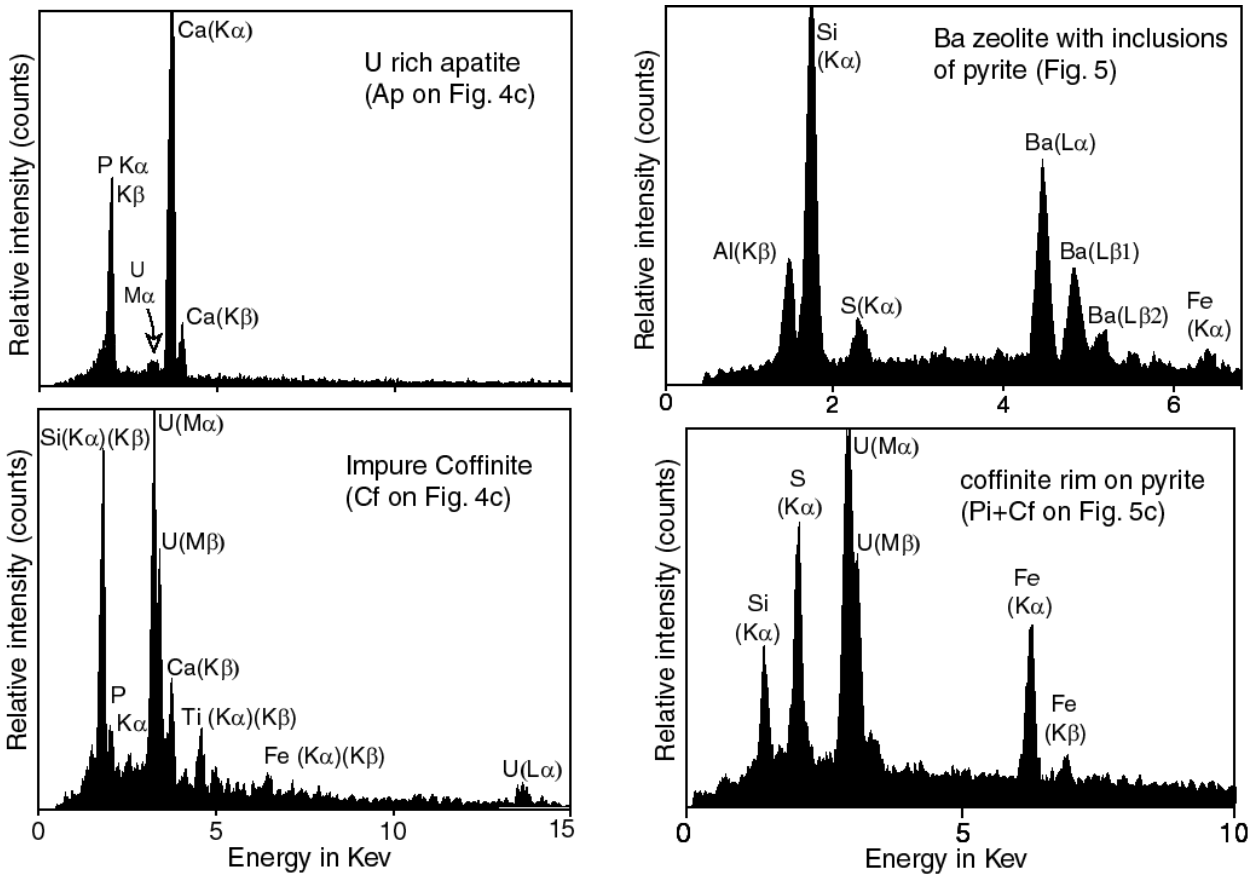

Figure 1-6. Selected energy dispersive x-ray spectra of key phases shown in Figures 4 and 5.

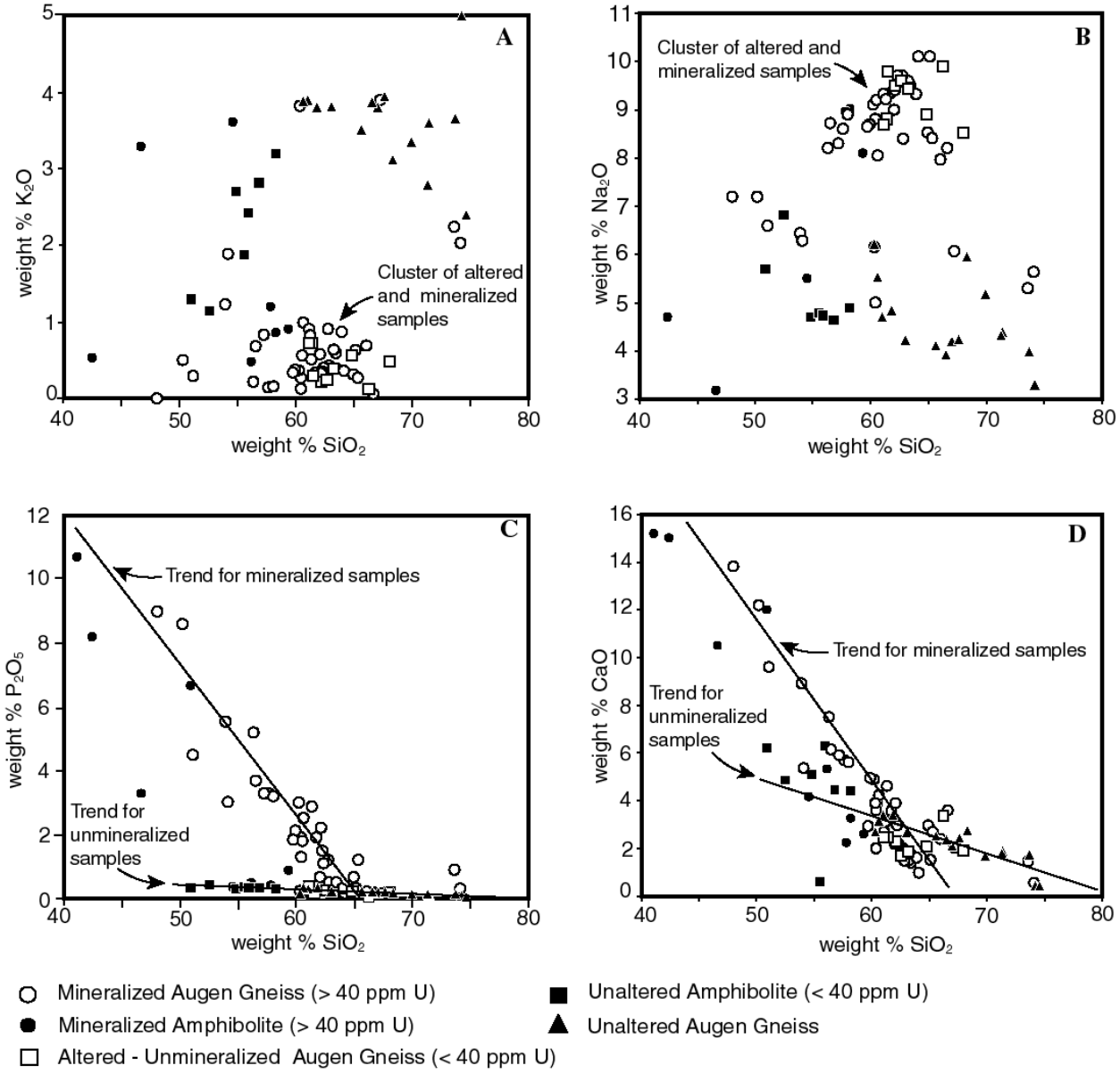

Figure 1-7. Major element whole rock data. (A) K_2O vs SiO_2 showing K depletion in altered and mineralized samples, (B) Na_2O vs SiO_2 showing Na enrichment in altered and mineralized samples, (C) P_2O_5 vs SiO_2 showing trend lines for unaltered augen gneiss ($y = -0.0141x + 1.13$; $R^2 = 0.706$; $n = 16$) and mineralized augen gneiss ($y = -0.474x + 31.1$; $R^2 = 0.885$; $n = 42$), (D) CaO vs SiO_2 showing trend lines for unaltered augen gneiss ($y = -0.158x + 12.9$; $R^2 = 0.786$; $n = 16$) and mineralized augen gneiss ($y = -0.671x + 45.1$; $R^2 = 0.905$; $n = 42$) (Whole rock data from Marline Uranium Corporation, 1983 and R. Ayuso, USGS, personal communication, 2001).

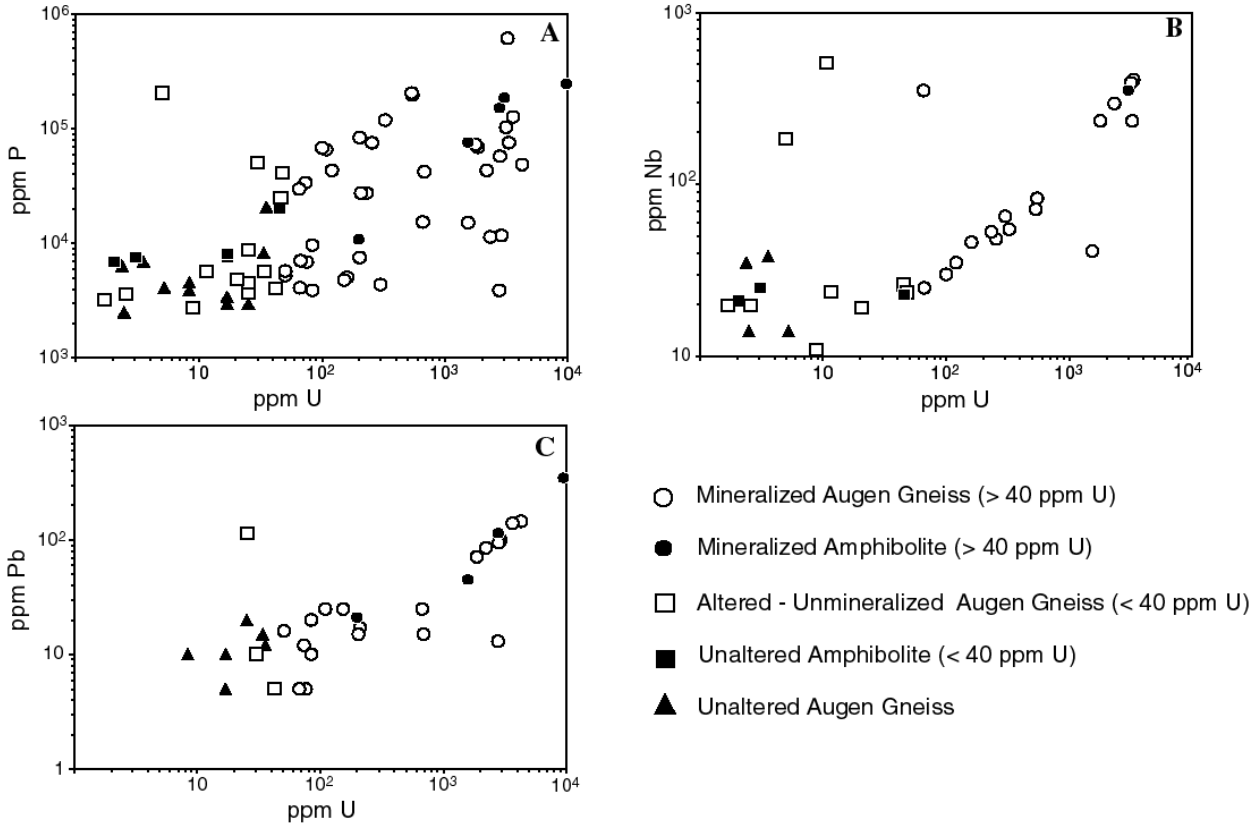

Figure 1-8. Trace element whole rock data. (A) scatter plot showing diffuse but consistent positive correlation between U and P. This correlation reflects the abundance of apatite within the primary ore assemblage. The correlation is diffuse because some U-mineralized samples do not contain apatite (e.g. the pitchblende-coffinite-calcite and pitchblende-coffinite-zeolite ores). (B) Niobium vs uranium for n = 20 mineralized samples showing positive correlation (R^2) = 0.88. The specific Nb bearing phase has not been unequivocally identified; however, textural relations and EDS spectra suggest that it may be contained within the fine-grained Ti oxides associated with the ore assemblages. (C) Lead vs uranium for n = 23 mineralized samples showing strong positive correlation (R^2 = 0.93). This correlation reflects the abundance of 1 - 5 mm diameter galena cubes intergrown with coffinite in high grade U-mineralized samples (Whole rock data from Marline Uranium Corporation, 1983 and R. Ayuso, USGS, personal communication, 2001).

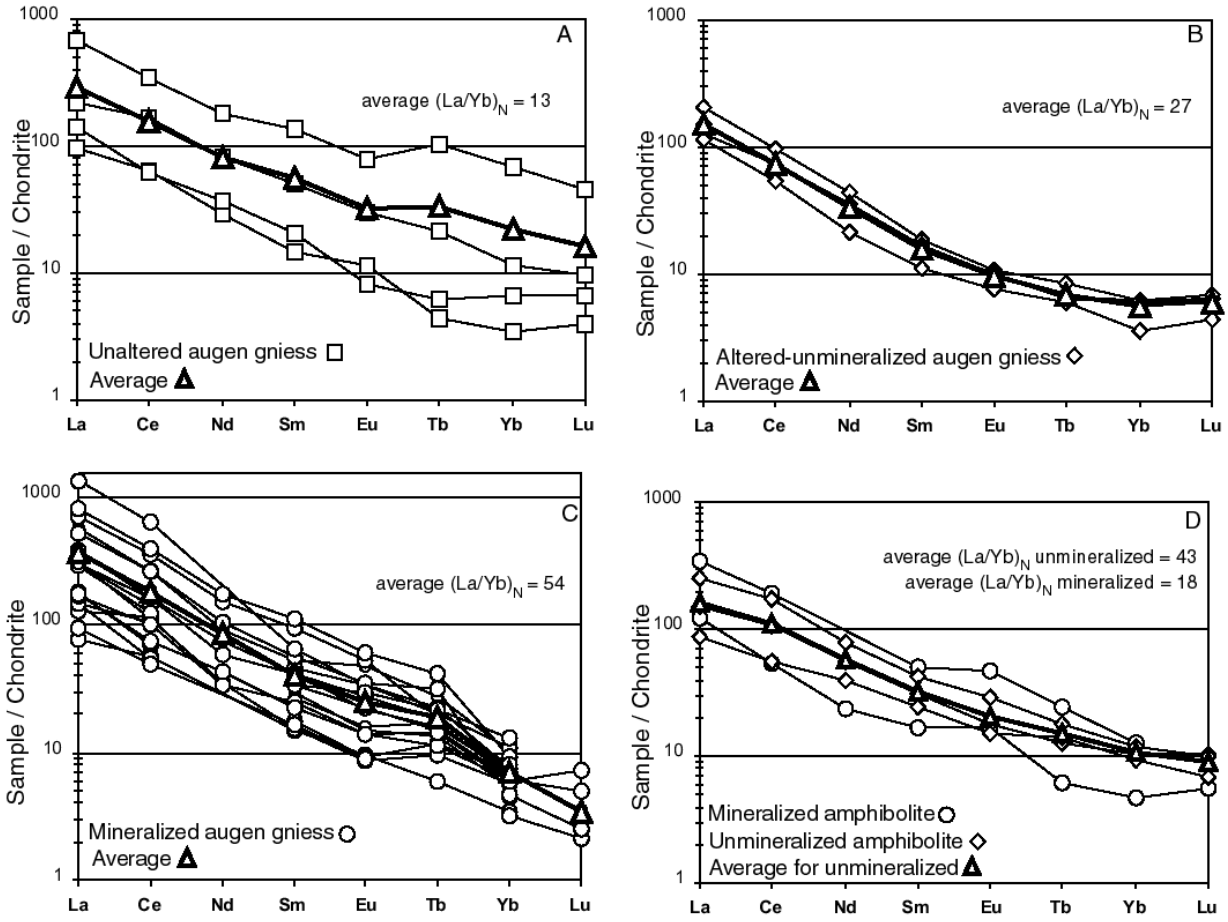

Figure 1-9. Chondrite normalized rare earth element diagrams: (A) unaltered augen gneiss: the range in values for the these samples reflects the lithologic heterogeneity of the host rock, protolith stratigraphy. (B) Altered but unmineralized augen gneiss: these data indicate that alteration events preceding U mineralization did not result in significant enrichment or depletion in rare earth elements. (C) Mineralized augen gneiss: samples containing the coffinite-apatite assemblage show significant enrichments in the light rare earth elements. (D) Mineralized and unmineralized amphibolites: mineralization did not result in significant enrichment in rare earth elements in amphibolite lithologies.

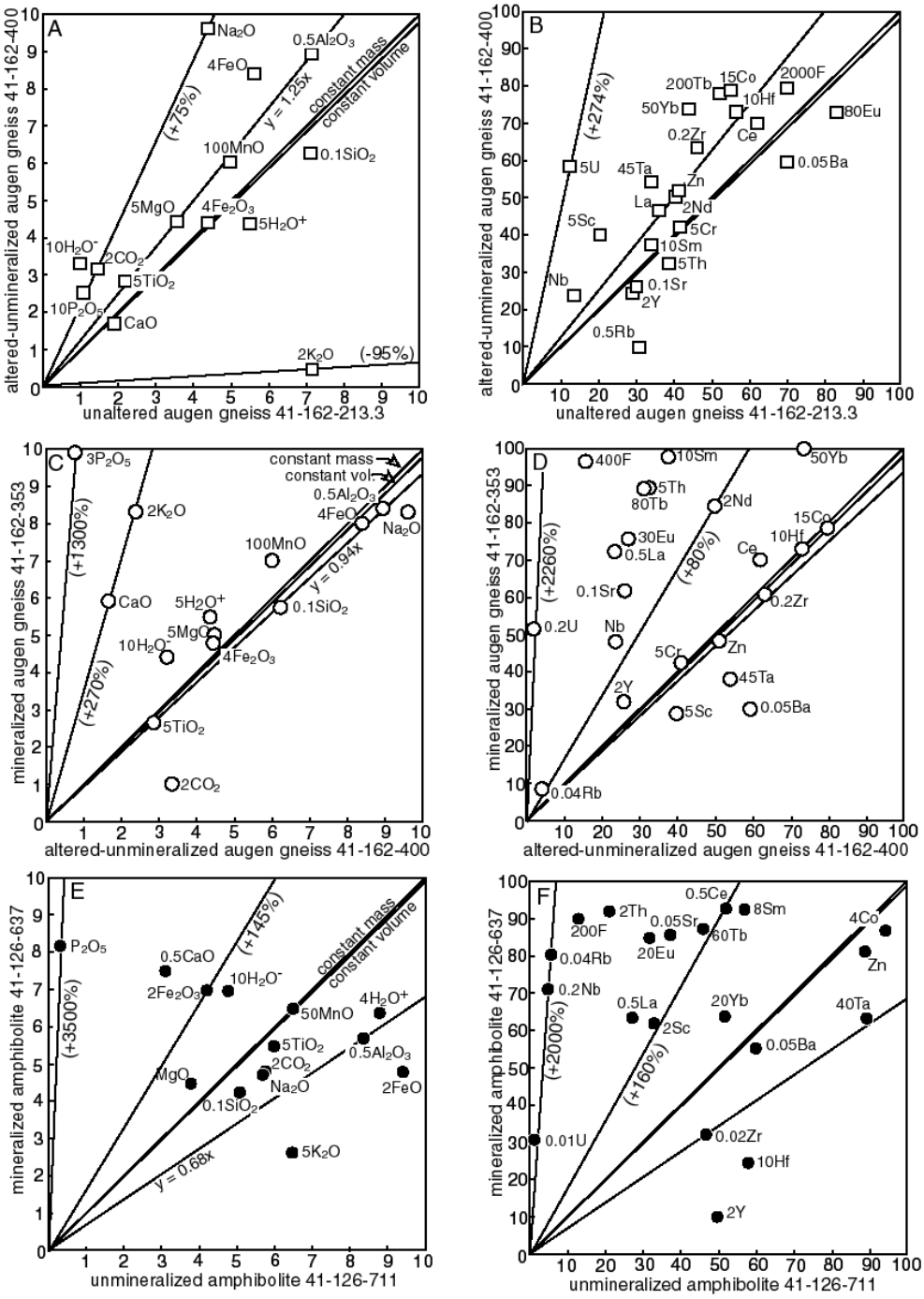

Figure 1-10. Isocon diagrams after the method of Grant, 1986 (concentration values scaled to fit within plot range). (A) Unaltered vs. altered augen gneiss - major elements. The slope to the constant alumina line (y = 1.25x) suggests that the system experienced an approximately 18% loss in volume during alteration; (B) unaltered vs. altered augen gneiss -trace elements; (C) altered vs. mineralized augen gneiss - major elements; (D) altered vs. mineralized augen gneiss - trace elements. The slope to the constant alumina line (y = 0.94x) suggests that the system experienced an approximately 7% gain in volume during alteration; (E) altered vs. mineralized amphibolites - major elements. The slope to the constant alumina line (y = 0.68x) suggests that the system experienced an approximately 48% gain in volume during alteration; (F) altered vs. mineralized augen gneiss - trace elements.

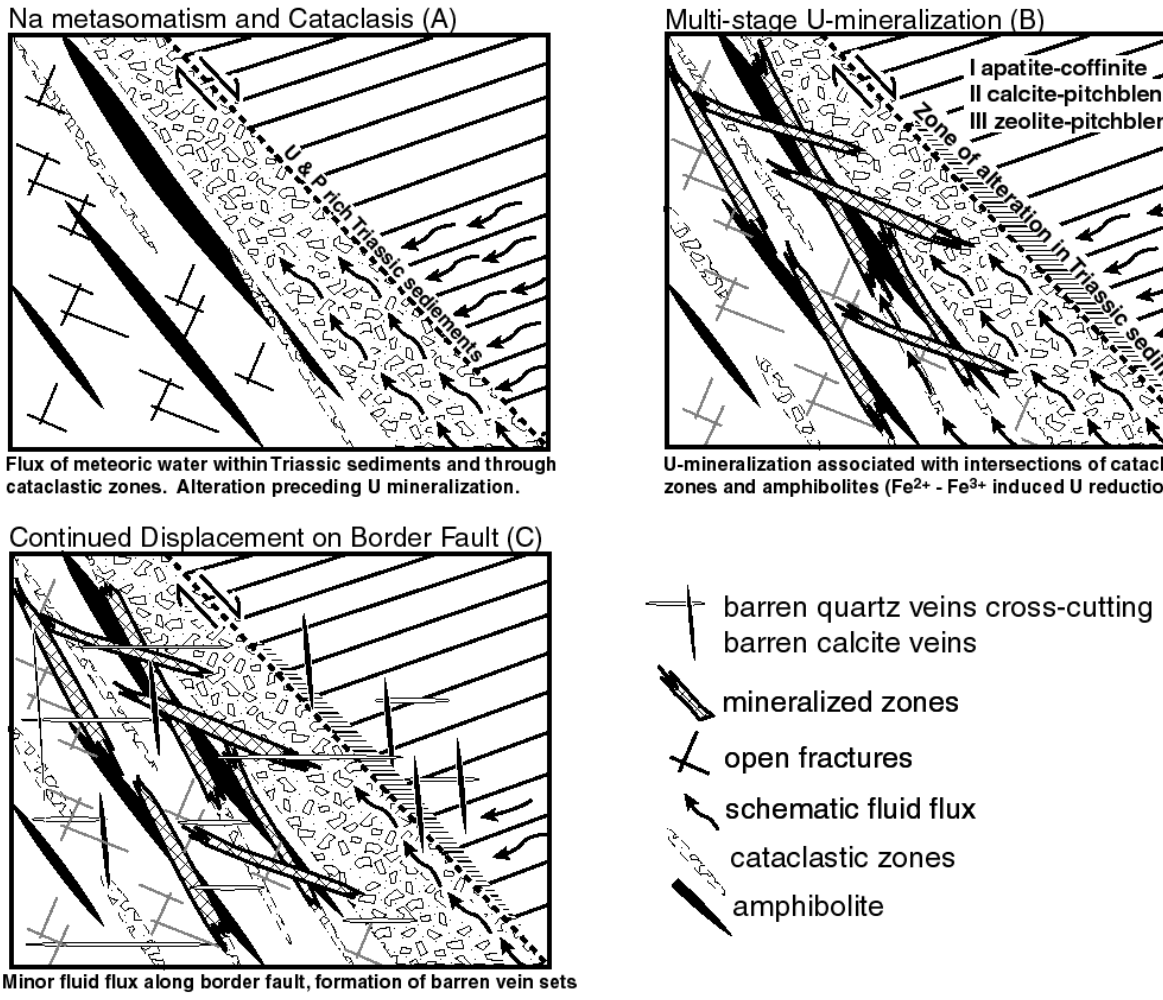

Figure 1-11. Conceptual model for the formation of the Coles Hill uranium deposit. (A) Alteration events preceding U- mineralization are dominated by Na-metasomatism and cataclasis along the Chatham fault zone. (B) In places where cataclastic zones intersect amphibolite Fe released during alteration of mafic minerals reduces the U in hydrothermal solution, thus leading to precipitation of ore assemblages. This is evidenced by the presence of hematitic halos around ore zones and the spatial association between altered amphibolites and U mineral assemblages. The source of U and P needed to produce the apatite-coffinite and other ore assemblages may have been Triassic carbonaceous shales and mudstones of the Cow Branch formation. This unit has been shown to contain organic rich, fossiliferous zones with high background concentrations of both U and P. (C) Uranium ore assemblages are cross-cut by non ore bearing quartz and calcite veins that formed during late stage displacement on the Triassic border fault.

Chapter 2: Uranium Fixation By Phosphate Mineralization During Oxidation and Chemical Weathering of the Coles Hill Uranium Deposit, Virginia

Abstract

The Coles Hill uranium deposit located in south-central Virginia represents an unparalleled natural laboratory for the study of phosphate based mineralogical fixation of uranium within oxidized, chemically weathered quartzo-feldspathic gneisses. Shallow drill core from this site preserve a sharp, continuous ferrous/ferric redox front separating gray, unweathered, uranium ore-bearing bedrock from incipiently weathered core sections that are pervasively coated by iron oxide and oxy-hydroxide minerals. This iron redox front occurs near a major discontinuity in uranium mineralogy with U(IV) assemblages (e.g. coffinite, uraninite) on the reducing side, and U(VI) assemblages (e.g. uranyl phosphates) on the oxidizing side. Uranyl phosphates also occur locally as fracture coatings approximately 1 centimeter below (on reducing side) the ferrous/ferric transition. This 1 centimeter thick interval below iron redox front contains both U(VI) assemblages as well as unaltered, ore-stage (primary) U(IV) assemblages and therefore, represents a uranium redox transition zone.

This discontinuity in uranium mineralogy, however, does not represent a major discontinuity in bulk uranium concentrations with sample groups from both oxidized and reduced sides of the front generally ranging from 500 to 1000 ppm. This observation suggests that the volume of shallow bedrock associated with the Coles Hill uranium deposit has acted as a closed system with respect to uranium mass transport during the oxidation and incipient chemical weathering processes.

The dominant mechanism by which uranium is being fixed during the redox transition is by the precipitation of U(VI) phosphate minerals. These secondary phases, which are of the Ba end member of the meta-autunite group (meta-uranocircite), occur within three texturally distinct mineral assemblages. Petrographic and mineral chemical evidence suggests that these assemblages formed contemporaneously and that the textural and mineralogical differences are a result of localized variations in micro-physical and micro-chemical properties of their host environments. These assemblages occur along ferric oxy-hydroxide stained fracture surfaces and boundaries between weathered primary host-rock minerals. This suggests that the Coles Hill U(VI) phosphate assemblages formed during incipient chemical weathering within the current

hydrologic system. Mineralogical and geochemical data from the Coles Hill site therefore indicate that, given high enough phosphate activity, uranium may be efficiently attenuated by phosphate mineral precipitation within oxidizing, fluid rich natural systems.

Introduction

The mobility of uranium in natural systems is fundamentally influenced by the oxidation potential of its ambient environment. The redox geochemistry of uranium has thus been studied intensively over the past several decades leading to a thorough understanding of the principles influencing uranium solubility in natural chemical systems. This previous work indicates that, in the absence of significant amounts of penta-valent vanadium, arsenic or phosphorous, uranium is soluble in oxidizing environments (e.g. Garrels and Christ, 1959, Langmuir, 1978, Ivanovich and Harmon, 1982). In uranium rich systems such as natural uranium deposits and uranium mill tailings the oxidation process typically involves destabilization of U(IV) minerals such as uraninite (UO_{2+x}) and coffinite ($USiO_4 \bullet nH_2O$) resulting in high concentrations of U(VI) aqueous species. For example, low pH (3.2), high Eh (858 millivolts) waters from the Osamu Utsumi uranium mine in Brazil have dissolved uranium concentrations as high as 10 ppm (Miekeley et al., 1992), is 500 times greater than the proposed US-EPA drinking water standard (Environmental Protection Agency, 1991)

Understanding the solubility of uranium is of critical importance to designing scientifically sound strategies for the remediation and long-term storage of uranium-bearing waste products. Alteration experiments performed on unirradiated UO_2 (analog for commercial spent nuclear fuel) in the absence of dissolved phosphate or vanadate indicate that the secondary U(VI) mineral paragenesis will involve the formation of soluble, metastable uranyl oxide hydrates (e.g. schoepite or dehydrated schoepite) followed by more stable uranyl silicates (e.g. uranophane) (Wronkiewicz et. al., 1992, 1996, Wronkiewicz and Buck, 1999). The secondary mineral sequence observed in these experiments is remarkably similar to the secondary U(VI) paragenesis documented for uraninite oxidation at the Nopal I uranium deposit (natural analogue for the proposed U.S. high-level nuclear waste repository at Yucca Mountain) (Leslie et. al., 1993, Pearcy et. al., 1994). These results thus suggest that in unsaturated, systems characterized by low concentrations of phosphate and vanadate, the solubility of uranium may be controlled by

secondary minerals such as schoepite or dehydrated schoepite initially, and later by the more stable uranyl silicates of the uranophane group.

If dissolved phosphate or vanadate levels are high, however, the solubility of uranium in oxidizing conditions may be minimized by the formation of relatively insoluble U(VI) minerals such as uranyl phosphates (e.g. autunite, log K_{sp} = -44.7; from Langmuir, 1997, Table A13.3) or uranyl vanadates, (e.g. carnotite, log K_{sp} = -56.3; from Langmuir, 1997, Table A13.3). Natural environments in which these low solubility U(VI) minerals form, may thus represent important natural laboratories for studying the natural attenuation of uranium under oxidizing conditions. Such studies may lead to important ideas about the design of new cost effective remediation strategies involving phosphate based soil amendments or reactive barrier systems. An excellent place to study such processes is the Coles Hill uranium deposit (Figure 2-1).

The Coles Hill deposit, located in the Piedmont Province of Virginia, consists of two connected coffinite-uraninite-apatite ore zones (Coles Hill north and south ore bodies; Figure 2-1) hosted in cataclastic zones that cross-cut quartzo-feldspathic augen gneiss. The southern body has been shown to contain approximately 22 million kilograms U_3O_8 with an average grade of 0.113% (958 ppm U) (Halladay, 1989). The north ore body has similar total reserves but at a slightly lower grade (Halladay, 1989). Data collected during exploration of the deposit (e.g. Marline Uranium Corporation, 1983) provides significant geologic and geochemical control on the primary ore zones (see Chapter 1). However, as the deposit was never mined, it represents a pristine geologic and hydrochemical system in which processes influencing the paleo- and present-day transport and retardation of uranium can be studied. This paper focuses on the environmental petrology and geochemistry of the "present-day" U(IV)-U(VI) redox transition zone and its relation to the ferrous/ferric front preserved within north ore zone of the Coles Hill uranium deposit.

Sample Collection and Analysis

For this study, mineralogical and geochemical assessments were performed on three typical core sections from the Coles Hill north orebody (Figure 2-2). Fresh and weathered bedrock samples analyzed were split from diamond bit core sections drilled during exploration of the Coles Hill deposit. Representative slabs were cut from each sample and mounted in epoxy, polished and coated with an approximately 250 angstrom thick film of carbon for analyses by

scanning electron microscope (SEM), energy dispersive x-ray spectrometry (EDS) and electron microprobe (EMP). All SEM, EDS and EMP analyses were performed at the Virginia Tech, Department of Geological Sciences, electron microbeam facilities using a CAM scanII electron microscope and Cameca SX-50 electron microprobe.

Hand specimens of each sample were pulverized using a tungsten carbide shatter box and samples were shipped to an internationally accredited commercial laboratory for major, minor and trace element analyses. Major and minor elements Si, Al, Fe, Mn, Mg, Ca, Na, K, Ti, P and LOI (measure of total volatile content) were analyzed by a lithium metaborate/tetraborate fusion inductively coupled plasma (ICP) technique, while all other elements were analyzed by bulk digestion, inductively coupled plasma mass spectrometry (ICP-MS). It was necessary to process relatively small sample volumes (< 0.5 kg) in order to assess each core section at the centimeter scale. Some variations in bulk concentration data may therefore contain notable geochemical "noise" caused by lithologic heterogeneity of the of the rock profile.

Ground water from the oxidized bedrock zone was sampled at a residential pump from a well that is cased off through the saprolite aquifer. Ground waters from the saprolite aquifer were sampled using polyethylene bailers after purging the well. Dissolved oxygen and pH were measured in situ after allowing the wells to recharge after purging. All samples were filtered (0.45 micron) and samples to be analyzed for uranium and other metals were preserved (acidified to pH < 2.0) using ultra pure nitric acid. Samples were shipped to an internationally accredited commercial laboratory for analyses by ICP-MS (for cations) and ion chromatography (for anions).

Rock-System Characterization of the Iron and Uranium Redox Transitions

In order to provide a geologic context for the mineralogical and geochemical data discussed below we also present results based on general geologic characterizations of field relationships, hand samples and thin sections of the three representative core sections. The Coles Hill primary uranium ore occurs within fractures and cataclastic zones that cross-cut augen gneisses along the northwest margin of the Danville Triassic basin (Figure 2-1). The host rocks consist of albite-quartz-chloritie/biotite-oligoclase-microcline augen gneiss interlayered with albite-chlorite/biotite-reibeckite/hornblende amphibolites (see Chapter 1). The augen gneisses are the most voluminous rock type in the study area and host the majority of the uranium ore.

Unweathered samples of this lithology are light to dark-gray and contain a penetrative foliation defined mostly by oriented chlorite and relict biotite. The foliation is cross-cut by both barren and uranium ore-bearing fracture zones. In shallow core sections (less than approximately 30 meters depth below surface) the ore-bearing, unweathered (gray) host rocks transition abruptly to partially weathered rock that is pervasively "stained" by secondary ferric mineral coatings. This front does not, however, represent a discontinuity in radioactivity, with samples from both above and below the interface ranging from 300 to 500 counts per second (background average: 200 cps).

In hand sample, the oxidized core is mottled dark red and yellow brown with localized centimeter-thick zones of black botryoidal coatings that are identified by SEM-EDS and EMP as micron-scale mixtures of iron and manganese oxides. An example of a hand-sample containing the redox front and associated secondary uranium minerals is shown in Figure 2-3. Petrographic observations indicate that the secondary ferric coatings are pervasive at the micron scale, occurring on fracture surfaces and as 1 to 10 micron thick films along grain boundaries between partially weathered primary minerals (e.g. feldspar, chlorite). Despite these and other indications of incipient weathering (e.g. feldspars to kaolinite), the oxidized samples consist of intact, solid rock that retains primary structures such as the gniessic foliation. The depth to the ferrous/ferric redox front varies with topography, and is located approximately 30 meters below the crest of Coles Hill to less than 20 meters below low lying fields. In areas with a high density of hydraulically active fractures (e.g. near the Triassic border fault, Figure 2-2) the front extends (discontinuously) to depths greater than 50 meters.

Macroscopic examination of the front in ultraviolet light reveals a strongly fluorescent, green to yellow mineral (white in Figure 2-3) that occurs as multi-granular coatings along fracture surfaces and pore spaces. Mineral chemical and XRD data (discussed below) confirm that these fluorescent mineral coatings consist mostly of U(VI) phosphates of the meta-autunite mineral group. This phase occurs predominantly in oxidized (ferric hydroxide stained) samples; however, it is also locally detectable (macroscopically) in fractures approximately 1 centimeter below (reducing side) of the iron staining front. This 1 cm thick interval contains both secondary U(VI) phosphates as well as unaltered primary U(IV) phases that have not yet interacted with the oxygenated ground water. This uranium redox transition zone, thus represents a key interval of centimeter scale redistribution of uranium within this system.

To better understand the processes leading to uranium fixation within the oxidized samples three representative core sections (41-174, depths 24.7 to 30.8 m; 41-173, depths 27.1 to 30.0 m; and 41-172, depths 27.1 to 28.0 m) containing both iron and uranium redox transitions were examined at the micron scale using SEM, EDS and EMP techniques.

Petrography and Mineral Chemistry

Unoxidized, primary uranium Ore

The Coles Hill primary ore contains three distinct U(IV)-mineral assemblages (see Chapter 1). The oldest and most abundant consists of fine-grained (10-20 microns long) fluor-apatite laths surrounded by thin (0.5–5 micron) rims of crypto-crystalline coffinite. Fracture zones that host this assemblage also contain minor amounts of uraninite, subhedral coffinite, chlorite, titanium oxides and accessory sulfides. The apatite-coffinite assemblage is cross-cut by fractures containing coarse-grained calcite, colloform uraninite, minor coffinite and accessory sulfides. These zones are cross-cut by fractures containing massive barium zeolite (harmotome), colloform uraninite, coffinite, pyrite, quartz and titanium oxides. All three primary uranium mineral assemblages are locally cross-cut by barren fracture zones and veins containing barite, quartz or calcite +/- sulfides.

To provide the mineral chemical background needed to interpret secondary mineral paragenesis during oxidation of the primary ore, compositions of typical coffinites from cores 41-174 (28.9 meters depth) and 41-173 (28.6 meters depth) were analyzed by electron microprobe (Table 2-1). These data yield a relatively consistent average composition of 67 weight percent UO_2, 17.5 weight percent SiO_2, 2.2 weight percent CaO, 0.7 weight percent P_2O_5, 0.6 weight percent BaO and 0.3 weight percent PbO. The most variable chemical component within the Coles Hill coffinites is PbO which ranges from below detection limits (less than 0.1 weight percent) to as high as 3 weight percent in intergown coffinite/ uraninite aggregates. This is an important observation as it has been shown by Finch and Ewing (1992) that the amount of radiogenic lead within primary U(IV) minerals strongly influences the paragenesis of secondary U(VI) alteration assemblages. For example, they show that U(VI)-Pb hydroxides may facilitate the growth of U(VI) phosphates by offering preferential nucleation sites (e.g. curite to autunite). However, no uranyl Pb minerals have been identified at the Coles Hill site.

The concentration of P_2O_5, in the Coles Hill coffinites, which also varies significantly (from 0.3 to 4 weight percent), is positively correlated with CaO suggesting that it is associated with inclusions of primary, ore-stage apatite. Another important mineral chemical observation is that the Coles Hill coffinites show consistent BaO concentrations of approximately 3,000 to 7,000 parts per million (BaO detection limit, 800 ppm; analyses by EMP). It is not clear whether Ba resides within the coffinite lattice or as separate sub-micron inclusions, but regardless of its exact chemical form, Ba from this and perhaps other sources (e.g. breakdown of Ba-zeolite, which is not found in the weathered zone overlying the deposit) appears to have played a critical role in the paragenesis of secondary U(VI) phases that form by oxidation of the primary ore.

Secondary uranium mineral assemblages

The U(VI) phosphate that coats fracture surfaces and pore spaces within oxidized ore-bearing core sections has been identified as by XRD, SEM-EDS and EMP as the barium end member of the meta-autunite mineral group (meta-uranocircite, ideal formula: $Ba[(UO_2)(PO_4)]_2 \bullet 6\text{-}8H_2O$ (Gains et. al., 1997)). A representative heavy mineral separate (SG > 3.32) sampled 4 centimeters above the redox front (on oxidizing side) in core 41-174 was examined by XRD and was found to consist mostly of apatite (primary) and meta-uranocircite (secondary) (Figure 2-4; R. Finch, 2001, personal communication).

Electron microprobe analyses of representative grains are shown in Table 2-2. These data indicate that meta-uranocircite forming from the alteration and dissolution of the Coles Hill primary U(IV) minerals is compositionally uniform with average oxide concentrations of 57.7 weight percent UO_3, 15.2 weight percent BaO, and 15 weight percent P_2O_5. Other cations that define autunite/meta-autunite end members (e.g. Ca, Mg, Sr, K, Pb) were analyzed for but were found to be below detection limits (less than 0.1 weight percent). When normalized to ideal water (12 weight percent as H_2O) the composition of meta-uranocircite from the oxidized bedrock of the Coles Hill uranium deposit are very similar to that of synthetic meta-uranocircite II reported by Vochten et. al., (1992).

Petrographic characterization of the Coles Hill meta-uranocircites reveal that they occur in three different textural forms each associated with a distinct mineral assemblage. No compositional difference was detected in crystals of different textural forms (Table 2-2). The relative ages of these assemblages are equivocal due to the lack of cross-cutting relationships.

Similarities in compositions and the lack of cross-cutting relations suggest that the different meta-uranocircite textural types formed during the same event (e.g. oxidation of primary U(IV) ore by oxygenated ground waters) and that the textural differences reflect differences in micro-physical and micro-chemical environments in which they formed. For clarity throughout the textural descriptions the distinct meta-uranocircite forms are designated type I, II, and III (designations do not imply relative age relationships).

Type I: meta-uranocircite - barium, calcium, manganese oxide assemblage:

The most conspicuous form (type I) occurs as concentrations of 0.5 – 2 millimeter long, tabular, euhedral crystals found on the surfaces of 0.5 – 5 millimeter wide open fractures. The type I meta-uranocircites are intimately associated with calcium-barium manganese oxides (Figure 2-5) and euhedral quartz crystals. The manganese minerals form 10 – 30 micron wide, botryoidal aggregates that commonly occur in dendritic growth patterns within the plane of the [001] surface of the meta-uranocircite. The intimate intergrowth of the meta-uranocircite crystals with these manganese oxides (Figure 2-5) suggests that they are part of the same assemblage.

The composition of the manganese minerals associated with the type I meta-uranocircite are variable. All EDS spectra of these grains show both calcium and barium (in varying proportions) in addition to the dominant manganese peak. Some of these spectra also contain distinct peaks of lead, iron and uranium suggesting that these manganese aggregates represent locally important sinks for these elements within this system.

Type II: meta-uranocircite – lanthanide phosphate assemblage

The type II meta-uranocircites occur as scaly aggregates of randomly oriented 10 – 50 micron long, euhedral to subhedral crystals coating surfaces of 50 – 100 micron wide fractures (Figure 2-6). As shown in Table 2-2 the type II and type I meta-uranocircites are compositionally indistinguishable. The difference between these two assemblages is that the type II crystals are not associated with manganese minerals but are intergrown with a secondary calcium, uranium, and lead bearing lanthanide phosphate. This mineral occurs in randomly

oriented masses of subhedral to euhedral prismatic crystals that are less than a micron wide and approximately 5 microns long (rhabdophane?).

These lanthanide phosphate micro-crystals occur with the type II meta-uranocircite aggregates, as coatings along open fractures within oxidized, apatite-rich, primary uranium ore zones. Locally the lanthanide phosphate occurs as coatings that precipitated on a substrate of randomly oriented, type II meta-uranocircite, while in other places the type II meta-uranocircite cross-cuts the lanthanide phosphate. These textural observations thus suggest that these two phases formed contemporaneously within the same assemblage. The coatings and pore fillings of lanthanide phosphate are closely associated with apatite rich primary ore zones suggesting a genetic relationship between the lanthanide phosphate and micro-chemical environments dominated by apatite (primary).

Typical EMP analyses, and EDS spectra of this lanthanide mineral are shown in Table 2-3 and Figure 2-6 respectively. These data indicate that this phase has an average composition of 28.4 weight percent P_2O_5, 20 weight percent La_2O_3, 17 weight percent Ce_2O_3, 4.7 weight percent Pr_2O_3, 7.5 weight percent Nd_2O_3, 5.3 weight percent CaO, 2.7 weight percent UO_3 and 2 weight percent PbO (Ba and Yb were below detection limits of approximately 0.1 weight percent, other rare earth elements were not analyzed for). These chemical data indicate that this mineral represents another locally important sink for uranium within the Coles Hill system.

Type III: monomineralic meta-uranocircite in grain-boundary fractures

Type III meta-uranocircite occur as anhedral fillings within 1 to 10 micron wide regions between partially weathered primary minerals and within 10 to 50 micron wide pore spaces (Figure 2-7). This uranyl phosphate form is observed most commonly at boundaries between albite-quartz, and albite-albite boundaries, but also occurs between quartz-quartz and quartz/albite-chlorite boundaries.

The Type III form is also pervasive within ore-stage apatite filled fractures in samples from above the ferrous/ferric redox front (oxidized samples). In these apatite dominated micro-environments the meta-uranocircite occurs as 5 – 10 micron thick rims surrounding fine grained fluor-apatite laths (Figure 2-8). These rims are composed of mono-mineralic, cryptocrystalline meta-uranocircite; however, locally 1 – 5 micron wide grains showing the [001] mineral cleavage are observed. Electron microprobe imaging (e.g. Figure 2-8) indicates that even

directly adjacent to the apatite laths the meta-uranocircite shows negligible counts of calcium. The thickness and textural style of the rims of meta-uranocircite on the primary ore-stage apatites are nearly identical to the rims of coffinite that occur around these grains within the unoxidized primary ore. This suggests that the type III meta-uranocircite within these zones may have formed by replacement of coffinite where the oxidizing fluids infiltrated grain-boundaries within the primary ore. This implies that the redistribution of uranium during oxidation was on the order of millimeters to microns (scale of uranium transport). The textural and mineralogical associations of all three secondary U(VI) phosphate assemblages are summarized in Figure 2-9.

Major, Minor and Trace Element Geochemistry Across Ferrous/Ferric Front

Whole rock samples from above and below the redox front have similar major element compositions (Table 2-4). For example the unoxidized sample group has an average (n = 8) composition of: 8.4 weight percent Na_2O, 64 weight percent SiO_2, 0.1 weight percent K_2O, 2.5 weight percent Fe_2O_3, and 1.9 weight percent LOI (estimate of total volatiles); while the oxidized sample group has an average (n = 7) composition of: 8.0 weight percent Na_2O, 66.5 weight percent SiO_2, 0.2 weight percent K_2O, 2.3 weight percent Fe_2O_3, and 2 weight percent LOI. The low concentrations of K_2O (consistently less than 1 weight percent) relative to Na_2O, for both sample groups, reflect sodium metasomatism associated with primary uranium mineralization (see Chapter 1). Sample DH173-28 (see Table 2-4) was excluded from the average of the oxidized samples because it contains an unusually large amount of fracture hosted meta-uranocircite. This sample is important, however, because it represents a geochemical signature dominated by the U(VI) mineral assemblages.

To assess the enrichment or depletion of elements within the three redox fronts average concentrations of selected major and trace elements in oxidized samples were normalized to averages for corresponding unoxidized samples (Figure 2-10). Therefore, elements plotting above unity in Figure 2-10 are enriched in the oxidized samples for that core and elements below unity are depleted. The irregular and inconsistent pattern in this plot reflects the inherent lithologic heterogeneity of each rock profile. Given this heterogeneity, most elements show no evidence for enrichment or depletion during the oxidation process. The only potential exceptions are Mg, which shows minor but consistent depletion in oxidized samples, and Ba which is consistently enriched (also to a minor extent) in oxidized samples (discussed below).

These results also suggest that there has been no major bulk mass or volume change across the redox front. This is based on the observation that elements shown to behave in a conservative manner during chemical weathering (e.g. Ti, Zr, Al) (Krauskopf, 1967, Nesbitt and Wilson, 1992) show no consistent variation from unity across the redox front. To further understand the geochemical trends associated with the redistribution of uranium within this environment, uranium and other key element concentrations were plotted as a function of depth for each core section (Figure 2-11).

Uranium concentration profiles across the ferrous/ferric front

In unoxidized samples uranium content varies from 138 to 1030 ppm with an average of 565 ppm, while the oxidized samples range from 305 to 3070 ppm with an average of 575 ppm (excluding the unusually uranium rich sample, DH173-28, from average). Uranium concentrations show significant variations within individual depth profiles (Figure 2-11); however, these variations are not systematically related to the location of the redox front. This result coupled with petrographic observations indicates that the variations in uranium reflect spatial heterogeneity of both primary and secondary uranium bearing assemblages. For example, sample DH173-28 which was sampled from approximately 15 centimeters above the redox front (oxidized side) in core 173, contains over 3000 ppm U and is characterized by a localized abundance of fractures coated with the secondary U(VI) phosphate assemblages. This sample thus reflects a geochemical signature strongly influenced by meta-uranocircite mineral chemistry.

On average uranium is not being significantly depleted or enriched across the Coles Hill oxidation fronts. This suggests that uranium is not being removed from the rock system during oxidation of the primary ore. Furthermore, the observation that meta-uranocircite commonly occurs between primary apatite grains in regions previously occupied by coffinite suggests that, at least locally the length scale of uranium redistribution may be on the order of millimeters (e.g. replacement of coffinite by meta-uranocircite in primary apatite-coffinite ore zones).

Sodium, potassium, and aluminum concentration profiles across the ferrous/ferric front

Potassium does not show systematic variation with depth in these cores; however, it does show significant enrichment (increases from 0.1 to 0.6 weight percent K_2O) in the uranium rich, oxidized sample 174-28. This sample also contains an unusually high concentration of Rb (33.5 ppm relative to 11 ppm average for oxidized samples). Although K was not detected in the meta-uranocircite samples analyzed by electron microprobe (detection limit approximately 0.1 weight percent) the whole rock observations suggest that the secondary U(VI) phosphates, (pervasive in sample 174-28) may contain K and Rb substitutions.

Concentrations of Al and Na in these rocks are controlled by albite abundance (the most common mineral in the host rocks) and they remain relatively uniform across the three core sections (excluding sample 174-28). These data suggest that, although some albite grains have undergone incipient chemical weathering to form kaolinite near the redox front, this process has not caused significant depletions in Na within the profiles.

Magnesium, barium, calcium and phosphorus concentration profiles across ferrous/ferric front

Concentrations of Mg decreases from greater than 0.6 weight percent MgO below the front to less than 0.4 weight percent MgO above the front in core 174. This trend is also evident in core 173 near the redox front and may reflect the incipient destruction of primary biotite and chlorite (the major sinks for Mg in reduced samples) and subsequent removal of Mg by ground waters (Mg not retained by secondary mineralization in oxidizing zone).

The average barium concentrations for the two sample groups are: 422 ppm for unoxidized samples and 974 ppm for oxidized samples (excluding sample 173-28). This enrichment in Ba above the redox front is most dramatic in core 174 where the concentration varies from 200 ppm below the front to values ranging from 450 to 1500 ppm in oxidized samples. This trend may be explained by the precipitation of the Ba U(VI) phosphate minerals and associated secondary barite which are pervasive as fracture coatings on the oxidized sections of core. The Ba enrichment trend is not as clearly defined in core 173, possibly due to a higher percentage of the hydrothermal barite and Ba-zeolite below the redox front.

The concentration profiles of Ca and P show more significant variations than other key elements. For example, P_2O_5 ranges from 1.1 to 8.5 weight percent in unoxidized samples and 1

to 4 weight percent in oxidized samples. Correspondingly, CaO varies from 1 to 11.8 weight percent in unoxidized samples and 1 to 5.7 in oxidized samples. As shown in the depth profiles, CaO varies in direct proportion to P_2O_5 in both oxidized and unoxidized samples. This strongly suggests that spatial variations in the amount of the primary ore-stage apatite assemblage controls the concentrations of these elements in these cores. The minor decoupling of the CaO, and P_2O_5 profiles in core 174 (particularly at 29 m depth) suggests that higher proportions of the non-apatite bearing primary ore assemblages are present in this section (e.g. uraninite -zeolite-sulfides, uraninite -calcite-sulfides).

Iron and titanium concentration profiles across the ferrous/ferric front

The iron concentration profiles show variations from 0.5 to 3.0 weight percent Fe_2O_3. These variations, however, are not systematically related to the location of the redox front, suggesting that they reflect spatial heterogeneity of primary iron minerals in the reduced samples (e.g. chlorite, biotite) and fracture coating ferric oxy-hydroxides in the oxidized samples. In contrast, titanium remains relatively constant across the redox front, suggesting a more uniform dissemination of primary Ti minerals (e.g. titanite, rutile) in these cores. This observation further supports our interpretation that the oxidation process did not result in substantial bulk mass or volume loss or gain (assuming Ti is conserved during chemical weathering; Krauskopf, 1967, Nesbitt and Wilson, 1992). This idea is also supported by the relative constant concentration profiles of other relatively immobile elements such as Al and Zr (not shown: see Table 2-4.).

Variations in chondrite normalized lanthanide elements across the ferrous/ferric front

Chondrite normalized lanthanide patterns for oxidized and reduced samples are shown in Figure 2-12. The patterns for the two sample groups are similar overall suggesting that there has not been significant fractionation of the lanthanides during the oxidation process. The reduced samples, however, do show more variation in ratios of light to heavy elements relative to oxidized samples. These variations may reflect the spatial variations in the volume percent of the primary coffinite-apatite assemblage. This explanation is supported by the observation that depth profiles of $(La/Yb)_N$ ratios (Figure 2-11) are parallel to both the CaO and P_2O_5 within theses core sections.

Uranium Mineral Stability and Aqueous Speciation

The chemistry of filtered (0.45 microns) ground waters from the shallow bedrock (oxidized zone) and overlying saprolite associated with the Coles Hill north orebody are shown in Table 2-5. The most important observation of the ground water investigation is that all filtered samples from the Coles Hill north orebody contain less than 15 parts per billion dissolved uranium (lower than the proposed EPA (1991) drinking water standard of 20 parts per billion). This suggests that the secondary phosphate minerals forming within the oxidized uranium ore zone are effective at immobilizing uranium within the present-day hydrologic system. To futher investigate this uranium fixation process ground water data have been used to assess both the solid and aqueous speciation of uranium for this system.

There is limited data from the specific depths under consideration; therefore, certain parameters (e.g. bicarbonate, nitrate and sulfate) were estimated using data collected by the Marline Uranium Corporation (1983) as part of an environmental baseline study of the deposit region. Sample DH2-10/12/00, which is from the saprolite aquifer overlying the north orebody, is also used in this analyses because it has been shown that, based on vertical hydraulic head relationships (Marline Corporation, 1983) saprolite ground waters recharge the bedrock aquifer. Thus, the DH2 sample is also representative of oxygenated water (up to 8 parts per million dissolved oxygen) that interacts with the primary ore near the ferrous/ferric redox front.

For mineral stability assessments the activities of ions in solution were calculated using the "Geochemists Workbench" software package (Bethke, 1998) which employs an extended form of the Debye-Huckle equation (Helgeson, 1969). Solubility data for meta-uranocircite, coffinite, uranophane, and schoepite are from Vochten et. al., (1992), Hemingway (1982), Nguyen, et. al., (1992), Grenthe et. al., (1992) respectively. Fluor-apatite and hydroxy-apatite solubility data are from Woods and Garrels (1987). Solubility data used for autunite (Ca end member) and H-autunite are from Muto, (1965) and Grenthe et. al., (1992) respectively and the data for saleeite (Mg-autunite), Na-autunite, and K-autunite is from Magalhaes et. al., (1985). Stability data for all aqueous species is from Grenthe et. al., 1992.

The Eh-pH stability field of the Ba-U(VI) phosphate found at Coles Hill is shown in Figure 2-13a. The estimated reaction path required to produce the observed assemblages is also shown. It implies that, given a pH range of 6-7 (measured in shallow ground waters from Coles

Hill), the transition from coffinite to meta-uranocircite occurs at an Eh of approximately 100 millivolts. At this pH the coffinite/meta-uranocirite boundary corresponds closely with the boundary between Fe(II) and Fe(III) (Fe^{2+} - $Fe(OH)_3$ transition). These Eh-pH estimates are thus in accord with the field observation that, in drill core form the Coles Hill deposit the ferrous/ferric front and uranous/uranyl transition zone are spatially associated (separated by approximately one centimeter). This estimate is also supported by the observation that the lanthanide phosphate associated with meta-uranocircite type II is depleted in cerium which could reflect the fact that the fluid from which this mineral formed was oxidizing enough for cerium to be fractionated from the other rare earth elements by CeO_2 precipitation. For the pH range at Coles Hill (6 - 7) the Ce^{3+}/CeO_2 transition is approximately 200 millivolts (Brookins, 1987).

Although Eh has not been directly measured for the Coles Hill fluids, values can be estimated by comparing the Coles Hill saprolite ground waters (e.g.sample DH2-10/12/00, Table 2-5) with similar weathered zone ground waters from the Morro do Ferro natural analogue site in Brazil (Nordstrom et. al, 1992). Ground waters from both Coles Hill and the Brazilian site have field pH values around 6.0 and dissolved oxygen values ranging from 4 – 8 ppm. For the Morro do Ferro samples the dissolved oxygen concentrations (4.3 – 8.5 ppm) correspond to Eh values of 504 – 525 millivolts (respectively) (Nordstrom et. al, 1992). It is thus estimated that ground waters from the Coles Hill weathered zone may have Eh values of a similar range (500 – 530 millivolts). Furthermore, the association of type I meta-uranocircite with manganese oxides implies that the Eh for this assemblage may have been as high as 700 millivolts indicating that the redox gradient preserved in these rocks involved highly oxidizing conditions.

In addition to the master variables Eh and pH, uranium speciation in this type of system is fundamentally influenced by the relative amounts of dissolved phosphate and carbonate. This is illustrated by plotting uranium speciation on a diagram of the log activity ratio $[(PO_4)^{2-}_{(total)}/HCO_3^-{}_{(total)}]$ vs pH (Figure 2-13b). This plot suggests that for a system with a uranium activity of $10^{-7.3}$ (representative of Coles Hill north orebody ground water) the lower stability limit of the observed U(VI) phosphate will range from a phosphate/carbonate activity ratio of approximately $10^{-4.0}$ at pH 5 to approximately $10^{-2..3}$ at pH 8. At ratios below this limit uranium is predicted to enter solution as a uranyl carbonate complex.

To better understand the secondary mineral stability and speciation within this system mineral saturation indices (SI = $\log_{10}$[ion activity product/solubility product of mineral]) and

fluid speciation were calculated from representative ground waters (Table 2-5) and plotted as a function of pH (Figure 14). Figure 2-14a shows that for the pH range of interest (6 – 7) Coles Hill shallow bedrock ground water is supersaturated with respect to meta-uranocircite (maximum SI = 3.0). Over this pH range the solution is undersaturated with respect to other important U(VI) phosphates. Of these, autunite (Ca endmember) is the least undersaturated (SI of approximately –0.8) while others such as chernikovite (H-autunite), saleeite (Mg-autunite), torbernite (Cu autunite), Na-autunite and K-autunite all have saturation indicies less than –2.0. Other important U(VI) phases such as schoepite and uranophane are also undersaturated within the Coles Hill ground water (SI = -2.0 and –3.0 respectively). This speciation model does however, predict that at pH > 7.8 the solution would be saturated with respect to uranophane, but waters of this type have not been recognized in the study area nor has uranophane been identified.

Figure 2-14b shows the aqueous uranium speciation for the shallow bedrock ground water from the Coles Hill north orebody. It indicates that major species at low pH would be UO_2^{2+} and to a lesser extent UO_2F^+. In the pH field of interest (6 – 7) however, the dominant species are $UO_2HPO_4^o(aq)$ and $UO_2CO_3^o(aq)$ with $UO_2(CO_3)^{2-}$ becoming dominant at pH > 6.5 (species stability constants form Grenthe, 1992). This diagram reiterates the observation that higher bicarbonate and pH values favor the formation of stable uranyl carbonate complexs which may facilitate the aqueous transport of relatively high concentrations of uranium.

Figure 2-14a also shows that this ground water is supersaturated with respect to fluor-apatite at pH > 5 and with respect to hydroxy-apatite at pH >6.5. To further investigate the role that apatite could play in influencing the formation of secondary U(VI) phosphates the speciation model discussed above was run again using different input constraints. For this second speciation calculation, instead of using measured dissolved phosphate levels for the ground water, phosphate concentrations were buffered by fluor-apatite as an infinite reactive solid. This model predicts that phosphate in solution would vary from approximately 200 ppb at pH = 5.0 to approximately 5 ppb at pH = 6.0 (assuming 17.1 ppm Ca^{2+} and 170 ppb F^- and using fluor-apatite solubility data from Woods and Garrels (1987)). Furthermore, this model predicts that the decrease in dissolved phosphate with increasing pH would cause the Coles Hill shallow bedrock ground water to become undersaturated with respect meta-uranocircite at a pH of approximately 5.7 (Figure 2-15). This prediction is, therefore, inaccurate as it does not agree with field observations that meta-uranocircite is forming from ground waters of pH = 6.0 within the

oxidized bedrock zone of the Coles Hill site and that no overgrowths or new (secondary) fluor-apatite crystals have been detected within this region. This suggests that the precipitation and growth of fluor-apatite is inhibited within this system. This inhibition of apatite growth may play an important role in the secondary U(VI) phosphate mineralization process as it allows for dissolved phosphate levels to remain high enough to saturate the solution with respect to the observed phase (meta-uranocircite).

Discussion

The sharpness of the redox front in the Coles Hill cores suggests that the reactions leading to their formation (e.g. oxidation of primary U(IV) and Fe(II) minerals) are occurring at rates that are fast relative to the transport rates of the reacting species (e.g. Levenspiel, 1972 and Romero, et. al., 1992). This interpretation is supported by the results of batch experiments showing that the transformation of primary ore from the Coles Hill deposit to U(VI) phosphate bearing assemblages can be achieved in less than forty days (Jerden and Sinha, 2001). The transition from the primary U(IV) assemblage to the meta-uranocircite assemblages may be modeled as:

$$\textbf{Coffinite} + H_2PO_4^- + 0.5\ Ba^{2+} + 0.5\ O_2(aq) + nH2O \rightarrow 0.5\ \textbf{Meta-uranocircite} + SiO_2(aq) \quad (1)$$

Rewritten in terms of grams this transition is:

$$\textbf{1g Coffinite} + 0.3g\ H_2PO_4^- + 0.2g\ Ba^{2+} + 0.05g\ O_2(aq) + nH2O \rightarrow 1.5g\ \textbf{Meta-uranocircite} + 0.2g\ SiO_2(aq) \quad (2)$$

Possible sources of phosphate needed for this reaction are primary ore-stage fluor-apatite and potentially the coffinite grains, which consistently contain over 5000 ppm P_2O_5 (present in lattice or as inclusions). The release of phosphate from the primary ore zones can be expressed by the generalized chemical reaction:

$$\textbf{Fluor-apatite} + 6H^+ \rightarrow 5Ca^{2+} + 3H_2PO_4^- + F^- \quad (3)$$

The most important source of barium within this system may be the Ba-zeolite (Harmotome) associated with the primary ore. The release of barium from the primary ore zones

can thus be expressed by the generalized chemical reaction (assuming aluminum released will be incorporated into kaolinite):

$$\text{Harmotome} + 2H^+ \rightarrow 5H_2O + Ba^{2+} + \text{Kaolinite} + 4SiO_2(aq) \quad (4)$$

Another potentially important source of barium in this system is the primary coffinite, which is shown by EMP analyses to consistently contain over 3000 ppm BaO (Table 2-1). Another interpretation is that the barium was not derived locally but was transported to the Coles Hill site by ground water (some local ground waters contain up to 800 ppb dissolved Ba; Marline Corporation, 1983).

Redox front formation and migration

The Coles Hill ferrous/ferric redox front appears to have formed by processes similar to those invoked to explain the formation of redox fronts exposed within the Osamu Utusmi uranium mine, Brazil (studied as part of the Pocos de Caldas natural analogue project). The Pocos de Caldas study (e.g. Romero et. al., 1992) showed that the iron redox fronts exposed within the shallow host rocks of the uranium deposit formed as oxygenated meteoric waters (containing approximately 10 mg/L dissolved O_2 at 20^{o}C) infiltrated through the soil/saprolite profile and were channeled along conductive fracture zones. The oxygen front propagates laterally away from the conductive fracture as O_2 is transported by molecular diffusion (e.g. concentration gradient driven transport) into the rock matrix along micro-fractures and grain boundaries. This process, which results in the formation of fracture parallel, redox "fingers" (e.g. Romero et. al., 1992), was found to be the major driving force in uranium migration at the site, with primary uraninite being rapidly dissolved at the oxygen front and reprecipitated on the unoxidized portion of the front.

The formation and propagation of the redox front studied as part of the Pocos de Caldas study is similar to the one at the Coles Hill site. However, the mechanisms of uranium redistribution at the two sites are distinctly different. This is illustrated by the observation that, at the Coles Hill site, uranium is being retained within the oxidized zone by the precipitation of U(VI) phosphates rather than forming secondary uraninite.

At Coles Hill, the mineral reactions occurring near the ferrous/ferric front (e.g. precipitation of Mn oxides and ferric oxides and oxy-hydroxides) indicate that primary minerals

are interacting with oxic fluids (Eh > 200 millivolts). To preserve the oxygenated nature of the waters that have moved through an approximately 15 m thick zone of soil and weathered rock without becoming anoxic, we suggest two possibilities: (1) localized "fast flow zones" allowing rapid infiltration of meteoric waters with minimal interaction with chemical reductants (e.g. organic matter), (2) low abundance of reductants (e.g. organic matter) within the soil/saprolite column. Hydrologic studies performed during exploration of the Coles Hill deposit show that within the study area ground waters from the saprolite aquifer are flowing down into the oxidized bedrock zone (Marline Corporation, 1983). Ground waters within this saprolite aquifer contain 4 – 8 ppm dissolved oxygen (Jerden and Sinha, 2001). These values are similar to those measured for shallow ground waters at the Morro do Ferro analogue site in Brazil (4.3 – 8.5 ppm) (Nordstrom, et al, 1992).

The probability of rapid infiltration through the soil/saprolite column is supported by the observation that localized regions within the Coles Hill weathered zone have high matrix and/or fracture permeability. These permeable zones have measured hydraulic conductivities (measured by packer tests) that can range to values as high as 40 cm/day (Marline Uranium Corporation, 1983). Similar hydraulic conductivities (around 20 cm/day) were measured for fractured rock associated with the iron redox fronts at the Osamu Utsumi mine (Pocos De Caldas study; Holmes et al., 1992).

Another important difference between the processes leading to the formation of the iron redox fronts studied as part of the Pocos de Caldas project and those at Coles Hill is that the former result from the dissolution of pyrite, while the major source of ferric iron at Coles Hill is the weathering of chlorite (weathering of accessory pyrite and biotite play a minor role). In this way the Coles Hill weathering profile is similar to that formed over the Koongara uranium deposit (north-central Australia) which was studied as part of the Alligator Rivers Natural Analogue Project. At Koongara the iron staining is shown to form through ferric hydroxide precipitated as a reaction product during the alteration of chlorite to vermiculite. Using generalized formulas for the minerals involved, this reaction can be written as:

Iron-rich Chlorite $[(Fe_3, Mg_2, Al_1)(Al_1Si_3)O_{10}(OH)_8] + 2H^+ + 5H_2O + nO_2(aq) \rightarrow$ **(5)**
Ferric coating $[2Fe(OH)_3]$ + Vermiculite $[(Fe_1, Mg_1, Al_1)(Al_1Si_3)O_{10}(OH)_2] + Mg^{2+}$.

The importance of this type of reaction as a source of iron for the ferric mineral coatings at the Coles Hill site is supported by petrographic and SEM-EDS data showing that the primary chlorite alters to ferric hydroxides and a (Fe,Mg)-bearing clay mineral (vermiculite?), as well as XRD data showing that overlying saprolites contain up to 20% (clay fraction) hydroxy interlayered vermiculite (Zelazny, 2000 personal communication).

The rate of iron redox front propagation within the Coles Hill profile is therefore dominantly influenced by the rate of chlorite weathering (e.g. Reaction 4). The propagation of the zone containing the secondary U(VI) minerals, however, is determined by the kinetics of weathering of the coffinite-apatite ore zones (e.g. Reactions 1 and 3). This may explain why the U(VI) phosphate assemblages locally occur in fractures approximately 1 centimeter below (on unoxidized side of) the ferrous/ferric redox front. For example, within a given micro-environment, if the rate of ferric iron release from chlorite weathering is slower than the rate of UO_2^{2+} and H_2PO_4 release from near-by coffinite – apatite zones secondary U(VI) phosphates may nucleate and grow within the portion of the oxygenated zone in which chlorite has not yet fully reacted to form detectable ferric staining. This mechanism accounts for both macroscopic and microscopic characteristics of the Coles Hill redox front.

Conclusion

The data presented above suggests that the volume of bedrock containing the ferrous/ferric redox front and uranous/uranyl transition zone at the Coles Hill uranium deposit has acted as a closed system with respect to uranium mass transport over the past tens of thousands of years (estimated length of time for redox front formation). The primary mechanism of uranium fixation within the oxidizing zone is the precipitation of secondary U(VI)-bearing mineral assemblages dominated by Ba-uranyl phosphates (meta-uranocircite). Ground water studies suggest that this mineral is capable of buffering dissolved uranium concentrations to values lower than 20 parts per billion. This process is facilitated by relatively high phosphate activities (e.g. $10^{-5.5} – 10^{5}$) and occurs at high Eh values and neutral to slightly acidic pH.

The Coles Hill uranium deposit thus represents an environmental system in which the natural attenuation of uranium transport is being achieved within an oxidizing environment. The phenomena involved in this process make this site a unique natural laboratory for the study of uranium attenuation with potential applications for the design, performance assessment, and

implementation of cost effective uranium remediation and containment strategies, such as soil amendments techniques and in-situ reactive barriers technologies.

References

Brookins, 1987. Eh-pH Diagrams for Geochemistry, New York, Springer-Verlag

Evensen, N. M., Hamilton, P. J., and O'Nions R. K., 1978, Rare earth abundances in chondritic meteorites, Geochimica Cosmochimica Acta, v. 42 p.1199-1212

Environmental Protection Agency, 1991, National primary drinking water standards for radionuclides, proposed rule, June, 1991, EPA Fact Sheet, Radionuclides in Drinking Water, 570/9-91-700

Finch, R. J., and Ewing, R. C., 1992. The corrosion of uraninite under oxidizing conditions, Journal of Nuclear Materials 190 133-156

Finch, R. J., and Murakami T., 1999, Systematics and paragenesis of uranium minerals, Reviews in Mineralogy, Volume 38: Uranium: Mineralogy, Geochemistry and the Environment, Burns, P. C., and Finch, R. (Eds)

Garrels R. M., and Christ C. L., 1959, Behavior of uranium minerals during oxidation. in Geochemistry and Mineralogy of the Colorado Plateau Uranium Ores., Garrels R. M., Larsen E. S., (Eds) US Geological Survey Professional Paper 320:81-89

Gaines, R. V., Skinner, H. C. W., Foord E. E., Mason B., Rosenzweig, A., King, V. T., Dowty E., 1997. Dana's New Mineralogy. 8th Edition. Wiley & Sons, New York, 1819 p.

Grenthe, I., Fuger, J., Konings, R J. M., Lemire, R. J., Muller, A. B., Nguyen-Trung Cregu, C., Wanner, H., 1992. (H. Wanner and I. Forest, eds.) Chemical Thermodynamics of Uranium, Nuclear Energy Agency, Amsterdam: Elsevier Science Publication

Halladay, C.R., 1989, The Swanson uranium deposit, Virginia: a structurally controlled U-P albitite deposit [abs.], in Uranium resources and geology of North America: Saskatoon, Canada, Proceedings of a technical committee meeting organized by the International Atomic Energy Agency, September 1987, p. 519

Hemingway, B.S., 1982. Thermodynamic properties of selected uranium compounds and aqueous species at 298.15 K and 1 bar at higher temperatures –Preliminary models for the origin of coffinite deposits. Open File Report 82-619, U.S. Geological Survey

Holmes, D. C., Pitty, A. E., Noy, D. J., 1992. Geomorphological and hydrogeological features of the Pocos de Caldas caldera analogue study sites, Journal of Geochemical Exploration, 45, 215-247

Ivonaovich, M. and Harmon, R. S. (Editors), 1982, Uranium Series Disequilibrium: Application to Environmental Problems. Oxford University Press, Oxford.

Jerden J. L., Jr., and Sinha, A. K., 2001a. Geology and geochemistry of the Coles Hill uranium deposit, Virginia, a unique example of hydrothermal apatite-coffinite-uraninite mineralization, *in review*: Economic Geology

Jerden J. L., Jr., and Sinha, A. K., 2001b. Mineralogical fixation of uranium during oxidation and chemical weathering of a coffinite-uraninite-apatite orebody, Virginia, Eleventh Annual V.M. Goldschmidt Conference, May 20-24, Hot Springs, Virginia, USA (oral presentation, no abstract given)

Kathren, R. L., 1984. Radioactivity in the Environment, Philadelphia, Harwood Academy Publications

Krauskopf, K. B., 1967. Introduction to Geochemistry, New York: McGraw-Hill

Langmuir, D., 1978. Uranium solution-minral equilibria at low temperatures with applications to sedimentary ore deposits, Geochimica et Cosmochimica Acta, v. 42 p. 547-569.

Langmuir, D., 1997. Aqueous Environmental Geochemistry, Upper Saddle River, New Jersey, Prentice-Hall Inc. 600 pp.

Leslie, B. W., Pearcy, E. C., Prikryl J. D., 1993, Oxidative alteration of uraninite at the Nopal I deposit, Mexico Possible contaminant transport and source term constraints for the proposed repository at Yucca Mountain, in Scientific Basis for Nuclear Waste Management XVI. Interrante CG, Pablan RT (Eds) Materials Research Symposium Proceedings v. 294, p. 505-512

Levenspiel, O., 1972. Chemical Reaction Engineering (2^{nd} edition) Wiley, Chichester, 1972

Marline Uranium Corporation, 1983, An evaluation of uranium development in Pittsylvania County Virginia: report submitted jointly by Marline Uranium Corporation and Union Carbide Corporation to the Virginia Uranium Administrative Group to the Virginia Uranium Administrative Group Pursuant to Section 45.1-285.1et seq of the Code of Virginia (1983) (Senate Bill 155), October, 15, 1983,

Menard, H. W., Jr., 1961. Some rates of regional erosion, Journal of Geology, 69, 154-161

Miekeley, N., Linsalate P., Osmond, J. K., 1992, Uranium and thorium isotopes in groundwaters from the Osamu Utsumi mine and Morro do Ferro natural analogue sites, Pocos de Caldas, Brazil, Journal of Geochemical Exploration, 45, 345-363

Muto T., 1965. Thermochemical stability of ningyoite. Mineralogical Journal 4 245-274

Nesbitt, H. W., and Wilson, R. E., 1992. Recent chemical weathering of basalts, American Journal of Science, 292, 740-777

Ngyuyen, S. N., Silva, R. J., Weed, H.C., and Andrews, J. E., Jr. 1992. Standard Gibbs free energies of formation at the temperature 303.15 K of four uranyl silicates: soddyite, uranophane, sodium boltwoodite and sodium weeksite. Journal of Chemical Thermodynamics, 24 359-376

Pavich, M. J., Brown, L., Valette-Silver, N., Klein, J., Middleton, R., 1985, ^{10}Be analysis of a Quaternary weathering profile in the Virginia Piedmont, Geology, 13, 39-41

Pearcy, E. C., Prikryl, J. D., Murphy, W. M., Leslie, B. W., 1994, Alteration of uraninite from the Nopal I deposit, Pena Blanca District, Chihuahua, Mexico compared to degradation of spent nuclear fuel in the proposed U.S. high-level nuclear waste repository at Yucca Mountain, Nevada, Applied Geochemistry, V. 9 p. 713-732

Romero, L., Neretnieks, I., and Moreno, L., 1992. Movement of the redox front at the Osamu utsumi uranium mine, Pocos de Caldas, Brazil, Journal of Geochemical Exploration, 45, 471-502

Vochten, R. F., Van Haverbeke, L., and Van Springel, K., 1992. Transformation of chernikovite into meta-uranocircite II, $Ba(UO_2)(PO_4)_2 \bullet 6H_2O$ and study of its solubility, Mineralogical Magazine, v.56, p.367-372

Woods, T. L., and Garrels R. M., 1987, Thermodynamic Values at low temperature for natural inorganic materials: an uncritical summary, Oxford University Press, New York, 242 pp.

Wronkiewicz, D. J., Bates J. K., Gerding T. J., Veleckis, E., Tani B. S., 1992, Uranium release and secondary phase formation during unsaturated testing of UO_2 at 90^oC, Journal of Nuclear Materials, v. 190, p. 107-127

Wronkiewicz, D. J., Bates J. K., Wolfe, S. F., Buck E. C., 1996, Ten-year results from unsaturated drip tests with UO2 at 90oC,: Implications for the corrosion of spent nuclear fuel, Journal of Nuclear Materials, v. 238, p. 78-95

Wronkiewicz, D. J., and Buck E. C., 1999, Uranium mineralogy and the geologic disposal of spent nuclear fuel, Reviews in Mineralogy, Volume 38: Uranium: Mineralogy, Geochemistry and the Environment, Burns, P. C., and Finch, R. (Eds)

Table 2-1. Electron microprobe analyses of coffinites from the Coles Hill primary ore zone.

	(1)	(2)	(3)	(4)	(5)	Average	(6)	(7)
SiO_2	17.69	17.56	17.40	17.36	17.22	17.45	10.59	16.06
UO_2	66.72	69.74	68.11	64.68	67.53	67.36	77.72	64.65
PbO	0.18	0.03	0.82	0.10	0.15	0.26	0.43	0.02
CaO	3.31	2.52	2.21	1.45	1.70	2.24	2.68	5.05
P_2O_5	1.13	0.69	0.91	0.43	0.46	0.73	0.33	4.13
BaO	0.64	0.63	0.44	0.69	0.82	0.64	0.39	0.54
Total	89.68	91.17	89.89	84.71	87.88	88.67	92.14	90.45

*ThO_2 was below detection limit of approximately 0.1 weight percent. Samples (1) - (3) from core 174, 102 meters depth, samples (4) - (7) from core 173, 90 meters depth Relative standard deviations of raw data (calculated from counting statistics) are: 1% or less for SiO_2 and UO_3; 2% or less for P_2O_5 and CaO; 1% - 3% for PbO and BaO.

Table 2-2. Electron microprobe analyses and mineral formula calculation of meta-uranocircites from oxidized bedrock associated with the Coles Hill uranium deposit.

	(1)	(2)	(3)	(4)	(5)	(6)	(7)	(8)
UO_3	56.96	57.19	57.91	58.10	57.56	57.95	58.86	58.86
P_2O_5	14.93	15.05	14.88	14.79	14.89	14.40	14.40	14.37
BaO	16.11	15.69	15.22	15.11	15.43	15.46	14.62	14.61
Total*	88.00	87.92	88.00	88.00	87.89	87.81	87.88	87.85
Ions based on 12 oxygen equivalents, ignoring interlayer H_2O								
U	1.95	1.95	1.97	1.98	1.96	2.00	2.02	2.02
P	2.06	2.06	2.04	2.04	2.05	2.00	1.99	1.99
Ba	1.03	1.00	0.97	0.96	0.98	0.99	0.94	0.94

*Total normalized to ideal H_2O. Totals of raw data are not representative due to dehydration of crystals in microprobe vacuum. Oxides CaO, SrO, MgO, Na2O, K2Oand PbO are below detection limit of approximately 0.1 weight percent. Relative standard deviations of raw data (calculated from counting statistics) are: 1% or less for UO_3 and 2% or less for P_2O_5 and BaO, (1), (4), (5) = Type III meta-uranocircite; (2), (3) = Type II meta-uranocircite; (6), (7), (8) = Type II meta-uranocircite (see text for description).

Table 2-3. Electron microprobe analyses of lanthanide phosphate associated with Type II meta-uranocircite, Coles Hill uranium deposit.

	(1)	(2)	(3)	(4)	(5)	(6)	(7)	Average
P_2O_5	27.76	27.82	28.25	28.30	28.47	28.73	29.59	28.42
La_2O_3	18.79	20.03	19.70	19.60	20.14	20.64	20.88	19.97
Ce_2O_3	18.32	18.14	16.70	17.15	16.70	15.80	16.60	17.06
Pr_2O_3	4.63	4.78	4.62	4.64	4.40	4.83	4.64	4.65
Nd_2O_3	6.88	7.65	7.65	7.60	7.36	7.64	7.90	7.52
Yb_2O_3	0.00	0.00	0.00	0.00	0.00	0.00	0.00	0.00
CaO	5.28	5.14	5.43	4.90	5.99	5.09	4.95	5.25
PbO	2.23	2.10	2.14	1.96	1.91	2.22	2.12	2.10
UO_3	2.61	2.72	2.61	2.62	2.67	2.84	2.96	2.72
Total:	86.49	88.37	87.09	86.77	87.65	87.78	89.65	87.69
(Ce_N/Ce_N)*	0.45	0.42	0.40	0.41	0.40	0.36	0.38	0.40

(N) value normalized to average chondrite of Evensen et. al., 1978. *Monitor of the size of the negative Ce anomally. Calculated by dividing Ce_N by an interpolated Ce value obtained by $(La_N+Pr_N)/2$ Relative standard deviations of raw data (calculated from counting statistics) are: 1.0% or less for P_2O_5; 2.0% or less for CaO; from 2% - 3% for La_2O_3, Ce_2O_3 and Nd_2O_3 and 3% to 4% for other elements. Low totals due to lack of data for other lanthanides and the possible presence of nH_2O All analyses from core 174, 25.5 meters depth.

Table 2-4a. Whole rock geochemistry of unoxidized samples of Coles Hill uranium ore (oxides in weight percent, others in parts per million).

	DH 174[+]	DH 174[+]	DH 174[+]	DH 173[+]	DH 173[+]	DH 173[+]	DH 172[+]	DH 172[+]	Average[+]
depth (m)	**30.8**	**29.0**	**28.4**	**29.0**	**28.7**	**28.4**	**28.0**	**27.7**	**----**
Na_2O	8.2	8.8	9.1	7.4	7.3	8.1	9.0	9.5	8.4
MgO	0.9	0.7	0.6	0.6	0.9	0.8	0.8	0.5	0.7
Al_2O_3	16.3	16.8	16.5	13.7	14.5	15.8	17.1	17.3	16.0
SiO_2	64.3	65.4	67.2	52.7	68.2	63.9	66.9	62.7	63.9
P_2O_5	1.4	1.5	1.1	8.5	1.1	1.1	0.3	1.8	2.1
K_2O	0.2	0.1	0.0	0.2	0.1	0.1	0.2	0.2	0.1
CaO	3.0	2.6	2.0	11.8	2.8	4.0	1.0	2.9	3.8
TiO_2	0.5	0.4	0.2	0.4	0.5	0.4	0.5	0.3	0.4
MnO	0.1	0.0	0.0	0.0	0.0	0.1	0.0	0.0	0.0
Fe_2O_3(t)	3.1	2.4	1.8	2.2	2.7	2.8	2.9	1.9	2.5
LOI	2.3	1.4	1.6	1.9	2.1	3.0	1.6	1.5	1.9
Total	100.2	100.1	100.3	99.5	100.3	100.1	100.2	98.6	99.9
V	99.6	94.4	58.6	104.9	92.7	95.7	112.9	91.5	93.8
Rb	7.2	6.1	2.2	7.0	6.5	9.4	8.7	6.1	6.6
Sr	181.9	245.3	147.2	1210.0	183.9	208.5	67.1	256.6	312.6
Y	10.7	14.1	14.5	37.1	21.4	22.7	9.4	12.8	17.8
Zr	214.3	263.2	140.1	182.1	220.1	235.2	285.3	146.6	210.9
Nb	14.0	15.8	12.2	18.2	20.5	22.8	13.3	10.7	15.9
Ba	164.5	196.3	126.1	171.9	790.9	1150.0	232.2	543.0	421.9
La	47.8	63.4	27.9	156.6	54.6	60.1	20.3	77.2	63.5
Ce	78.0	100.4	47.6	255.0	92.1	100.2	41.8	129.9	105.6
Pr	7.0	9.4	4.6	24.3	8.6	9.8	4.2	11.1	9.9
Nd	24.1	32.4	16.9	79.6	30.6	33.3	14.9	35.4	33.4
Sm	3.6	4.6	3.1	9.5	5.3	5.5	2.5	4.5	4.8
Eu	1.1	1.3	0.8	2.6	1.1	0.9	0.7	1.0	1.2
Gd	2.6	3.5	2.6	7.3	4.0	5.0	1.8	2.7	3.7
Tb	0.4	0.5	0.4	1.0	0.7	0.8	0.3	0.4	0.6
Dy	2.0	2.8	2.4	6.0	3.8	4.5	1.5	2.1	3.1
Ho	0.4	0.5	0.5	1.2	0.7	0.9	0.3	0.4	0.6
Er	1.1	1.5	1.7	3.4	2.1	2.7	1.0	1.2	1.8
Tm	0.2	0.2	0.3	0.4	0.3	0.4	0.2	0.2	0.3
Yb	1.3	1.6	1.5	2.3	2.3	2.5	1.2	1.3	1.7
Lu	0.2	0.2	0.2	0.3	0.3	0.4	0.2	0.2	0.3
Hf	5.8	6.4	3.9	0.8	5.7	6.3	6.9	1.3	4.6
Pb	10.0	19.5	10.1	16.0	14.4	23.1	13.2	23.0	16.2
Th	13.8	14.0	31.5	22.0	20.0	31.4	7.5	18.1	19.8
U	138.2	521.0	211.2	706.4	1030.0	955.5	496.3	459.9	564.8
$(La/Yb)_N$	25.7	27.5	12.3	46.8	16.4	16.0	11.4	41.6	24.7
(Eu_N/Eu_N^*)	1.0	1.0	0.8	0.9	0.7	0.5	1.0	0.8	0.9
(Ce_N/Ce_N^*)	0.9	0.9	0.9	0.9	0.9	0.9	1.0	0.9	0.9

(t) Total iron as Fe_2O_3, (N) normalized to average chondrite of Evensen et. al., 1978. # Average for uranium in oxidized ore samples does not include sample DH 173-28m (Ce_N/Ce_N^*) monitor of the size of the negative Ce anomally. Calculated by dividing Ce_N by an interpolated Ce value obtained by $(La_N+Pr_N)/2$ (Eu_N/Eu_N^*) monitor of Eu anomally. Calculated by dividing Eu_N by an interpolated Eu value obtained by $(Sm_N+Gd_N)/2$.

Table 2-4b. Whole rock geochemistry of oxidized samples of Coles Hill uranium ore (oxides in weight percent, others in parts per million).

	DH 174	DH 174	DH 173	DH 173	DH 173	DH 173	DH 172	DH 172	Average[#]
depth (m)	**27.1**	**24.7**	**28.0**	**27.7**	**27.4**	**27.1**	**27.4**	**27.1**	**----**
Na_2O	8.2	8.4	5.6	8.8	8.5	8.2	8.2	8.5	8.0
MgO	0.4	0.3	0.5	0.4	0.3	0.7	0.6	0.5	0.5
Al_2O_3	16.1	16.5	12.1	16.7	16.0	16.3	15.8	16.6	15.8
SiO_2	68.2	64.9	75.6	65.3	61.7	63.1	68.3	64.4	66.5
P_2O_5	0.7	1.9	0.9	1.8	4.1	2.1	1.2	2.1	1.9
K_2O	0.2	0.1	0.6	0.2	0.1	0.2	0.1	0.1	0.2
CaO	1.0	2.9	1.2	2.5	5.7	3.0	1.9	2.8	2.6
TiO_2	0.5	0.4	0.4	0.4	0.2	0.4	0.5	0.5	0.4
MnO	0.0	0.0	0.0	0.0	0.0	0.0	0.0	0.0	0.0
Fe_2O_3(t)	2.8	2.2	1.5	2.4	1.6	3.5	2.3	2.6	2.3
LOI	2.0	2.0	2.0	1.9	1.8	2.6	1.6	2.1	2.0
Total	100.1	99.7	100.3	100.5	100.0	100.1	100.5	100.1	100.2
V	97.5	80.3	89.9	79.2	38.0	109.6	74.2	89.6	82.3
Rb	7.8	6.0	33.6	7.1	7.6	10.4	5.0	7.9	10.7
Sr	110.9	301.2	100.4	252.1	606.1	310.6	189.2	297.9	271.1
Y	13.0	15.1	21.1	16.6	19.0	28.9	25.5	21.4	20.1
Zr	285.9	236.1	242.9	198.2	145.7	111.1	234.1	159.9	201.7
Nb	26.1	25.5	13.4	21.7	16.2	16.4	21.1	24.4	20.6
Ba	447.0	1530.0	1340.0	1120.0	666.5	909.5	862.4	916.6	974.0
La	30.5	45.0	31.7	41.2	73.5	69.2	66.3	82.1	54.9
Ce	53.5	70.9	57.6	69.2	101.2	112.8	107.3	129.0	87.7
Pr	5.0	6.9	6.0	6.8	10.7	10.5	10.5	11.9	8.5
Nd	18.6	24.5	21.9	24.2	35.8	37.1	35.5	40.9	29.8
Sm	3.5	4.0	4.3	4.0	5.2	6.1	5.7	6.2	4.9
Eu	0.9	0.9	1.0	0.9	1.0	1.2	1.1	1.2	1.0
Gd	2.9	3.4	3.4	3.2	3.9	4.8	5.0	4.9	4.0
Tb	0.4	0.5	0.6	0.5	0.5	0.8	0.8	0.8	0.6
Dy	2.6	2.9	3.5	2.7	2.9	4.6	4.6	4.3	3.5
Ho	0.5	0.6	0.7	0.6	0.6	0.9	0.9	0.8	0.7
Er	1.4	1.6	2.2	1.8	1.8	3.0	2.6	2.2	2.1
Tm	0.2	0.2	0.3	0.3	0.3	0.5	0.4	0.3	0.3
Yb	1.5	1.5	2.1	1.7	1.6	2.7	2.4	2.2	2.0
Lu	0.2	0.2	0.3	0.3	0.3	0.4	0.3	0.3	0.3
Hf	7.2	6.2	5.9	1.2	0.5	1.1	6.2	4.3	4.1
Pb	31.5	23.4	11.7	19.9	18.8	28.3	18.7	35.0	23.4
Th	22.1	17.5	12.1	15.9	33.3	19.0	24.7	21.8	20.8
U	304.9	474.9	3070.0	452.1	1210.0	717.1	336.2	528.0	574.7
$(La/Yb)_N$	13.5	19.7	10.0	16.4	30.4	17.5	18.7	25.2	18.9
(Eu_N/Eu_N^*)	0.9	0.7	0.7	0.7	0.7	0.7	0.6	0.6	0.7
(Ce_N/Ce_N^*)	0.9	0.9	0.9	0.9	0.8	0.9	0.9	0.9	0.9

(t) Total iron as Fe_2O_3, (N) normalized to average chondrite of Evensen et. al., 1978. # Average for uranium in oxidized ore samples does not include sample DH 173-28m (Ce_N/Ce_N^*) monitor of the size of the negative Ce anomally. Calculated by dividing Ce_N by an interpolated Ce value obtained by $(La_N+Pr_N)/2$ (Eu_N/Eu_N^*) monitor of Eu anomally. Calculated by dividing Eu_N by an interpolated Eu value obtained by $(Sm_N+Gd_N)/2$.

Table 2-5. Selected ground water analyses from the weathered zone overlying the Coles Hill north orebody.

	(1)	(2)	(3)	(4)
Field pH	5.90	6.00	6.00	6.00
Field DO (ppm)	8.00	----	----	3.00
Major Constituents (ppm)				
Na	10.17	12.20	14.00	12.20
Mg	0.73	4.22	2.30	4.22
Si	16.28	16.10	----	16.10
K	0.26	0.12	0.40	0.12
Ca	3.00	17.10	8.70	17.10
HCO_3	----	----	23.00	23.00
SO_4	4.88	----	0.50	4.90
Cl	3.13	----	34.00	34.00
Selected Minor & Trace Constituents (ppb)				
Al	26.56	< 2.0	< 500.00	< 2.0
Mn	11.99	4.17	29.00	4.20
Fe	30.25	78.38	64.00	64.00
Cu	1.01	----	120.00	120.00
Sr	28.84	83.62	----	83.60
Ba	331.72	682.71	2600.00	683.00
Pb	0.11	0.18	< 5.00	< 5.0
U	4.95	13.94	13.00	13.90
NO_3 (as N)	210.00	----	2300.00	2300.00
F	170.00	----	----	170.00
PO_4 (as P)	100.00	----	320.00	300.00
VO_4 (as V)	0.81	0.68	< 5.00	< 5.00

(1) = Ground water from saprolite aquifer (from well adjacent to 41-173, see Fig. 2-2),
(2) = Ground water from residential well tapping oxidized bedrock zone,
(3) Ground water from oxidized bedrock zone sampled and analyzed by the Marline Corporation, 1983,
(4) = Representative ground water composition used for speciation calculations, estimated by synthesizing data from the Marline Corporation (1983) environmental baseline study of the deposit region with new data collected by the authors.

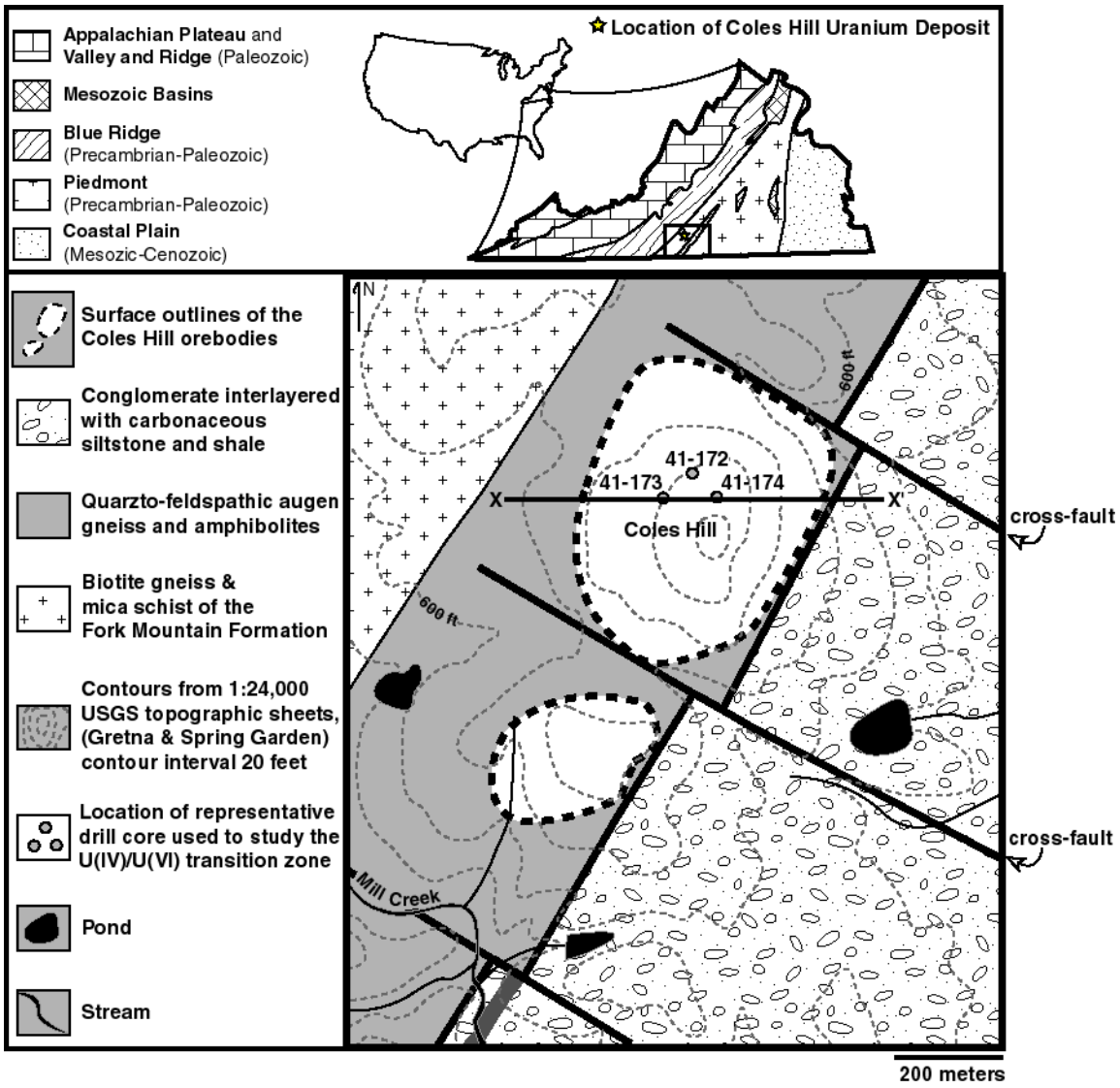

Figure 2-1. Location and geologic setting of the Coles Hill uranium deposit. Representative drill cores studied for this project are shown within the northern most orebody of the deposit.

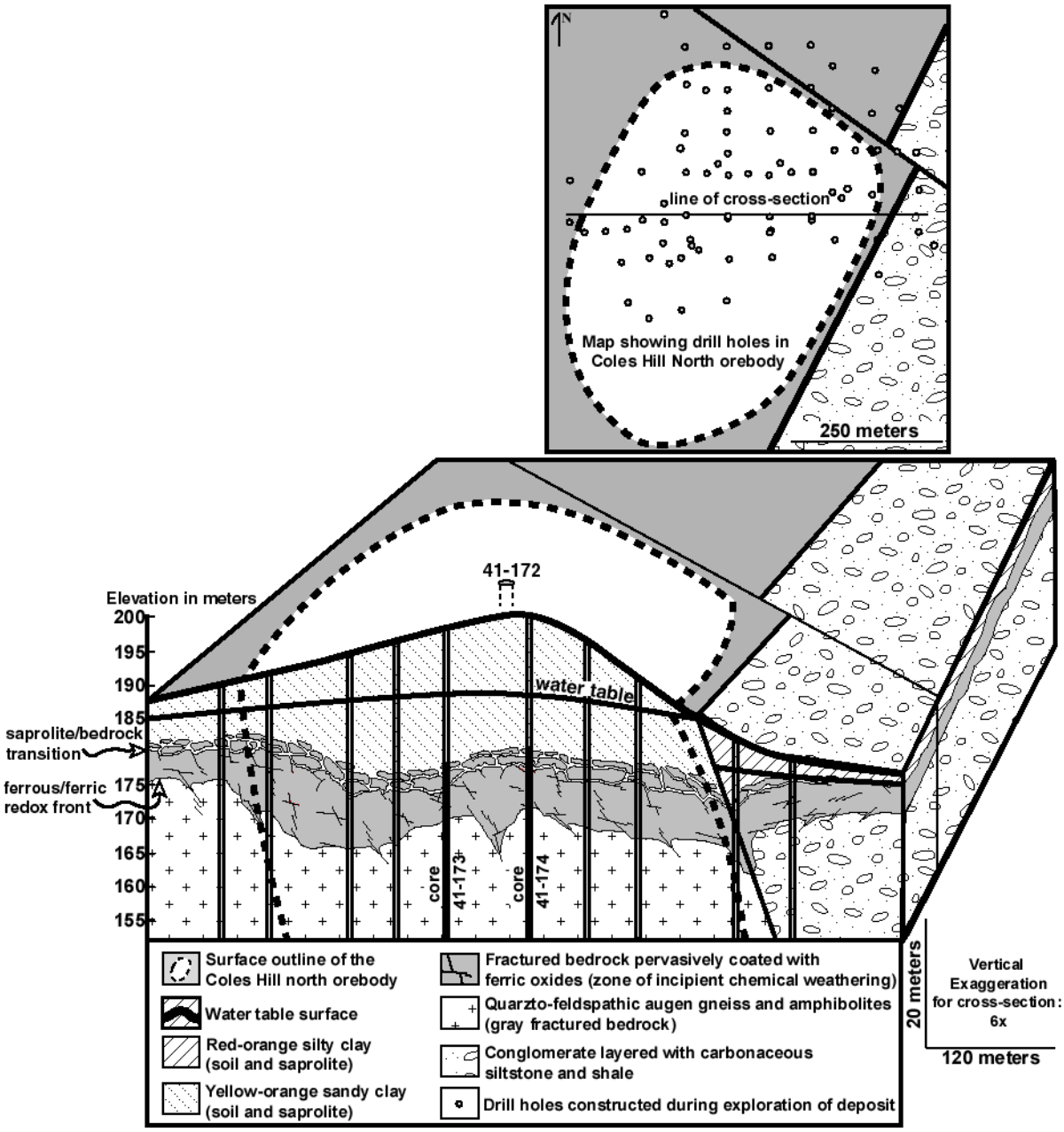

Figure 2-2. Geologic cross-section through weathered zone overlying the Coles Hill uranium deposit. This section, which was plotted using exploration drill hole logs (drill hole locations shown on map view), indicates that the zone of ferric oxide stained bedrock (zone of incipient chemical weathering) is continuous but varies in thickness and depth within the study area. The three core sections identified in the cross-section were used to characterize the mineralogy and geochemistry of uranium at redox fronts where primary U(IV) ore is exposed to oxidizing groundwaters.

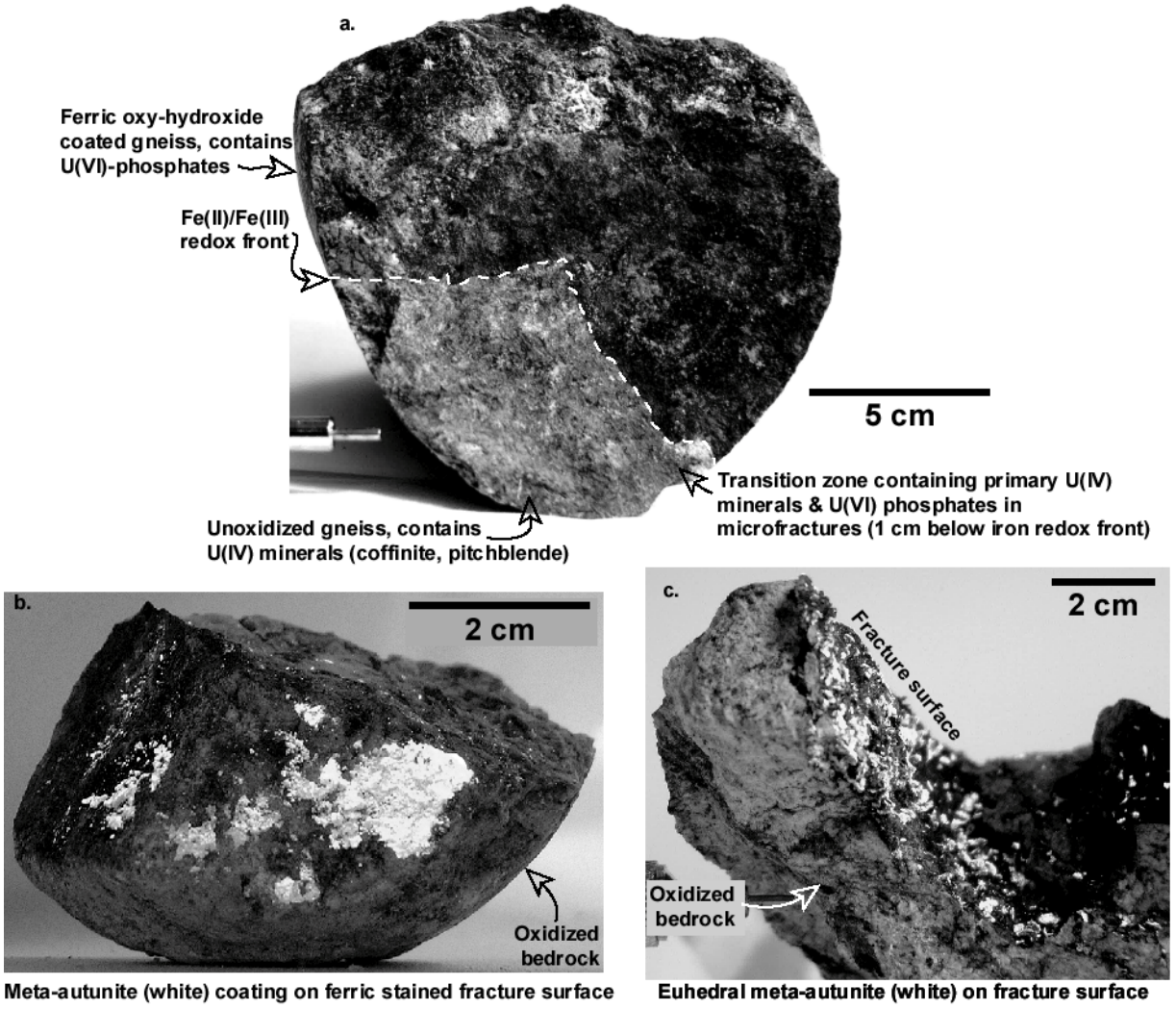

Figure 2-3. Hand samples of core from near the ferrous/ferric redox front preserved in uranium ore bearing bedrock from the Coles Hill uranium deposit. (a) hand sample showing iron and uranium redox fronts (sample from 41-173, 28.1 m depth). The front migrates as oxidizing (meteoric) waters infiltrate primary bedrock along grain-boundary micro-fractures, thus the irregular shape of the ferrous/ferric interface is caused by variations in grain-boundary permeability. (b) U(VI) phosphate coating (white) on hand sample of oxidized uranium ore (photograph taken in ultraviolet light; core 41-174, 27.1 m depth), (c) Concentrations of euhedral U(VI) phosphate crystals (white) on open fracture surface within oxidized uranium bearing core (photograph taken in ultraviolet light; core 41-172, 27.4 m depth).

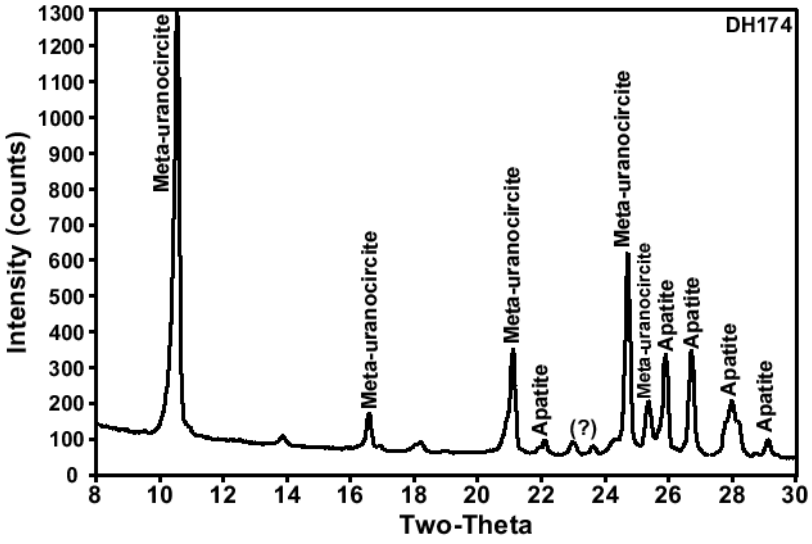

Figure 2-4. X ray diffraction pattern of a representative heavy mineral separate (SG > 3.32) sampled 4 centimeters above the redox front (on oxidizing side) in core 41-174 was examined by XRD and was found to consist mostly of apatite (primary) and meta-uranocircite (secondary) (data from R. Finch, 2001, personal communication).

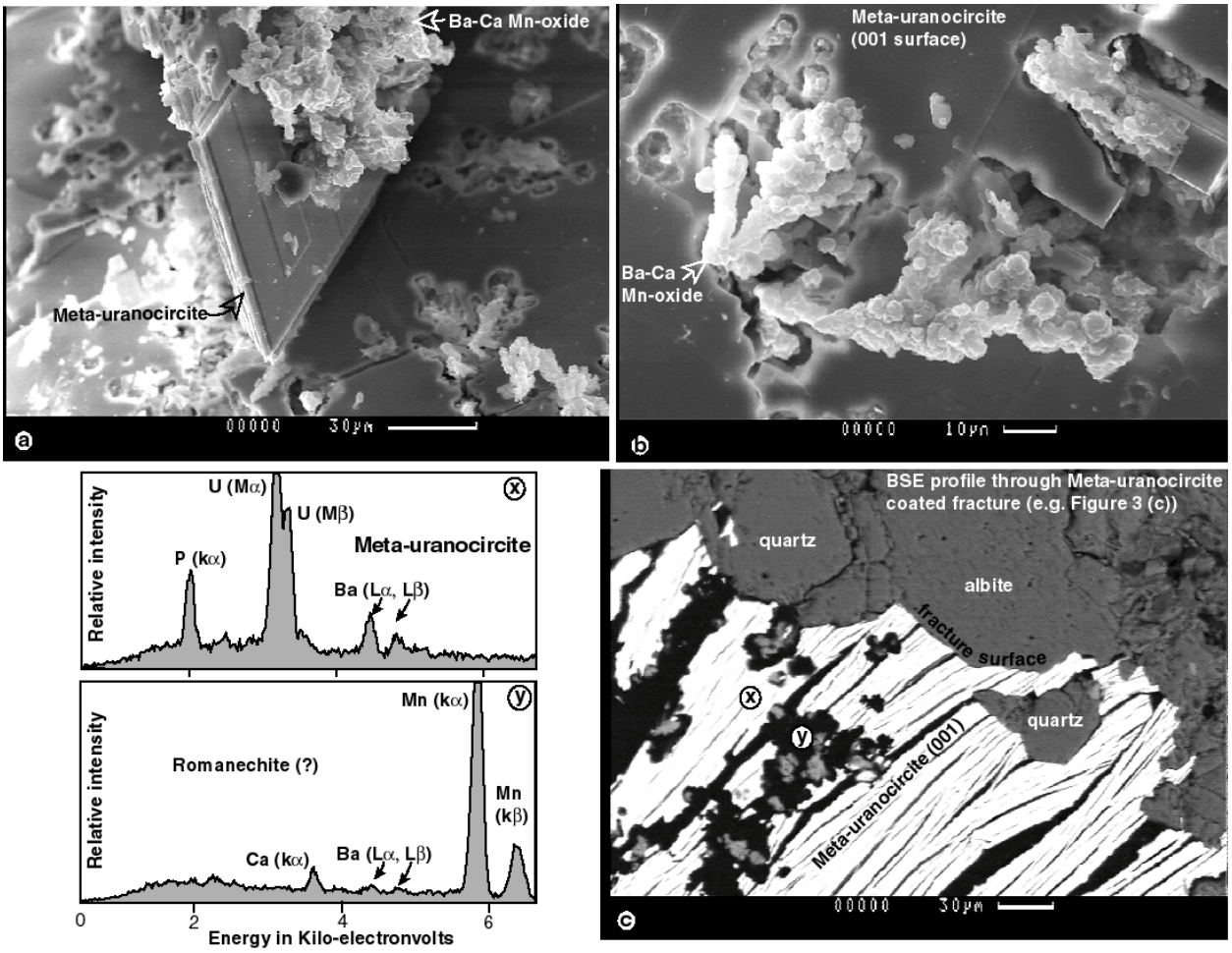

Figure 2-5. Electron images of the Type I meta-uranocircite assemblage. (a) Scanning electron image (SEM) of euhedral meta-uranocircite crystal associated with a Ba-Ca Mn-oxide (sample from core 41-173, 26 m depth). (b) Enlarged view of Ba-Ca Mn-oxide growing on meta-uranocircite substrate (sample from core 41-173, 26 m depth). (c) back scatter electron (BSE) image of thin section cut across a meta-uranocircite coated fracture surface (sample from 41-174, 27 m depth). Energy dispersive x-ray spectra (EDS) illustrating compositions of U(VI) phosphate and Mn-oxide phases.

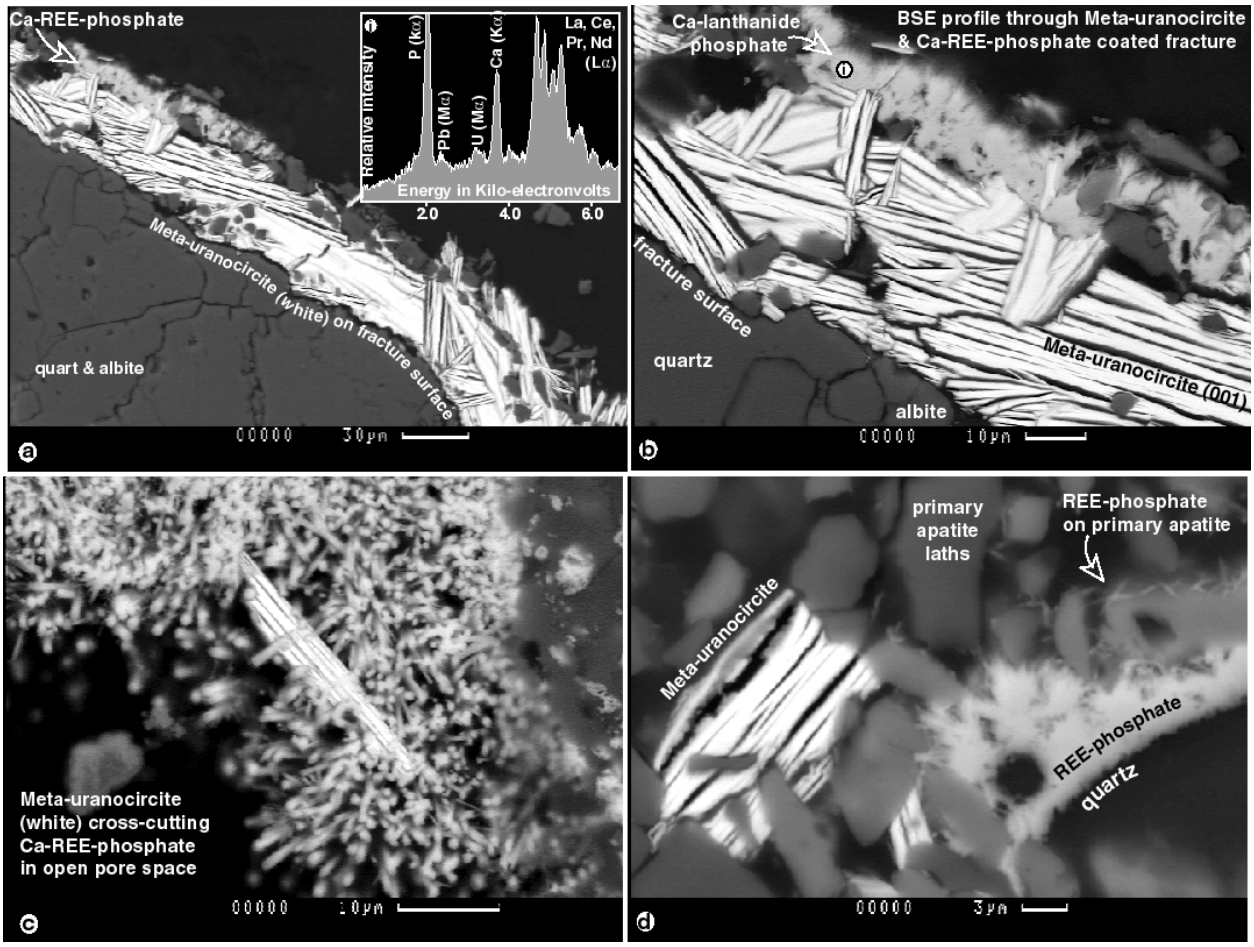

Figure 2-6. Back scatter electron images (BSE) of the Type II meta-uranocircite assemblage. (a) BSE profile (from thinsection) of Ba meta-autunite (meta-uranocircite) coating a fracture surface within the host rock quartz-feldspar gneiss. Meta-uranocircite is overgrown by a Ca rich lanthanide phosphate (REE-phosphate) identified by energy dispersive x-ray spectra (sample from core 41-174, 25.5 m depth). (b) Enlarged view of upper portion of fracture shown in (a) showing textural association between the U-bearing secondary phosphate minerals. (c) Enlarged view of textural association between meta-uranocircite and REE-phosphate in a open pore space within the host rock gneiss (sample from core 41-174, 25 m depth). (d) Meta-uranocircite and REE-phosphate associated with primary, ore-stage apatite. Note microcrystals of REE phosphate on surface of apatite lath (sample from core 41-174, 25.5 m depth).

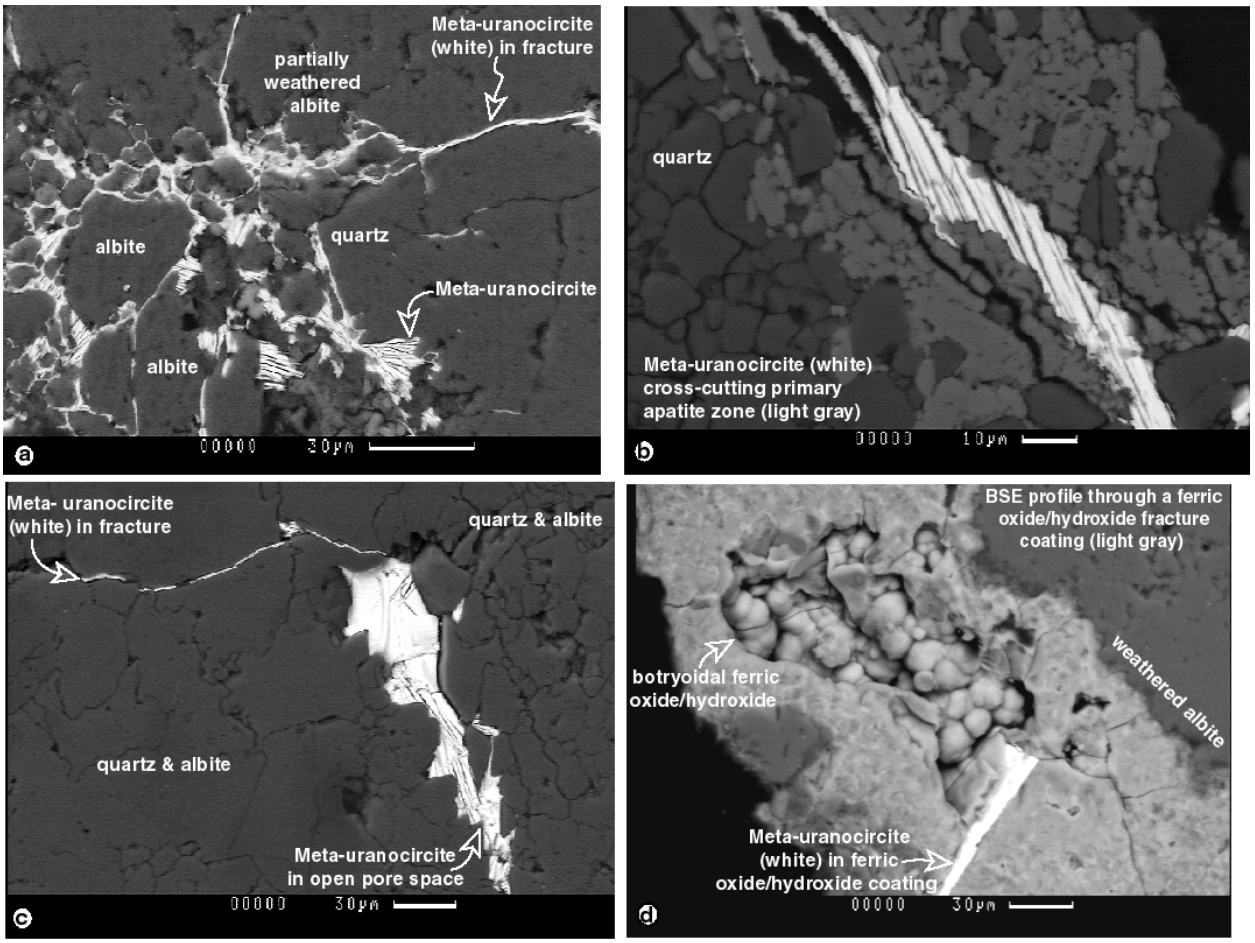

Figure 2-7. Backscatter electron images of the Type III meta-uranocircite assemblage. (a) Meta-uranocircite filling in grain boundaries between weathered primary minerals (mainly albite) (sample from core 41-172, 26 m depth). (b) Fracture filled with meta-uranocircite within primary, ore-stage apatite zone (sample from core 41-173, 27.4 m depth). (c) Mono-minerallic occurrence of meta-uranocircite within open pore space and fracture within quartz-feldspar gneiss (sample from core 41-173, 27 m depth). (d) Meta-uranocircite grain within ferric oxides/oxy-hydroxides fracture coating (sample from core 41-174, 27 m depth).

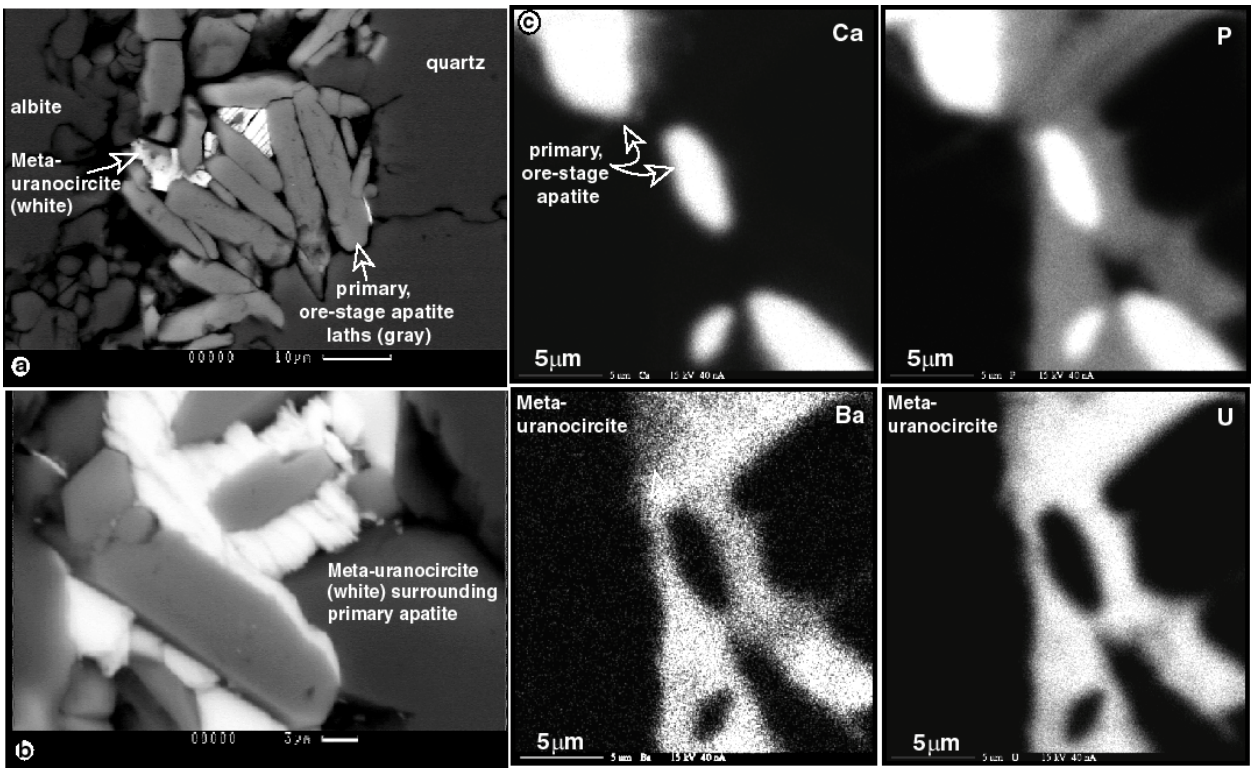

Figure 2-8. Backscatter electron images (a & b) and electron-microprobe x-ray maps (c) of the Type III meta-uranocircite assemblage. (a) BSE showing meta-uranocircite within grain-boundaries between primary, ore-stage apatite laths (sample from core 41-173, 28 m depth). (b) BSE showing meta-uranocircite surrounding primary, ore-stage apatite grains (sample from core 41-172, 27.4 m depth). (c) X-ray maps for elements Ca, P, Ba, U showing that even directly adjacent to the primary apatite grains the secondary uranium phosphate is of the Ba end member of the meta-autunite group (operating conditions for x-ray maps 15 kilovolts, 40 nanoamps).

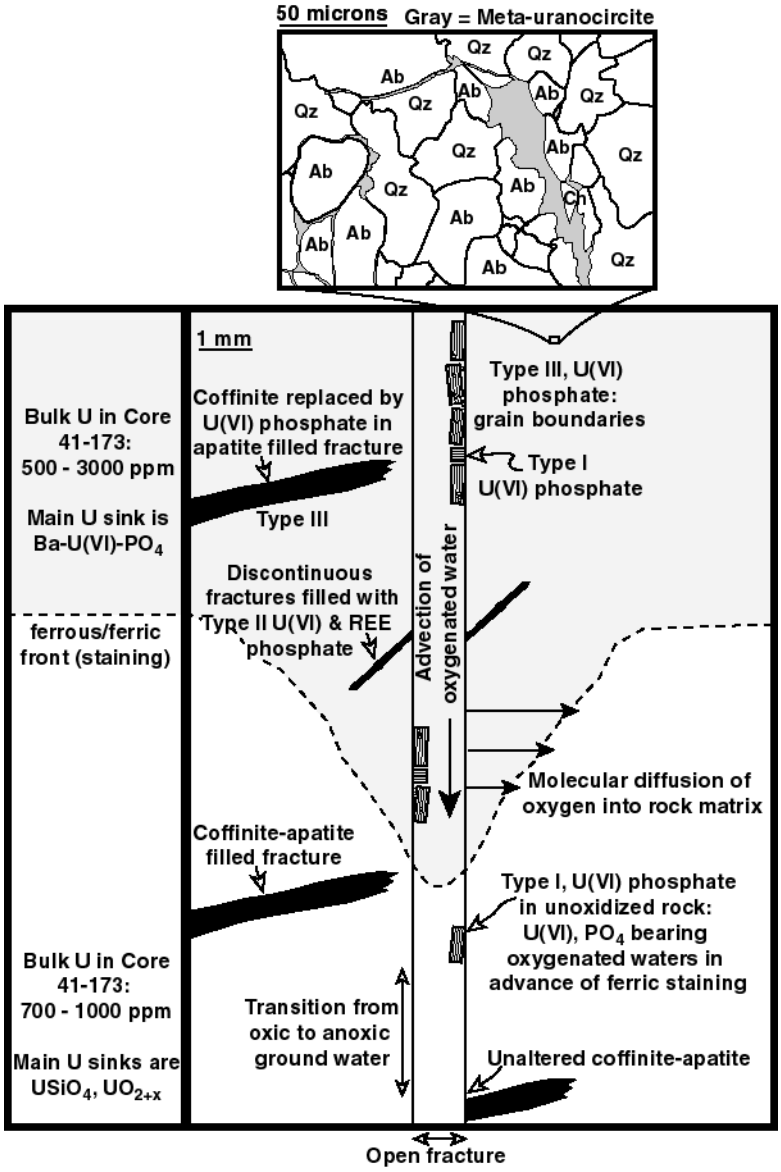

Figure 2-9. Illustration showing the micro-chemical and micro-physical domains associated with the three U(VI) phosphate assemblages (compiled from SEM and petrographic observations).

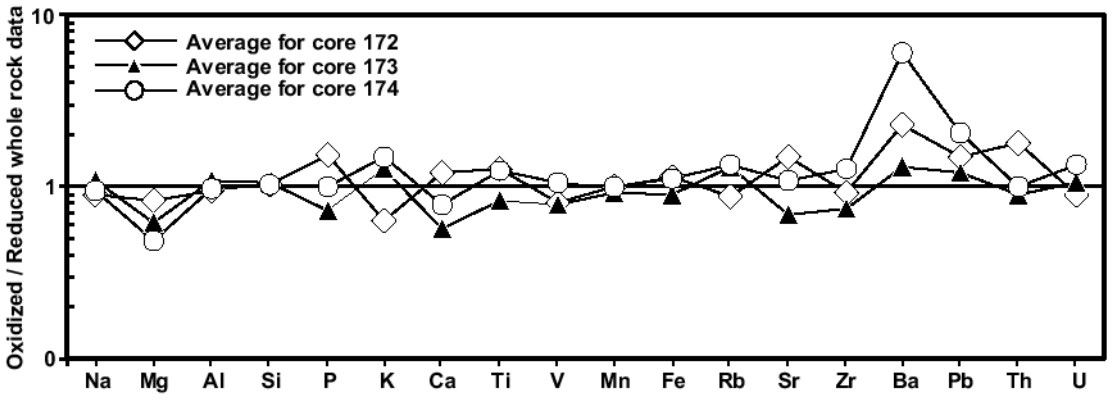

Figure 2-10. Average concentrations of selected major and trace elements in oxidized samples normalized to averages for the corresponding reduced samples. Samples consistently plotting above unity are enriched in the oxidized samples while those consistently plotting below are depleted in the oxidized samples. The irregular variation in the data is caused by the inherent lithologic heterogeneity of the sampled core sections.

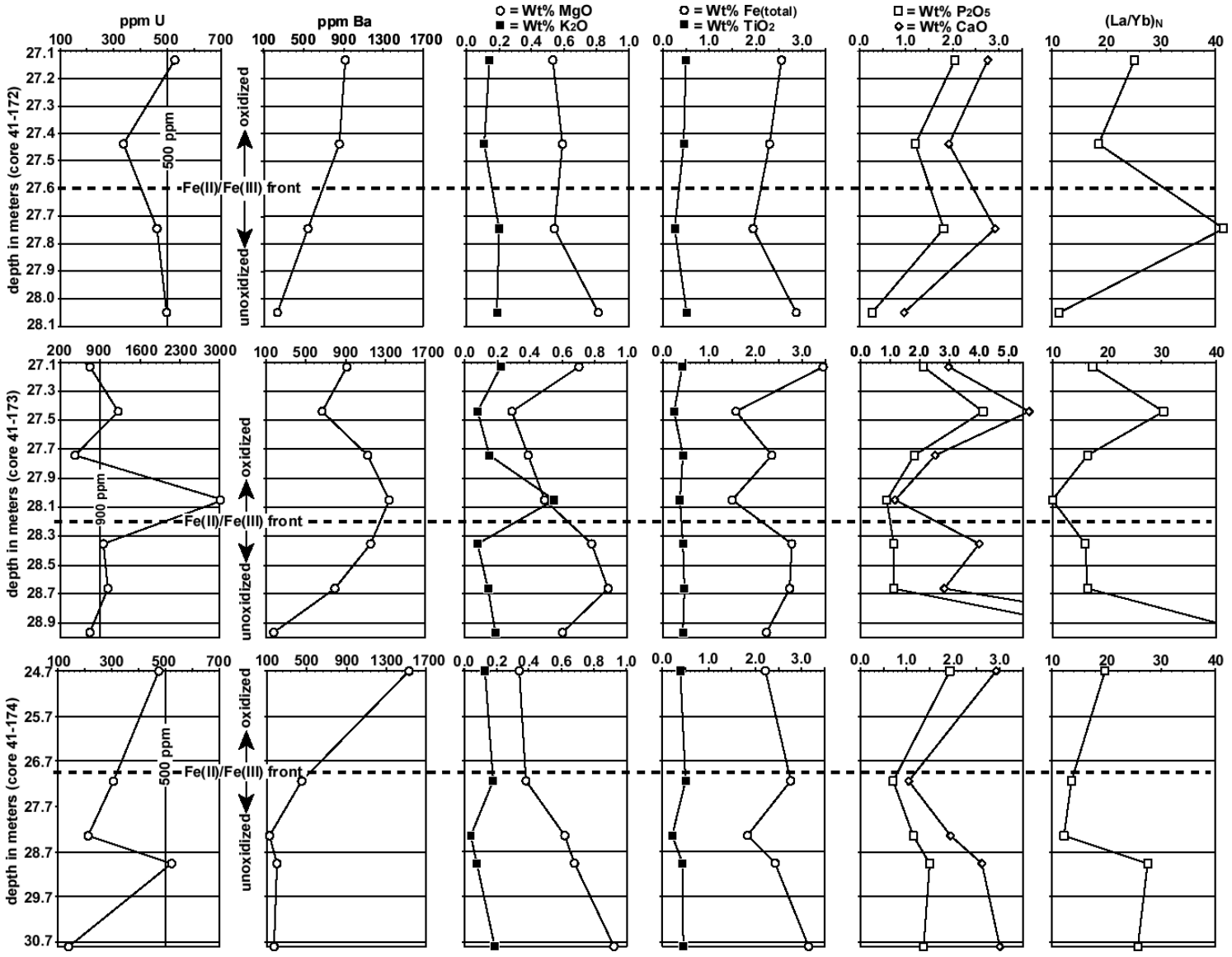

Figure 2-11. Concentration-depth profiles across redox fronts in representative core sections. The observation that oxidized samples have the same range in uranium as unoxidized samples suggests that the volume of rock containing these core behaved as a closed system with respect to uranium transport during oxidiation of the primary ore. The fluctuations noted in these profiles are due to differences in primary uranium concentrations (e.g. localization of primary ore zones) and/or by centimeter scale redistribution of uranium associated with the growth of Ba meta-autunite on fractures and grain boundaries.

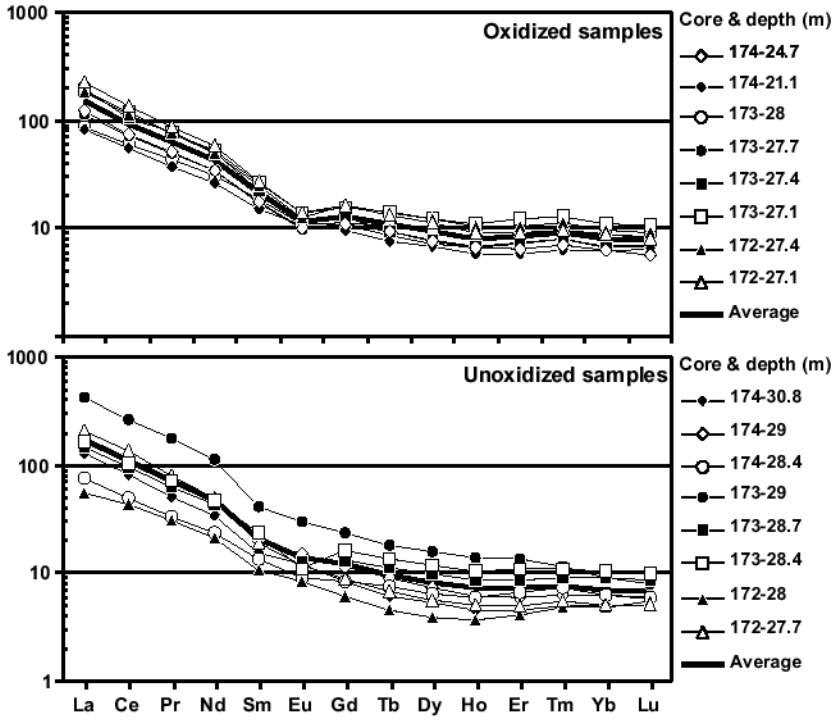

Figure 2-12. Chondrite normalized lanthanide patterns for oxidized and reduced samples. Normalizing values from Evensen et. al., 1978.

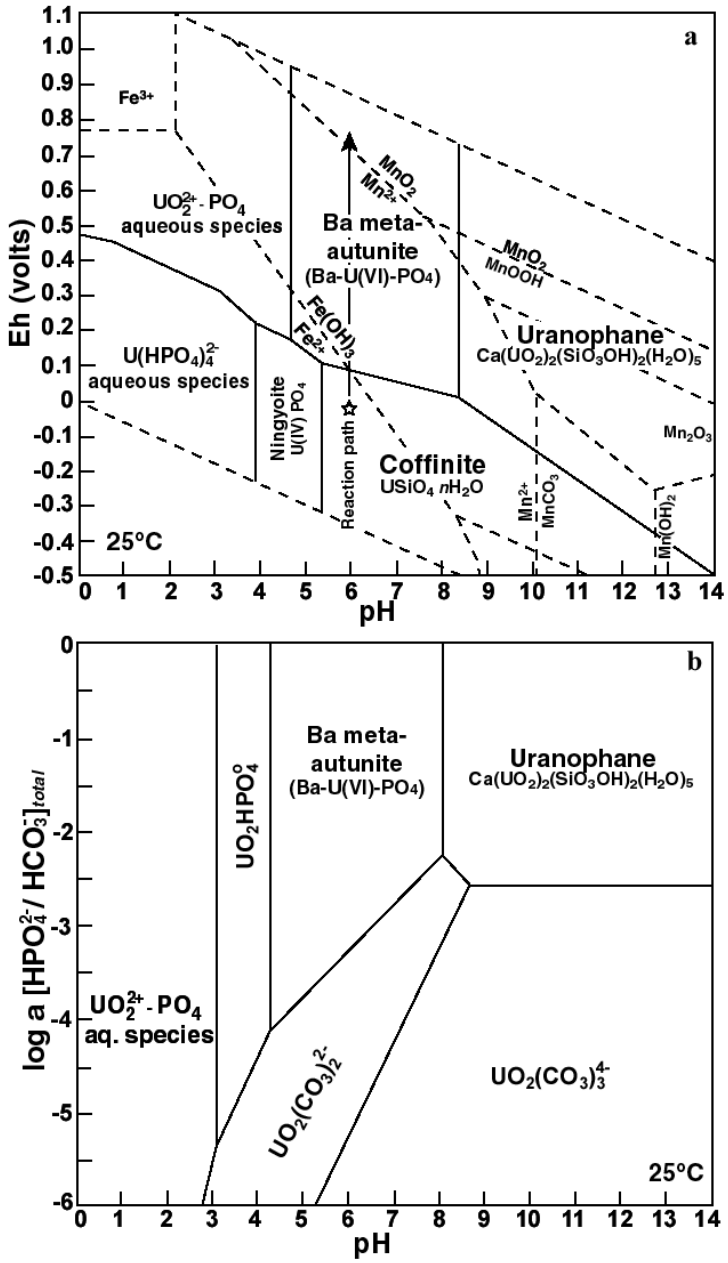

Figure 2-13. Activity diagrams showing the stability field of meta-uranocircite (Ba meta-autunite) for the Coles Hill shallow bedrock ground water system. (a) Eh-pH diagram for the Coles Hill system showing estimated reaction path (based on mineralogical observations) during oxidation of the primary ore (activities calculated from measured groundwater composition: $O_2(aq) = 10^{-4}$, $Na^+ = 10^{-3.3}$, $Mg^{2+} = 10^{-3.8}$, $SiO_2(aq) = 10^{-3.2}$, $K^+ = 10^{-5.5}$, $Ca^{2+} = 10^{-3.5}$, $Ba^{2+} = 10^{-5.4}$, $U = 10^{-7.3}$, $HCO_3^- = 10^{-3.4}$, $SO_4^{2-} = 10^{-4.4}$ and $HPO_4^{2-} = 10^{-5.1}$. For sources of solubility data see text. (b) Activity diagram showing U(VI) mineral stability for the Coles Hill system as a function of the activity ratio of dissolved phosphate to carbonate vs pH. Activities of other ions are the same as used for 12a.

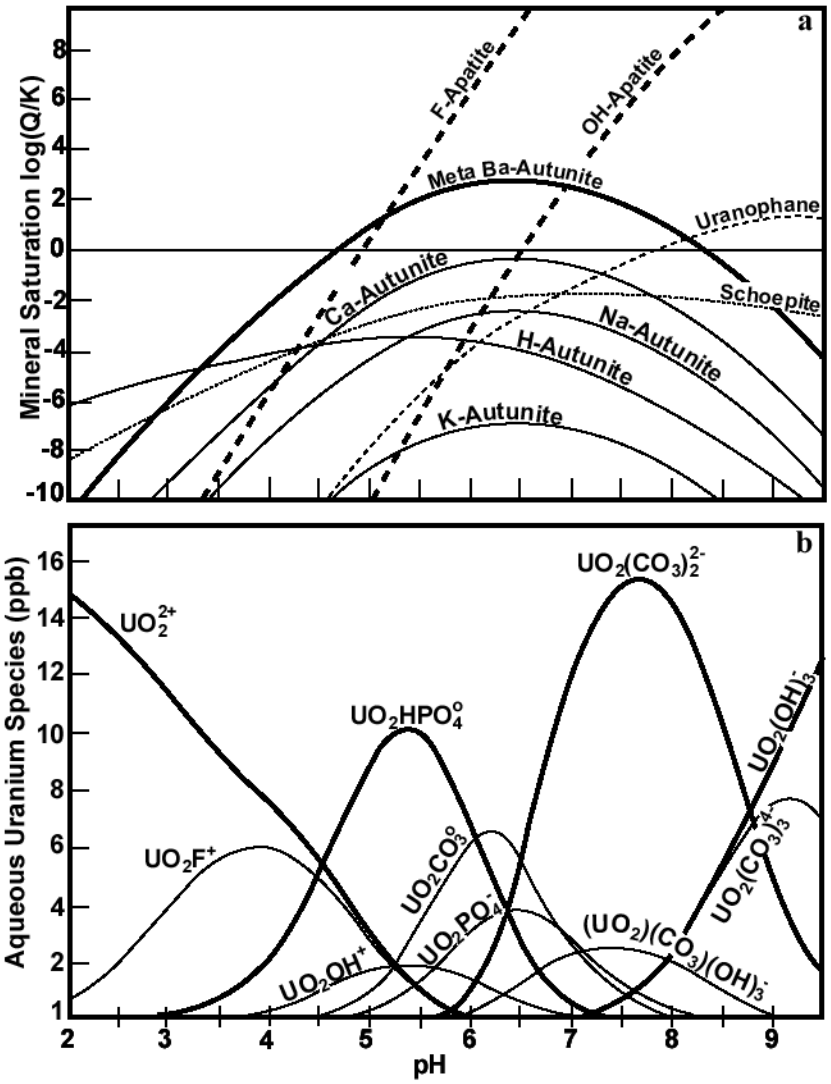

Figure 2-14. Speciation diagrams for ground water from the shallow bedrock zone associated with the Coles Hill north orebody. The water composition used to produce these diagrams is shown in Table 5. (a) Solid phase speciation diagram showing saturation indices for potentially important uranium minerals plotted as a function of pH. (b) Aqueous speciation for the same ground water sample showing the importance of uranyl phosphate complexes with in the pH range of interest (6 – 7).

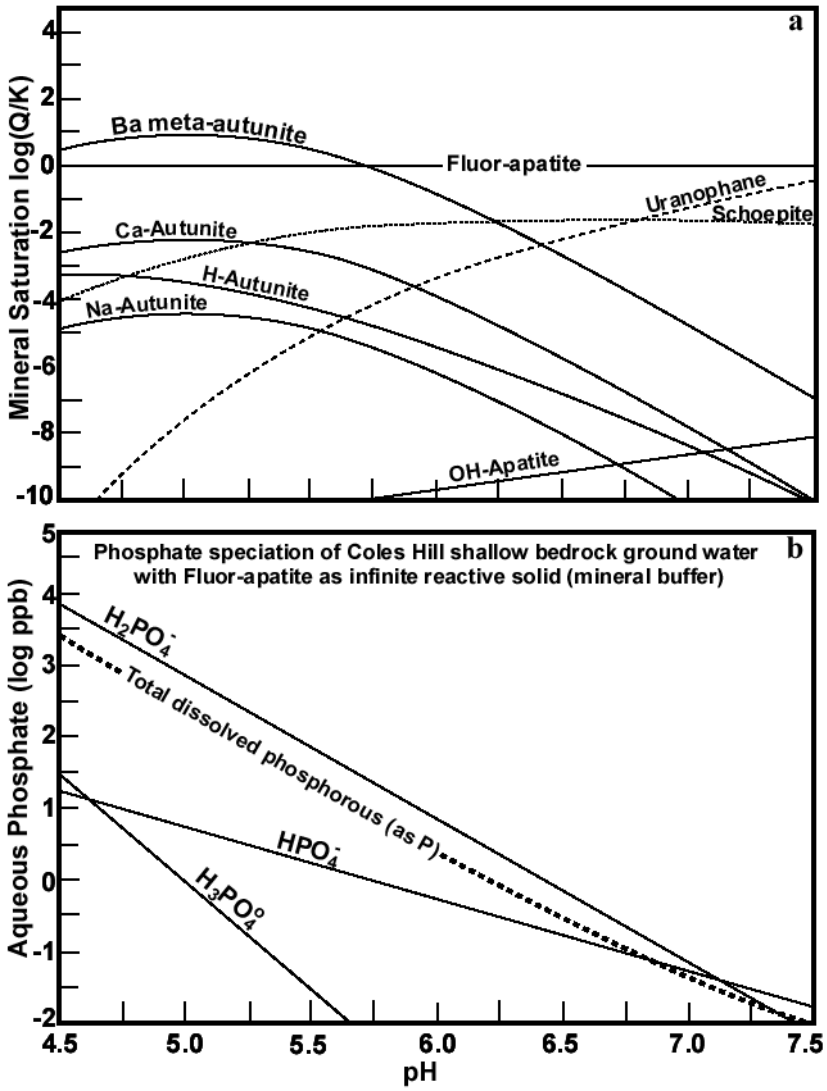

Figure 2-15. Speciation diagrams for the same ground water sample used in Figure 13 assuming that the solubility of dissolved phosphate is controlled by fluor-apatite (water composition used to produce these diagrams is shown in Table 5). Note restricted saturation domain of Ba meta-autunite due to rapid decrease in phosphate concentrations with increasing pH. (a) Solid phase speciation diagram showing saturation indices for potentially important uranium minerals plotted as a function of pH. (b) Aqueous speciation for the same ground water sample showing the predicted rapid decrease in phosphate in the pH range of 6 – 7.

Chapter 3. Mineralogical Fixation of Uranium in an Oxidizing, Saturated/Unsaturated Saprolite-Soil Column: Chemical Weathering of the Coles Hill Uranium Deposit, Virginia

Abstract

Geochemical and mineralogical studies of the twenty meter thick soil-saprolite profile developed over the Coles Hill uranium deposit, in Virginia, indicate that uranium transport may be inhibited or naturally attenuated by phosphate mineralization in oxidizing environments. The characterization of gradients in bulk geochemistry and soil pH as a function of depth within the weathered zone constrain geochemical processes that influence the dispersal of uranium within this system. Assessments of textural relations and chemical compositions of key secondary mineral assemblages reveals the distribution and mineralogical associations of uranium with depth within the profile. Speciation and mineral saturation modeling using ground waters collected from the lower portion of the saprolite-soil column has further constrained our understanding of the aqueous chemistry and mineralogical fixation of uranium within this system.

In the lower part of this profile U(VI) phosphate bearing, oxidized bedrock transitions to ground water saturated saprolites which have bulk U concentrations ranging from 1000 to 1400 ppm, and also contain abundant U(VI) phosphate minerals of the meta-autunite mineral group. Ground water samples extracted from the saturated saprolite zone that contain these U(VI) phosphate minerals have dissolved uranium concentrations ranging from 5 to 15 ppb (below the proposed drinking water standard of 20 ppb; US-EPA, 1991), and illustrates the effectiveness of the natural attenuation processes operating at this site.

Above the water table, bulk U concentrations drop to an average value of 250 ppm and the U(VI) phosphate minerals of the type found in the saturated saprolite are not present. The pH estimates of pore waters from this zone suggest that this unsaturated soil environment is too acidic for meta-autunite to be stabilized. Within this unsaturated zone uranium is primarily associated with an aluminum phosphate of the crandallite mineral group, and with P sorbed to ferric hydroxide mineral coatings. Results from field based studies of the major uranium reservoirs at Coles Hill have been supplemented by solid and aqueous phase speciation modeling. The results of this study suggest that uranium is mobilized within the relatively low pH (<5.0) unsaturated environment and is then reprecipitated below the water table as low solubility U(VI) phosphates due to near neutral pH conditions (around 6.0) and relatively high

activity ratios of dissolved phosphate to carbonate (e.g. log $[H_2PO_4^-/HCO_3^-] > -3$). This natural attenuation process may have been active for at least the past 500,000 years and thus has important implications for understanding the long term behavior of uranium within near surface environments.

Introduction

The development and implementation of scientifically sound strategies for the containment and remediation of heavy metal and radionuclide contaminants requires knowledge of the long term behavior of these elements in natural geologic systems. An element of particular concern is uranium, which occurs in high concentrations at many contaminated sites across the US (e.g. Eisenbud and Gesell, 1997) and is the major constituent of commercial spent nuclear fuel (Shoesmith and Sunder, 1992). Research over the past several decades has led to the identification and characterization of many of the fundamental environmental parameters that influence the mobility of uranium in specific types of hydrogeologic environments.

One of the most important geologic settings in this regard is Yucca Mountain site, which is being investigated as the potential disposal facility for much of the high level nuclear waste generated in the US (Nuclear Waste Policy Amendments Act, 1987). This site is promising as a long-term repository because it occurs within an arid climate and is hydrologically unsaturated, thus reducing the risk that uranium and other waste elements will enter the local hydrosphere. The Yucca Mountain project has produced a comprehensive database for understanding radionuclide transport and retardation within arid, unsaturated environments. However, due to the location of low level waste facilities and uranium contaminated sites in the eastern US, the environmental transport of radionuclides in humid, fluid-rich systems is also an important national scientific issue. This issue is currently being addressed by geochemical and mineralogical investigations of the natural attenuation of uranium at the Coles Hill uranium deposit located in Virginia (Figure 3-1).

The Coles Hill site represents an excellent locale for studying the environmental retardation of uranium in fluid saturated, oxidizing systems. The uniqueness of the site stems in part from an extensive geologic and hydrologic database generated during exploration of the deposit (which was never actually mined). One of the primary goals of the Coles Hill project is to generate a field-based data set that may be used to constrain how the processes that control

uranium dispersal vary over geologic time scales within heterogeneous rock-soil-ground water systems.

The Coles Hill deposit is located in the Piedmont Physiographic Province of Virginia and consists of two uranium orebodies (Coles Hill north and south orebodies; Figure 3-1) that connect at depth. The ore consists primarily of coffinite ($USiO_4 \bullet nH_2O$), fluor-apatite ($Ca_5(PO_4)_3F$) and uraninite (UO_{2+x}) and is hosted in cataclastic zones that cross-cut quartzo-feldspathic augen gneisses. The southern ore body has been shown to contain approximately 22 million kilograms U_3O_8 with an average grade of 0.113% (958 ppm U) (Halladay, 1989). The north ore body has similar total reserves but at a slightly lower grade (Halladay, 1989). Data collected during exploration of the deposit provides significant geologic and geochemical control on the primary ore zones (see Chapter 1). The deposit was never mined, however, and thus represents an undisturbed natural system in which processes influencing the paleo- and present-day transport and retardation of uranium can be studied. This paper examines the geochemical behavior of uranium within an oxygenated weathering profile developed over the uranium deposit. It focuses specifically on the role played by the precipitation of secondary uranium minerals, and the association between uranium and phosphorus within the environment.

Sample Collection and Analytical Methods

For this study, mineralogical and geochemical data were gathered on four representative stratigraphic columns through the weathered zone (Figure 3-1); however, most of the detailed characterization of uranium mineralogy and geochemistry were focused on holes DH1 and DH2 located near the center of the Coles Hill north orebody. Sampling of shallow zones (< 2 meters) was performed by hand augering. Sampling of deeper zones (down to 20 meters) was made possible by the Virginia Division of Mineral Resources who provided use of their auger drill rig (technical support by R. Berquist and W. Henika). Samples of weathered materials were collected from distinct saprolite/soil horizons based on variations in color, grain size and proportion of relict bedrock grains. All saprolite and soil samples were dried immediately after collection within a laminar flow, clean air (+100) environment. Representative samples retaining textural integrity were impregnated with epoxy, polished and coated with an approximately 250 angstrom thick film of carbon for analyses by scanning electron microscope (SEM), energy dispersive x-ray spectrometry (EDS) and electron microprobe (EMP). Examinations of mineral

surfaces was performed by SEM on unconsolidated samples mounted on aluminum stubs using double-sided carbon tape. All SEM, EDS and EMP analyses were performed at the Virginia Tech, Department of Geological Sciences, electron microbeam facilities using a CAM scanII electron microscope and Cameca SX-50 electron microprobe.

Hand specimens of each sample were pulverized using a tungsten carbide shatter box and samples were shipped to an internationally accredited commercial laboratory for major, minor and trace element analyses. Major and minor elements Si, Al, Fe, Mn, Mg, Ca, Na, K, Ti, P and LOI (measure of total volatile content) were analyzed by a lithium metaborate/tetraborate fusion inductively coupled plasma (ICP) technique, while all other elements were analyzed by bulk digestion, inductively coupled plasma mass spectrometry (ICP-MS). It was necessary to process relatively small sample volumes (< 0.5 kg) in order to assess each core section at the centimeter scale. Some variations in bulk concentration data may therefore contain notable geochemical "noise" caused by lithologic heterogeneity of the rock profile.

Soil pH was measured by the method of Hendershot et al, (1993). This procedure involves weighing out 10 grams of dried soil (room temperature) into a beaker, adding 20 mL of distilled/deionized water and stirring for 30 minutes, letting the mixture stand for 1 hour then measuring the pH of the supernatant with a standard pH probe. Replicates of each sample were within +/- 0.1 pH unit.

Ground waters from the base of the weathered zone were sampled at wells produced during auger sampling (e.g. from the same columns from which solid samples were taken). The water samples were obtained using polyethylene bailers after purging the wells. Dissolved oxygen and pH were measured in situ after allowing the wells to recharge after purging. All samples were filtered (0.45 micron), and samples to be analyzed for uranium and other metals were acidified to pH < 2.0 using ultra pure nitric acid. Samples were shipped to an internationally accredited commercial laboratory for analyses by ICP-MS (for cations) and ion chromatography (for anions).

Results: Rock System Description

As shown in Figure 3-2 the weathered zone overlying the Coles Hill uranium deposit consists of four chemically and physically distinct intervals. These include (from base to surface) (1) unweathered bedrock, (2) incipiently weathered bedrock that is pervasively "stained"

by ferric oxide and oxy-hydroxide mineral coatings, (3) saprolite (C) soil horizon consisting of soft, incoherent material that forms in place by chemical weathering and retains structures present in the underlying, unweathered bedrock, (definition paraphrased from Jackson, 1997) and (4) unsaturated pedogenic soils (O, A, B soil horizons; terminology from Foth, 1984). In the study area the water table occurs within the C horizon, therefore, this interval may be subdivided into a ground water saturated saprolite zone and an unsaturated saprolite zone.

The Coles Hill weathering profile is typical of weathered zones developed from crystalline bedrock in the eastern US and is particularly similar to the rock/saprolite/soil sequence investigated in detail by Pavich, et al. (1985) and Pavich (1986, 1989). For example, as with the Coles Hill site, this sequence also occurs in the Virginia Piedmont, is formed from quartzo-feldspathic bedrock (Occoquan Granite), has a similar thickness as the study area profile, and contains similar chemically and physically distinct intervals (listed above). The work by Pavich, et al. (1985) and Pavich (1986, 1989) thus provides a useful background data set that can be used in the present study to better understand the saprolite/soil forming processes and thus enhance our ability to identify and model the key chemical weathering processes responsible for the distribution of uranium within the Coles Hill profile.

Unweathered bedrock

The host rocks of the primary (hydrothermal) uranium ore zones are albite-quartz-chlorite/biotite-oligoclase-microcline augen gneiss interlayered with albite-chlorite/biotite-reibeckite/hornblende amphibolites (see Chapter 1). The majority of the uranium ore within the study area is hosted within the the augen gneiss. Samples of this lithology are light to dark gray and contain a penetrative northeast striking, southeast dipping foliation defined by relict biotite and chlorite. The foliation is cross-cut by both barren and uranium ore-bearing fracture zones.

Incipiently weathered, oxidized bedrock

The interval of incipiently weathered, ferric iron stained bedrock varies from 1 to 8 meters in thickness due to variations in the relative abundances of hydrologically active fractures. This partially weathered, but intact bedrock has the same major mineral composition as the underlying augen gneiss; but also contains textural evidence for the weathering reactions:

chlorite → vermiculite + $Fe(OH)_3$ and albite → kaolinite. This iron redox transition within the Coles Hill profile has been described in Chapter 2 of this work.

Saprolite (C-horizon)

As with most Piedmont weathering zones, the thickest interval within the Coles Hill profile is the saprolite zone. Within the study area the thickness of this interval varies from 25 meters under hill crests to 10 meters below surrounding low lying pastures. This interval contains the water table, which also varies in depth as a function of topography (Figure 3-2). Thus observations made at the Coles Hill site agree with the observation of Pavich (1986) that within a given Piedmont drainage basin the saprolite represents an important porous and permeable ground water reservoir.

Hand-samples of both saturated and unsaturated saprolites contain centimeter to millimeter thick interlayers of reddish brown, orange yellow and white powdery material that parallel the strike and dip of the relict foliation and compositional layering. Texturally the saprolite is classified as a sandy-clay, however, it locally contains lenses and layers of a dark red, finer-grained material that also parallel the relict foliation. Black lenses consisting of compositionally variable manganese oxides (composition determined by SEM-EDS and EMP; discussed below) are locally present within the plane of the relict foliation as well as along surfaces of steeply dipping open fractures (joints) with apertures of approximately 0.5 to 1 millimeter. These observations suggest that in addition to flow thorough macroscopic pore spaces, ground waters within the saprolite zone may also be channeled along the relict foliation surfaces as well as discontinuous open fractures. Similar types of flow paths were documented for the Virginia Piedmont saprolite zone studied by Pavich (1989).

Pedogenic soil (O, A and B horizons)

The pedogenic soil interval varies in thickness from 3 to 5 meters throughout the study area. It consists of an upper 5 – 10 centimeter O horizon characterized by dark brown organic rich material containing abundant plant roots and leaf litter. This is underlain by an approximately 40 centimeter thick A horizon, which is light brown to reddish brown in color and contains localized plant roots and minor lenses of dark brown organic rich material (e.g. decaying plant tissue). This is underlain by a 60 – 100 centimeter thick dark red, fine-grained

(silty clay to clay) B horizon which is devoid of macroscopically observable organic matter (soil horizon terminology from Foth, 1984).

Age of weathering profile

The Coles Hill saprolite/soil column has not yet been dated directly, however, its age is constrained by studies of the rates of saprolite production in similar weathering profiles in the Piedmont physiographic province of the eastern US (Thomas, 1994). For example, using Be^{10} methods Pavich (1985) calculated a rate of saprolite production of 20 meters per million years for the Occoquan granite saprolite profile located in northern Virginia. Using stream base-flow geochemistry, Pavich (1986, 1989) also calculated a minimum saprolite production rate of 4 meters per million years for the same profile. Similarly, a mass balance study of saprolite formation in the Maryland Piedmont by Cleaves et. al. (1970) yielded formation rates ranging from 5 – 8 meters per million years. These studies thus suggest a range of saprolite formation rates of 4 – 20 meters per million years, for the mid-Atlantic to southeastern Piedmont Province.

Using the maximum rate of saprolite production measured by Pavich (1989) and given the average saprolite zone thickness of 10 meters for the Coles Hill site (Figure 3-2) the suggested minimum age for the study area profile is 500,000 years. This estimate provides a general constraint for the time scale over which the processes controlling the distribution of uranium have been active within the weathered zone overlying the Coles Hill deposit and further illustrates the uniqueness of the Coles Hill site for study of the long-term geochemical behavior of uranium within a fluid rich, oxidizing environment.

Uranium Mineral Petrography and Mineral Chemistry

The mineralogy of the Coles Hill weathering profile varies continuously as a function of depth, with each horizon bearing distinct mineral assemblages that reflect the variations in the extent of chemical weathering. Although uranium mineralogy is variable from zone to zone, there is a general association between phosphorous and uranium throughout the profile (e.g. by sorption or macroscopic mineral precipitation). Thus, an understanding of the processes that control uranium mobility at the Coles Hill site requires detailed characterization of the mineral textures, paragenesis, and mineral chemistry of these distinct uranium mineral zones.

Unweathered primary ore host rocks and oxidized bedrock zones

The primary uranium ore consists of three distinct fracture hosted assemblages (listed in order of relative age, oldest first): (1) coffinite ($USiO_4 \bullet nH_2O$)–apatite associated with albite, chlorite, anatase and sulfides, (2) uraninite/coffinite–calcite associated with sulfides, (3) uraninite/coffinite – Ba zeolite (harmotome) associated with anatase and sulfides. Based on the common occurrence and uniform distribution of the coffinite-apatite zones within cores, it is estimated that the majority of the total uranium reserves for the deposit are associated with this assemblage. Within shallow bedrock core sections the gray host rocks containing the primary ore abruptly transition to a zone of pervasively ferric iron "stained" rock in which the feldspars are partially weathered and the primary U(IV) phases have been altered to produce U(VI) assemblages (see Chapter 2).

The dominant U(VI) mineral in the oxidized bedrock zone is the Ba end member of the meta-autunite mineral group (meta-uranocircite) (see Chapter 2). It was also found that this secondary uranium phosphate occurs approximately 1 cm below the ferrous/ferric "staining" front suggesting that oxygenated waters capable of precipitating U(VI) phases are present in advance of the iron redox interface. These studies of the redox transition zone (as defined by the Fe(II)/Fe(III) and U(IV)/U(VI) couples) suggest that the volume of rock represented by the shallow cores from the Coles Hill deposit has acted as a closed system with respect to uranium transport. This is supported not only by petrographic observations (e.g. widespread, uniform occurrence of U(VI) minerals) but also by whole rock geochemistry that show both oxidized and reduced sections of core have the same range in bulk uranium (500 – 1000 ppm). The geochemistry and mineral chemistry of the primary ore and secondary U(VI) assemblages that occur in the oxidized bedrock zone are discussed in Chapters 1 and 2.

Saturated saprolite (lower C horizon)

Uranium within the ground water saturated saprolite zone is also associated with U(VI) phosphate minerals of the meta-autunite group. They are readily identifiable in both hand sample and thin section based on their color (lemon yellow), strong fluorescence (green) in ultraviolet light and distinct [001] basal cleavage. In hand sample these U(VI) phosphates are most commonly disseminated throughout a matrix consisting mostly of kaolinite, partially weathered albite and quartz (Figure 3-3). However, they locally occur in 1 – 5 mm long grain aggregates

(Figure 3-3) and in discontinuous linear bands of individual crystals that parallel relict foliation surfaces. Petrographic examination reveals three distinct textural forms: (1) 100 – 500 micron long single grains or grain aggregates disseminated throughout a matrix of iron oxy-hydroxide coated clay minerals, weathered feldspars and relic quartz (Figure 3-4b), (2) 0.5 – 1 millimeter long grain aggregates associated with relict quartz grains, (3) 20 - 40 micron long grains, that are disseminated throughout the clay rich (mostly kaolinite) matrix (Figure 3-4a,c). These finer-grained U(VI) phosphates are also locally concentrated within 1 cm long, 5 mm thick lenses of black granular material consisting mostly of 5 – 10 micron diameter barium-calcium manganese oxide grains(Figure 3-4d).

A sample from 18.3 meters depth in auger hole DH1 also locally contains trace amounts of relict aggregates of oxidized bedrock that are coated with 500 micron long, meta-uranocircite crystals intergrown with botryoidal barium-calcium manganese oxides. This assemblage is identical in form and composition to the type I meta-uranocircite assemblage observed within the underlying oxidized, uranium ore zone (see Chapter 2). The presence of these aggregates within the saprolite zone thus suggests that the meta-uranocircite formed during the initial stages of oxidation of the primary ore is stable or at least meta-stable within the groundwater saturated saprolite zone. However, the abundance of all U(VI) phosphate decreases abruptly above the present-day water table.

U(VI) phosphate mineral chemistry

The XRD pattern for a typical heavy mineral separate (specific gravity > 2.9) of saprolite from below the water table is shown in Figure 3-5a. These data exhibit significant peaks for apatite (relict) and meta-uranocircite as well as kaolinite. Major element compositions of the meta-uranocircites were characterized by EMP (Table 3-1 and Figure 3-6). These data indicate that unlike the compositionally uniform meta-uranocircite that occurs in the oxidized bedrock zone the U(VI) phosphates occurring in the saturated saprolites have variable compositions that range from $(Ba(UO_2)_2(PO_4)_2{\bullet}nH_2O)$ to $(Ba_{0.1}Ca_{0.9})(UO_2)_2(PO_4)_2{\bullet}nH_2O)$ to $(Ba_{0.1}Ca_{0.7}Sr_{0.1})(UO_2)_2(PO_4)_2{\bullet}nH_2O)$. This compositional variation is present within single grains that show an interlayering of calcium rich zones within crystals that are dominantly of the barium rich end member, meta-uranocircite. The layers are 1 to 5 microns in thickness,

discontinuous and parallel the "mica-like" interlayer site marked by a perfect {001} cleavage (Figure 3-6).

The observed compositional variation noted within single U(VI) phosphate grains from the saturated saprolite zone is interpreted to have resulted from an ion exchange process along the [001] crystallographic direction. This plane corresponds to the interlayer site of the autunite and meta-autunite structure which accommodates hydrated alkali, alkaline and metal cations. For the Coles Hill meta-autunite minerals this exchange process can be written as: $Ba(UO_2)_2(PO_4)_2 \bullet nH_2O + Ca = Ca(UO_2)_2(PO_4)_2 \bullet nH_2O + Ba$. A similar type of compositional interlayering in natural autunite minerals has been observed in samples from the Shinkolobwe uranium deposit in central Africa (Suzuki, et. al., 1998). However, unlike the Coles Hill samples the mixed-phase autunites from Shinkolobwe contain nannometer-scale, interlayers of a magnesium end member, saleeitie and a copper end member, metatorbernite (Suzuki, et. al., 1998).

Uranium mineralogy in unsaturated saprolites and pedogenic soil

In the unsaturated saprolites and pedogenic soil zones uranium is also coupled with phosphorus, however, the mineralogy controlling this association is significantly different from that observed in the saturated zones. The two main sinks for uranium in the unsaturated horizons are: (1) uranium associated with an aluminum phosphate mineral of the crandallite group (Figures 3-7 and 3-8), (2) uranium associated with phosphorus and iron oxy-hydroxide mineral coatings (Figures 3-9 and 3-10).

The XRD pattern for a typical heavy mineral separate (specific gravity > 2.9) from the pedogenic soil zone is shown in Figure 3-5b. These data exhibit significant peaks for crandallite and minor peaks for goethite and hematite, as well as quartz and kaolinite (present due to non-ideal mineral separation). The crandallite group mineral occurs in two textural forms: (1) as large (100 to 500 microns long) irregularly shaped grains associated with relict quartz and intergrown with botyroidal (Ca, Ba) manganese oxides (Figure 3-7a,b,c), (2) irregular masses (50 – 100 microns in diameter) that surround other soil minerals (quartz, kaolitite, weathered feldspars) (Figure 3-7d). Electron microprobe data for the crandallite (Table 3-2) indicates that it generally contains 31 weight percent Al_2O_3, 26 weight percent P_2O_5, 2 weight percent CaO, 2.5 weight percent SrO, 15 weight percent BaO and 1.4 weight percent UO_3. Crandallite minerals of similar

composition (Ca-Ba) have also been shown to contain up to 1.3 wt% UO_3 (Sadig et. al., 1988). It is not clear if uranium associated with the crandallite grains is present within the crystal lattice, as inclusions or as an adsorbed species; however, microprobe transects across selected grains reveal that uranium is positively correlated with phosphate, and negatively correlated with manganese (Figure 3-8). The samples with higher phosphate abundance are interpreted as relatively pure crandallite analyses (devoid of kaolinite and manganese oxide inclusions) while the manganese rich areas are likely the result of both crandallite and intergrown manganese minerals. Thus, within these zones uranium is partitioned into the Al phosphates to a greater extent than into the manganese oxides.

The association between uranium, phosphorus and iron oxy-hydroxide minerals is less well understood. Textural examples of this association are shown in Figure 3-9, and are chemically characterized in Figure 3-10 and Table 3-3. A representative analyses of one of these zones contains 43 weight percent Fe_2O_3(total), 7 weight percent P_2O_5 and 6 weight percent UO_3, as well as 5 weight percent Al_2O_3 and 10 weight percent SiO_2 from the kaolinite, quartz substrate. The chemical data show positive correlations between BaO vs UO_3 as well as P_2O_5 vs UO_3. The phosphate vs uranium correlation is somewhat diffuse due to two samples that have high uranium and low phosphate relative to the other samples. These two samples correspond to ones with relatively low total iron. No discrete uranium phosphate minerals have been identified by SEM within these zones. Furthermore the ratios of P_2O_5 to BaO and P_2O_5 to CaO are too high in these areas to be explained solely by the presence of meta-autunite minerals. This suggests that these correlations may reflect sorption process. Non uranium bearing iron phosphate minerals (strengite?) occur as accessory minerals within many unsaturated zone samples (Figure 3-9c). These grains generally occur as 15 micron wide fibrous masses with a radial growth pattern and generally occur near colliform (Ca, Ba) manganese oxides (Figure 3-9c).

To better understand the processes leading to the formation of the mineral assemblages discussed above these textural and mineral chemical data are supplemented by bulk geochemical analyses of representative saprolite/soil columns overlying the Coles Hill deposit.

Bulk Geochemistry

Concentration profiles of key elements within the Coles Hill weathered zone have been used to characterize the dominant soil forming processes controlling the dispersal of uranium within this system. Analyses were preformed on representative samples from auger holes DH1, DH2, DH3, DH5 and DH6 (see Figures 3-1 and 3-2 for locations). The following discussion will focus on auger hole DH1 and DH2 which sample profiles formed from chemical weathering of the primary Coles Hill deposit. Data from the other auger holes will be discussed in support of observations made from the DH1 and DH2 columns.

Major element bulk geochemistry

The bulk chemistry of the Coles Hill weathered zone is dominated by five major constituents: SiO_2, Al_2O_3, Na_2O, total iron (reported as Fe_2O_3) and loss on ignition (LOI: measure of total volatiles) (Tables 3-4 and 3-5). When plotted as a function of depth within the weathered column (Figure 3-11) these parameters show discontinuities corresponding to the four mineralogically distinct saprolite/soil zones discussed above (Figure 3-2b).

The saturated saprolites (lower C-horizon on Figure 3-2b) are characterized by SiO_2, Al_2O_3, Na_2O and Fe_2O_3 concentrations similar to those found within the unweathered bedrock underlying this part of the study area. Alumina and silica, however do show subtle gradients within this zone. For example, in both DH1 and DH6, SiO_2 varies from around 67 weight percent at the deepest samples to approximately 64 weight percent near the water table; conversely, Al_2O_3 varies from approximately 16 weight percent in the deepest sample up to around 20 weight percent near the water table. A similar gradient in Al_2O_3 is also present in the saturated saprolite zone of DH2; however, SiO_2 concentrations in this hole are relatively constant and similar to bedrock values of 67 weight percent. Loss on ignition values in the saturated saprolites are on average twice as high as those found in the underlying unweathered rock (2.0 vs. 4.0 weight percent respectively). This suggests that volatiles added to the bulk solid during chemical weathering are present even in the lowest portions of the saprolite/soil column.

In the unsaturated saprolite zone, there are pronounced gradients in Na_2O and LOI. For example, in all auger holes associated with the Coles Hill north orebody (DH1, DH2 and DH6) Na_2O values decrease continuously from greater than 6 weight percent below the water table to less than 1 weight percent within the upper 2 meters of the profile. Over the same interval LOI

varies from less than 4.0 weight percent for samples from below the water table to greater than 10 weight percent in samples from the upper two meters. The gradients for Al_2O_3 and Fe_2O_3 in these holes are similar to the LOI in that they increase in concentration towards the surface.

The Al_2O_3 and Fe_2O_3 gradients, however, are most pronounced in the upper five meters of the profile. For example, in the representative auger hole DH1 there is a increase in Al_2O_3 content from less than 20 weight percent below 5.0 meters depth to greater than 25 weight percent from 5.0 – 0.6 meters depth (B-horizon on Figure 3-2b). The abundance of aluminum then decreases back down to 20 weight percent at less than 0.6 meters depth. This Al_2O_3 increase is also evident in the DH2 column (Figure 3-12). Similarly iron increases from less than 4 weight percent below 5.0 meters depth to greater than 5 weight percent in the shallower region. The depth profile for silica in this zone is antithetic to alumina. For example in DH1, SiO_2 varies from greater than 64 weight percent below 5.0 meters depth to less than 60 weigh percent above 5.0 and then increases back to values greater than 65 weight percent near the surface (less than 0.6 meters depth). Macroscopic examination of this upper interval reveals that the increase in silica within the upper 60 centimeters of the profile corresponds to an abundance of relict quartz grains (sand to gravel size). Soil forming processes responsible for the major element concentration trends have also influenced the depth profiles of minor and trace elements.

Selected minor and trace element bulk geochemistry

Abundances of minor and trace elements that reflect processes influencing the dispersal of uranium within the Coles Hill weathered zone are those associated with the primary and secondary phosphate mineral assemblages (P, Ca, Sr, Ba, Ce) and are given in Tables 3-4 and 3-5. Titanium and zirconium concentrations were also measured to assess changes in bulk mass (volume) throughout the soil profile.

In both DH1 and DH2 phosphorus and calcium show peak concentrations below the water table (greater than 3000 and 5000 parts per million respectively). The covariance of these two elements suggests that measured abundances are controlled by apatite. This is also supported by the observation that relict rock fragments containing apatite persist near the base of the DH1 column. Auger hole DH6 does not show this apatite control because it is on the periphery of the deposit, and therefore the underlying bedrock contains relatively low amounts of the apatite-coffinite ore assemblage. Within the shallow portion of the saturated saprolite zone and above

the water table both phosphorus and calcium concentrations decrease and the trends are no longer parallel (Figures 3-11 and 3-12). This suggests that, within the shallow saturated zone, as well as in the unsaturated zone apatite is no longer the dominant mineral controlling these profiles.

Strontium, barium and cerium concentrations are all relatively constant from below the water table up to three meters depth in auger holes DH1, DH2 and DH6 (Figures 3-11 and 3-12). At depths ranging from 2.1 meters to 0.6 meters depth in DH1 strontium, barium and cerium concentrations increase by a factor of at least two. These zones also correspond to peaks in phosphorus abundance. Unlike those noted in DH1, the strontium, barium and cerium rich region of the DH2 column (3.4 meters) includes abundant lenses of black granular manganese oxide minerals such as those discussed earlier (e.g. Figure 3-9). This zone contains approximately 8270 parts per million manganese, which is 17 times greater than the average value for the entire Coles Hill profile.

In DH1, DH2 and DH6 titanium concentrations increase with decreasing depth. For example in DH1 titanium concentrations are around 3000 parts per million within the saturated saprolite zone and increase to values greater than 4000 parts per million within the upper 5 meters of the profile. Zirconium concentrations also increase as the surface is approached within the weathering profile. The range of zirconium concentrations within the DH1 and DH2 columns is generally from 200 to 400 parts per million and the depth profiles for this element are relatively discontinuous due to the spatial heterogeneity of zircon distributions within the primary host rock. The relative increases in titanium and zirconium in the upper parts of the weathering profile may reflect secondary enrichment due to removal of other materials (e.g. by leaching) from the upper part of the column. This concept is explored in more detail below.

Bulk uranium with depth

The soil forming processes responsible for the bulk geochemical trends described above have also strongly influenced the distribution of uranium within the Coles Hill weathering profile. In both of the auger holes drilled directly over the Coles Hill north orebody (DH1 and DH2) the uranium depth profile shows a pronounced peak associated with the water table. For example, saturated saprolites from both holes contain over 1200 parts per million uranium within the zone of seasonal water table fluctuation. In DH1 uranium content remains around 1000 parts

per million below the water table (Figure 3-11). In DH2, however, the uranium content drops to values ranging from 200 to 600 parts per million below the uranium peak (Figure 3-12), auggesting that the lower portion of the saturated saprolite zone in DH2 formed from rocks containing less primary uranium that those from which the DH1 saprolites formed.

In the unsaturated zones of both DH1 and DH2 uranium concentrations decrease to values ranging from 200 to 300 parts per million in the B-horizon (Figures 3-11 and 3-12) to less than 70 parts per million within the upper meter of the profile. As shown in the DH1 profile, uranium concentrations in the unsaturated zone are relatively uniform (Figure 3-11) suggesting that this column has reached a steady state with respect to it uranium retardation capacity.

Uranium depth profiles from two holes off the deposit were characterized for comparison. The DH3 saprolite/soil column, which formed from a non-mineralized quartzo-feldspathic host rock, has uranium concentrations that range from 6.6 parts per million at the base of the hole (8.5 meters depth) up to approximately 10 parts per million in the upper meter. Limited samples from auger hole DH5 indicate that soils formed from the Triassic sedimentary rocks that are down the hydrologic gradient from the deposit also contain approximately 10 parts per million uranium (in both saturated and unsaturated zones). Thus, despite the relatively high uranium concentrations in the saprolites and soils formed over the Coles Hill north orebody (>1000 ppm) there is no evidence for the lateral dispersion of uranium from the mineralized zone.

Bulk Mass Loss Associated with Chemical Weathering of the Coles Hill Ore

Three possible models are considered for relating the concentration gradients in uranium and major elements present within the Coles Hill profile: (1) the variations reflect pre-existing lithologic heterogeneity of the protolith (closed system behavior), (2) an element may be artificially “enriched” or “depleted” by the removal (leaching) or addition (deposition) of other major elements (bulk mass change), (3) enrichments or depletion may be due to actual precipitation or dissolution of an element or by sorption or desorption processes. Thus in order to constrain which of these explanations applies to (or most strongly influenced) a given concentration profile, it is necessary to take into account any bulk mass loss or gain within the profile. This is accomplished by normalizing the concentration data from the weathered profile to

corresponding data for the unweathered protolith (e.g. Goldich, 1938; Krauskopf, 1967; Nesbitt and Wilson, 1992; Langmuir, 1997).

Based on its location, geologic setting and geochemistry the unweathered portion of core section 41-173 was chosen as the protolith for the DH1 saprolite-soil profile (for discussion of core see Chapter 2). A sample from 28.4 meters depth was chosen for the calculations because it most closely matches the "typical" Coles Hill primary ore in terms of uranium grade, phosphorus content, grain-size and structure (e.g. ore bearing brittle fractures cross-cutting protomylonitic foliation).

The percent mass loss for individual samples in the DH1 saprolite/soil column were estimated by assuming that titanium and zirconium remain immobile (conservative) during the weathering process. This assumption has been used successfully in numerous other weathering studies (e.g. Nesbitt and Wilson, 1992; Nesbitt and Markovics, 1997) and is supported at the Coles Hill site by the observation that anatase/rutile grains (dominant titanium mineral) and zircon (dominant zirconium mineral) show little signs of chemical alteration throughout the profile. The zirconium concentrations, however, do show some variation (e.g. Figure 3-11) suggesting heterogeneous distributions of zircon within the primary ore and host rocks. Thus, titanium has been used as the normalizing parameter for this study.

To calculate the bulk mass loss within the profile (DH1 and DH2) major and trace element data from soils and saprolites were normalized based on the titanium concentration of their protolith (2818 ppm in drill core 41-173-28.4). The calculations were performed using the method demonstrated by Langmuir, 1997 (volatile content of weathered samples estimated by LOI). The bulk mass loss of the DH2 profile was calculated using the same representative protolith sample. Mass change results for the DH1 and DH2 profiles are shown in Figure 3-13.

Bulk mass loss as a function of depth

Within the saturated saprolite zone of DH1 (18.3 to 11 meters depth) bulk mass loss varies from 4% at the base to 15% near the water table (top of this interval). In the overlying lower unit of the unsaturated saprolites (10.4 to 5.5 meters depth) bulk mass loss varies discontinuously from 18% in lower samples up to 26% in upper portions of this interval. The values continue to increase in the upper unsaturated saprolite zone from 28% mass loss at the base to a maximum value of 50% mass loss in the upper portion of this interval. In the upper

part of the profile (2.1 meters depth to ground surface) the mass loss varies discontinuously from 35% to 45%. Although mass loss variations are not continuous within individual horizons the overall trend in the DH1 profile is that samples at the base of the column have experienced minor to negligible mass change while those higher in the column have experienced up to 50% bulk mass loss. The apparent "noise" within this profile may reflect minor inherent lithologic heterogeneity rather than true variations in mass loss.

The DH2 column shows the same overall trend for bulk mass change with the percentage of mass loss increasing towards the surface for most of the profile. However, the extent or absolute amount of mass loss experienced by this profile is lower than DH1. For example, bulk mass change estimates from below the water table in DH2 yield values ranging from 9% mass loss to 3% mass gain with an average value near zero suggesting that the mass loss within the saturated saprolite zone in this profile is negligible. Above the water table, however, mass loss estimates increase to a range of 30% to 46% which is comparable to those found in DH1. Thus, although the two profiles show similar overall trends and maximum mass loss values in the unsaturated zone these data suggest that DH2 is not as extensively chemically weathered as the DH1 profile.

Studies of mass changes in another Virginia saprolite weathering profile (Occoquan profile of Pavich, 1986 and 1989), analogous to the Coles Hill study area, yielded maximum bulk mass loss values of 75%. This value is higher than the maximum measured in the Coles Hill study area (50%); however, the ranges of mass loss values from the two sites are comparable. The similarities in bulk mass loss and major element data from the Occoquan and Coles Hill sites thus suggest that the chemical weathering processes responsible for the concentration profiles are not site specific, but represent fundamental mechanisms for soil development in the Mid Atlantic to south eastern regions of the US. Furthermore, these types of geochemical trends have also been observed in relation to lateritic soil development (e.g. Warber, et al., 1992) suggesting the global significance of these processes.

Major, Minor and Trace Element Enrichment/Depletion

In order to constrain the processes causing the bulk mass loss trends for the Coles Hill weathered zone as well as to assess the relative enrichments and depletions of key minor and trace elements the mass gain/loss percentages for individual elements were calculated using the

titanium normalized concentration data from the DH1 and DH2 profiles. Individual gain/loss values were calculated using the following relation: $(100 \times [C^{i}_{\text{Weathered sample}} - C^{i}_{\text{Protolith}}] / C^{i}_{\text{Protolith}})$ (where C = concentration in ppm of element i). The representative DH1 profile is used to describe enrichment/depletion trends and the percent loss/gain for selected elements in the DH1 are given in Table 3-6.

Sodium is depleted throughout the profile but the extent of deletion varies continuously from 7 percent loss at the base to 99 percent loss in the near surface. The aluminum gain/loss profile is erratic, but generally shows minor enrichment towards the base of the profile (approximately 7 percent gain in the saturated saprolites) and more significant enrichment (up to 25 percent gain) within the upper five meters of the unsaturated zone. This enrichment zone corresponds with the aluminum concentration increase shown in Figure 3-11. Silicon is depleted throughout the profile with the extent of depletion varying from approximately 15 percent loss in the saturated saprolites to approximately 50 percent within the upper five meters of the unsaturated zone. The iron gain/loss profile is also erratic showing regions of both minor enrichment and depletion within the saturated saprolites and lower unsaturated zone. Within the upper five meters of the profile, however, iron is consistently enriched to as much as 85 percent gain. The total volatile content (as monitored by LOI) is enriched throughout the profile but the extent of enrichment increases in magnitude towards the surface. For example, within the saturated saprolites LOI shows a 40 – 80 percent gain while in the upper five meters of the unsaturated zone enrichment values are consistently over 300 percent.

Although the entire profile is depleted in both phosphorus and calcium relative to the underlying uranium ore bearing bedrock, the lower portion of the saturated saprolite zone is less depleted in these elements than the rest of the column. This observation is interpreted to reflect the loss of primary apatite (e.g. by dissolution) within the lower portion of the weathering profile. Calcium is depleted by approximately 65 percent in the lower part of the saturated saprolite zone and by greater than 90 percent throughout the rest of the profile. Phosphorus is depleted by approximately 40 percent within the lower portion of the saturated saprolites but shows depletion values greater than 80 percent for all but two of the other samples in DH1. These two samples have depletion values of 61 and 67 percent and are 0.6 and 2.1 meters depth respectively.

Strontium is depleted by approximately 45 percent in the lower saturated saprolite but increases in depletion to values as high as 85 percent in the upper five meters. However, this trend becomes discontinuous within the upper two meters, showing significant enrichments of 100 percent and 13 percent at depths 0.6 and 2.1 meters. Barium shows a similar pattern with 30 percent depletion in the saturated saprolites and up to 70 percent depletion in the unsaturated zone. The barium depletion value drops to 5 percent at 2.1 meters and changes to 78 percent enrichment at 0.6 meters. The cerium trend is more erratic varying between 20 percent depletion and 20 percent gain throughout the profile. This trend does however show significant enrichments of 193 percent and 143 at depths 0.6 and 2.1 meters respectively.

The uranium gain/loss trend shows 13 percent gain in the saturated saprolites and progressive depletion from 20 percent loss within the zone of water table fluctuation to values around 90 percent in the upper five meters. Similar to the profiles just described uranium is less depleted at depths 0.6 and 2.1 meters depth where it records 86 percent and 77 percent depletion respectively. The enrichment/depletion trends for these major, minor and trace elements reflect four dominant mineralogical trends described above: (1) progressive conversion of albite to kaolinite throughout the profile, (2) dissolution of apatite in the lower part of the profile, (3) formation of U(VI) phosphate minerals of the meta-autunite group below the water table, (4) formation of crandallite group minerals in the upper part of the profile (especially evident at depths 0.6 and 2.1 meters depth). In order to further constrain the geochemical processes responsible for these trends ground waters from the saturated portion of the weathering zone have been used to assess both the solid and aqueous speciation within this system.

Uranium Mineral Stability and Aqueous Speciation

The chemistry of filtered (0.45 microns) ground waters from the saprolite aquifer overlying the Coles Hill north orebody are shown in Table 3-7. The data suggests that oxygenated waters (up to 8 ppm dissolved oxygen) in contact with uranium rich saprolite (up to 1000 ppm in bulk solid) contain 3 to 5 parts per billion dissolved uranium. Similar observations of low uranium concentrations in ground waters in equilibrium with autunite have been reported by Dall'aglio et al, (1974). This work, which was a study of secondary uranium mineralization in the Sila Plateau in Calabria Italy, reported uranium concentrations as low as 0.55 parts per billion for waters believed to be in equilibrium with autunite (Dall'aglio et al, 1974). In order to refine

our understanding of the process responsible for the retardation of uranium transport at the Coles Hill site, ground waters from the saturated saprolite zone have been used to assess both the solid and aqueous speciation of uranium for this system.

The saprolite ground waters have similar compositions to those sampled from the underlying shallow bedrock region (e.g. Table 2-5). This is most likely due to infiltration of waters from the saprolite zone into the underlying bedrock zone. This interpretation is in accord with studies of vertical hydraulic head relationships studied by the Marline Uranium Corporation (1983).

For mineral stability assessments the activities of ions in solution were calculated using the "Geochemists Workbench" software package (Bethke, 1998) which employs an extended form of the Debye-Huckle equation (Helgeson, 1969). Solubility data for meta-uranocircite, coffinite, uranophane, and schoepite are from Vochten et. al., (1992), Hemingway (1982), Nguyen, et. al., (1992), and Grenthe et. al., (1992) respectively. Fluor-apatite and hydroxy-apatite solubility data are from Woods and Garrels (1987). Solubility data used for autunite (Ca end member) and H-autunite are from Muto, (1965) and Grenthe et. al., (1992) respectively, the data for saleeite (Mg-autunite), Na-autunite, and K-autunite are from Magalhaes et. al., (1985) and variscite and strengite are from Lindsay (1979). Stability data for all aqueous species are from Grenthe et. al., 1992.

Figure 3-14 shows the Eh-pH diagram for the saturated saprolite zone overlying the Coles Hill north orebody. In comparison to the oxidized bedrock zone the stability field of the U(VI) phosphate has a more narrow pH range for the saprolite ground water due to relatively lower phosphate and uranium concentrations. Also shown on Figure 3-14 is the estimated reaction path way for the weathering of the Coles Hill uranium ore. The path starts in the coffinite field at low pH (unoxidized bedrock zone) and moves up in Eh at a pH of 6.0 (measured value for both saprolite and bedrock ground waters) and crosses the coffinite/meta-uranocircite boundary at an Eh of approximately 100 millivolts. This transition closely corresponds to the ferrous/ferric iron redox transition (see Chapter 2). Further up in the profile (unsaturated zone) the estimated pore water pH drops from 6.0 to around 4.5. As shown on Figure 3-14 this shift could lead to destabilization of the meta-autunite group minerals thus explaining the rarity of these minerals within the unsaturated portion of the column.

Figure 3-15 shows saturation indices (SI = $\log_{10}$[ion activity product/solubility product of mineral]) for important uranium and phosphate minerals calculated using the saprolite ground water chemistry. The mineral stability modeling indicates that over a pH range of 5.3 to 7.5 saprolite water is supersaturated with respect to Ba meta-autunite (SI of approximately 1.0). Over this same range the solution is undersaturated with respect to other uranyl phosphate phases such as autunite (Ca end member), chernikovite (H-autunite), saleeite (Mg-autunite), torbernite (Cu autunite), Na-autunite and K-autunite all of which have saturation indices below –2.0. Other important U(VI) phases such as schoepite and uranophane are also undersaturated in these waters.

Aqueous speciation of saprolite aquifer ground water is shown in Figure 3-15b. Similar to speciation of ground waters from the underlying oxidized bedrock the dominant species at low pH (< 5.0) are predicted to be UO_2^{2+} and UO_2F^{+}. At a pH of approximately 5.5 uranium is predicted to form a uranyl phosphate complex (e.g. $UO_2HPO_4^{o}(aq)$) while at pH > 5.5 its speciation will be dominated by carbonate complexes such as $UO_2CO_3^{o}(aq)$ with $UO_2(CO_3)_2^{2-}$ (species stability constants form Grenthe, 1992). These modeling results again demonstrate that higher bicarbonate and pH values favor the formation of stable uranyl carbonate complexes which may facilitate the aqueous transport of relatively high concentrations of uranium.

Therefore, as discussed in Chapter 2, the key parameter influencing the stability of the U(VI) phosphate minerals is the ratio of dissolved phosphate to carbonate. Low values of this ratio enhance the solubility of uranium by the formation of stable uranyl carbonate complexes. Thus, in order to constrain the systematics of uranium geochemistry in this environment it is necessary to identify the processes that control inorganic phosphate concentrations within the different geochemical reservoirs of the Coles Hill profile.

Over the pH range of interest within the saturated saprolite zone (5.0 to 7.0) apatite is likely to control the dissolved phosphate levels. The solubility of fluor-apatite over this range varies from approximately 10^{-5} molar phosphate at pH near 5.0 to less than $10^{-8.5}$ molar phosphate at pH 7.0 (Fig 3-16). Hydroxy-apatite is relatively soluble, varying from near $10^{-2.5}$ molar phosphate at pH = 5.0 to near 10^{-7} molar phosphate at pH = 7.0 (Lindsay, 1979). Within the unsaturated zone where pore water pH values are estimated to decrease to as low as 4.5, phosphate solubility may be controlled by the iron and aluminum phosphates strengite and

variscite. The solubility of these minerals are similar and vary from approximately $10^{-4.5}$ molar phosphate at pH = 5 to approximately $10^{-6.5}$ molar phosphate at pH = 3 (Figure 3-15).

Fluorine rich apatite is abundant within the primary ore, and relict grains have been recognized within the base of the weathered profile (e.g. DH1 16.8 and 18.3 meters depth). Iron and aluminum phosphates are also present within the profile but only within the unsaturated zone. If it is assumed that apatite controls phosphate solubility at pH > 6, and strengite will control phosphate solubility at pH < 6, a diagram such as that shown in Figure 3-16 can be used to predict the amount of dissolved phosphate for a given pH value. This diagram shows a maximum in phosphate solubility at pH = 5. This implies that as weathering proceeds and the apatite from the uranium ore and host rocks is exposed to the low pH (4.5 to 5.5) pore waters in the unsaturated zone, it will begin to dissolve thus making relatively high concentrations of phosphate available for transport downward towards the water table.

When this phosphate reaches the water table, rather than forming fluor-apatite it combines with available uranium to produce meta-autunite minerals within the zone just below the water table. This model is supported by the bulk geochemical depth profiles for calcium and phosphate discussed above as well as the observation that no new apatite crystals or overgrowths have been noted within the saturated saprolites.

Discussion: Uranium Dispersal and Fixation within the Weathered Zone Overlying the Coles Hill Deposit

The mineralogical and geochemical results discussed above are summarized in Figure 3-17 which is a generalization of the representative DH1 profile. The gradients in bulk geochemistry within the weathered zone overlying the Coles Hill north orebody reflect the action of soil forming processes which have also fundamentally influenced the distribution of uranium within this system. The unsaturated zone is more highly weathered than the saturated saprolites and weathering intensity increases towards the surface. These depth profiles of SiO_2, Al_2O_3, Na_2O and LOI are strongly influenced by the conversion of albite, which makes up more than 30 volume percent of the bedrock in the area, to kaolinite, which is the most abundant mineral in Coles Hill soil samples (Zelazny, 2000 personal communication). This reaction, which can be written as $2\text{Albite} + H_2O + H^+ \rightarrow \text{Kaolinite} + Na^+ + 4SiO_2(aq)$ leads to the loss of silica and sodium thus enriching the residual material in aluminum.

The upper two meters are the most highly weathered material in the profile consisting mostly of kaolinite, vermiculite, montmorillonite and gibbsite (Zelazny, 2000 personal communication). This zone corresponds to an A-horizon in which the action of organic acids and dissolved CO_2 have lead to extensive weathering and leaching of materials to lower depths in the profile. Below the A-horizon but still within the upper five meters an aluminum enriched B-horizon has formed where physically transported clays and metals leached from overlying horizons have accumulated.

High bulk concentrations of both Ca and P below 14 meters appear to be controlled by apatite. Above that zone apatite may have been dissolved due to lowering pH values. The relatively high phosphorus, strontium, barium and cerium concentrations in the shallow portion of the DH1 column are interpreted as reflecting abundant crandallite group minerals (e.g. Figure 3-7).

In the upper two meters, the phosphate depth profile is controlled by uranium bearing aluminum phosphates of the crandallite group. The local peaks in phosphorus concentration caused by the abundance of this mineral correspond to peaks in uranium, barium, strontium, and lanthanides. This suggests that the aluminum phosphate is the dominant sink for both uranium and the rare earth elements within the upper five meters of the profile. The similar peak in strontium, barium and cerium noted in the DH2 column appears to be related to an abundance of compositionally complex manganese oxides (e.g. romanachite). Geochemical discontinuities in the upper half meter; however, may be heavily influenced by soil amendments such as lime and fertilizer as well as extensive leaching by organic acids produced within this zone.

Much of our understanding of U(VI) phosphate minerals in weathering environments similar to the Coles Hill region stems largely from studies of Koongara uranium deposit in northwest Australia (e.g. Airey, 1986; Isobe et al, 1992; Sato et al, 1997; Murakami et al 1997). The Koongara deposit is located in a wet, humid environment and is overlain by an approximately 40 meter thick weathered zone (Airey, 1986). This weathered zone contains a secondary uranium ore body consisting largely of the U(VI) phosphate saleeite (Mg-autunite).

The major difference between the Coles Hill system and the Koongara site is that, as shown by the work of Murakami et al (1997), ground waters within the weathered zone overlying the Koongara uranium deposit are currently undersaturated ($SI < 0$) with respect to the observed U(VI) phosphate mineral (saleeite). Furthermore, Muakami et al (1997) describe SEM

observations suggesting that autunite minerals at the Koongara site are currently dissolving leading to the formation of a uranium dispersal "plume" down gradient from the secondary ore body. Conversely, at the Coles Hill site ground waters are saturated with respect to the observed U(VI) phosphate mineral which explains its wide-spread and disseminated occurrence within the saturated saprolite and oxidized bedrock zones.

Another important result of the Koongara project (e.g. Murakami et al, 1997) was the discovery of microcrystals (10 – 50 nanometers) of saleeite and meta-torbernite (Cu meta-autunite) within fracture coating aggregates of iron oxide minerals. Since the crystal structures of these minerals differ from the local structure of U(VI) complexes adsorbed to ferrihydrite the presence of these crystals could not be explained by adsorption alone (Murakami et al, 1997). Their explanation rather involves the following three steps: (1) chlorite from the primary host rocks weathers resulting in the formation of ferrihydrite, (2) phosphorus in ground water adsorbs or coprecipitates onto the ferrihydrite surface, (3) sorbed phosphorus is released from the iron oxide substrate as the ferrihydrite recrystalizes (ages) to form more stable minerals goethite and/or hematite, (4) the phosphorus thus released combines with adsorbed or dissolved uranium, magnesium and/or copper at the iron oxide mineral surface leading to surface precipitation of the U(VI) phosphate microcrystals.

Microcrystals of this type have not been identified within samples from the Coles Hill profile (no TEM studies have yet been completed); however, the correlation between phosphorus and uranium associated with iron oxide mineral coatings in some samples (e.g. Figure 3-10) may reflect the type of process documented at the Koongara site.

Uranium transport within the Coles Hill profile

As described above the bulk uranium concentration profile for the representative DH1 column varies from approximately 200 parts per million in the unsaturated zone to values greater than 1000 parts per million within the saturated saprolite zone (Figure 3-11 and 3-12). There are two ways to explain this trend. One possibility is that the upper portion of the weathered zone formed from primary rocks with low uranium contents. The second possibility is that the entire profile formed from originally uranium rich rocks, but that uranium has been leached from the upper part of the sequence during soil forming processes. The fact that the uranium discontinuity corresponds to the water table in both drill holes DH1 and DH2 supports the second possibility

because it is likely that the change in geochemical parameters associated with the transition from unsaturated to saturated conditions will strongly influence uranium solubility. This is evidenced by the observation that the sharp decrease in uranium above the water table corresponds to sharp decreases in pH and a corresponding increase in LOI (total volatile content). Both of these trends reflect soil forming processes, specifically the increase in soil pore water acidity and the perhaps related increase in clay content. It is thus suggested that the soil forming processes responsible for these trends are related to the uranium profile.

The relatively high bulk uranium concentrations (> 1000 ppm) within the saturated saprolite zone are associated with disseminated U(VI) phosphates of the meta-autunite mineral group. Above the water table these meta-autunite group minerals are unstable due to the lower pH environment. Uranium released from their breakdown is partitioned into three distinct reservoirs in the unsaturated zone: (1) uranium associated with phosphorus sorbed to iron oxy-hydroxide surfaces, (2) uranium associated with aluminum phosphates of the crandallite group, (3) uranium partitioned into the fluid phase and leached back down to the water table. When this uranium leached from the upper portions of the profile encounters the higher pH environment at the saturated zone it may reprecipitate as new meta-autunite minerals. This would explain the observations that the unsaturated zone is depleted in uranium relative to other reservoirs within the profile and that the water table region is enriched relative to other zones. A similar process has been postulated to explain the distribution of uranium and uranium series measurements within autunite occurrences in the Sila Plateau in Calabria Italy (Dall'aglio et al, 1974). Here it was shown based on radioactive disequilibria that autunite minerals are dissolving within the unsaturated zone (Ra>U) and reprecipitating below the water table (uranium excess) (Dall'aglio et al, 1974). Although radioactive disequilibria studies have not yet been performed on the Coles Hill U(VI) phosphates, the lack of meta-autunite in the unsaturated zone and their abundance below the water table, suggests that a similar process is at work at the Coles Hill site. Also similar to observations at Coles Hill, the studies of the Italian autunite occurrences indicate that the U(VI) phosphate mineralization is restricted to a geologic environment that contains relatively low dissolved carbonate ($10^{-3.5}$ log molar HCO_3^-) and thus a high dissolved phosphate to carbonate ratio (log HPO_4^-/HCO_3^- = -2) relative to the surrounding region.

The Coles Hill saprolite profile is estimated to be approximately 500 thousand years old (Pavich, 1986, 1989; Cleaves et al, 1970). This implies that the U(VI) phosphates within the

saturated saprolite zone may have persisted for hundreds of thousands of years. This result is also not unprecedented as it was shown by Finch et al (1996) using $^{234}U/^{238}U$ and $^{230}Th/^{234}U$ disequilibria methods that some U(VI) phases from the Shikolobwe mine in Zaire have experienced no major preferential loss of uranium since their formation over 100,000 years ago. Furthermore, ages greater than 300,000 years have been reported for secondary U(VI) minerals in Sweden (Lofvendahal and Holm, 1980). These results reiterate the potential important implications studying such natural occurrences of uranyl minerals may have on understanding the long-term geochemical behavior of uranium in different types of geologic environments.

Based on the field and mineralogical observations described above as well as the previous work the Coles Hill profile is interpreted as a dynamic system in which uranium is being actively leached from the unsaturated zone (meta-autunite dissolution) and reprecipitated (as meta-autunite) below the water table. This type of process may have been active for hundreds of thousands of years. The fact that the uranium concentration within the unsaturated zone remains relatively constant (approximately 200 ppm) below one meter depth suggests that the upper part of this zone has reached steady state conditions with regards to its uranium retardation capacity.

Conclusion

The study of the geochemistry and mineralogy of the weathering profile overlying the Coles Hill uranium deposit has shown that natural attenuation of uranium within oxidizing, fluid rich environments may occur if certain geologic and geochemical criteria are met. Understanding these criteria requires characterization and modeling of key phenomena on a variety of scales ranging from the size of the deposit (hundreds of meters) to the mineral-grain scale (microns to nanometers). The results of this study suggest that uranium that is mobilized within the relatively low pH (<5.0) unsaturated environment is being reprecipitated below the water table as low solubility U(VI) phosphates due to near neutral pH conditions (around 6.0) and relatively high activity ratios of dissolved phosphate to carbonate (e.g. $\log [H_2PO_4^-/HCO_3^-] > -3$). This natural attenuation process may have been active for at least the past 500,000 years and thus has important implications for understanding the long term behavior of uranium within near surface environments typical of the eastern US.

References

Airey, P. L., 1986, Radionuclide migration around uranium ore bodies in the Alligator Rivers Region of the Northern Territory of Australia-Analogue of radioactive waste repositories-A review, Chemical Geology, Vol. 55, pp. 255 – 268

Brookins, 1987. Eh-pH Diagrams for Geochemistry, New York, Springer-Verlag

Bruno, J., De Pablo, J., Duro, L., and Figuerola, E., 1995, Experimental study and modeling of the U(VI)-Fe(OH), surface precipitation/coprecipitation equilibria, Geochimica et Cosmochimica Acta, Vol. 59, pp. 4113 – 4123

Cleaves, E. T., Godfrey, A. E. and Bricker, O. P., 1970, Geochemical balance of a small watershed and its geomorphic implications, Geological Society of America Bulletin, V. 81, p. 3015-3032

Evensen, N. M., Hamilton, P. J., and O'Nions R. K., 1978, Rare earth abundance's in chondritic meteorites, Geochimica Cosmochimica Acta, v. 42 p.1199-1212

Environmental Protection Agency, 1991, National primary drinking water standards for radionuclides, proposed rule, June, 1991, EPA Fact Sheet, Radionuclides in Drinking Water, 570/9-91-700

Eisenbud, M., Gesell, T. F., 1997, Environmental radioactivity from natural, industrial and military sources, (fourth edition), Academic Press, San Diego, 656 pp.

Finch, R. J., and Ewing, R. C., 1992. The corrosion of uraninite under oxidizing conditions, Journal of Nuclear Materials 190 133-156

Finch, R. J., and Murakami T., 1999, Systematics and paragenesis of uranium minerals, Reviews in Mineralogy, Volume 38: Uranium: Mineralogy, Geochemistry and the Environment, Burns, P. C., and Finch, R. (Eds)

Finch, R. J., Suuksi, J., Rasilainen, K., and Ewing R. C., 1996, Uranium-series ages of secondary uranium minerals with applications to the long-term evolution of spent nuclear fuel, Materials Research Symposium Proceedings, v. 412, p. 823 - 830

Foth, H. D., 1984, Fundamentals of Soil Science. 7th edition, New York, John Wiley and Sons

Garrels R. M., and Christ C. L., 1959, Behavior of uranium minerals during oxidation. in Geochemistry and Mineralogy of the Colorado Plateau Uranium Ores., Garrels R. M., Larsen E. S., (Eds) US Geological Survey Professional Paper 320:81-89

Gaines, R. V., Skinner, H. C. W., Foord E. E., Mason B., Rosenzweig, A., King, V. T., Dowty E., 1997. Dana's New Mineralogy. 8th Edition. Wiley & Sons, New York, 1819 p.

Goldich, S. S., 1938, A study in rock weathering, Geology, V. 46, p. 17-58

Grenthe, I., Fuger, J., Konings, R J. M., Lemire, R. J., Muller, A. B., Nguyen-Trung Cregu, C., Wanner, H., 1992. (H. Wanner and I. Forest, eds.) Chemical Thermodynamics of Uranium, Nuclear Energy Agency, Amsterdam: Elsevier Science Publication

Halladay, C.R., 1989, The Swanson uranium deposit, Virginia: a structurally controlled U-P albitite deposit [abs.], in Uranium resources and geology of North America: Saskatoon, Canada, Proceedings of a technical committee meeting organized by the International Atomic Energy Agency, September 1987, p. 519

Hemingway, B.S., 1982. Thermodynamic properties of selected uranium compounds and aqueous species at 298.15 K and 1 bar at higher temperatures –Preliminary models for the origin of coffinite deposits. Open File Report 82-619, U.S. Geological Survey

Hendershot, W. H., Lalande, H., and Duquette, M., 1993, Soil reaction and exchangeable acidity, in Soil Sampling and Methods of Analysis, Carter, Ed., Canadian Society of Soil Science, Lewis Publishers

Ivonaovich, M. and Harmon, R. S. (Editors), 1982, Uranium Series Disequilibrium: Application to Environmental Problems. Oxford University Press, Oxford.

Isobe, H., Murakami, T., Ewing, R. C., 1992, Alteration of uranium minerals in the Koongarra deposit, Australia: Unweathered zone, Journal of Nuclear Materials, v. 190 pp. 174-187

Jackson, J. A. (ed.), 1997, Glossary of Geology, American Geological Institute, Alexandria Virginia.

Jerden J. L., Jr., and Sinha, A. K., 2001a. Geology and geochemistry of the Coles Hill uranium deposit, Virginia, a unique example of hydrothermal apatite-coffinite-uraninite mineralization, *in review*: Economic Geology

Jerden J. L., Jr., and Sinha, A. K., 2001b. Mineralogical fixation of uranium during oxidation and chemical weathering of a coffinite-uraninite-apatite orebody, Virginia, Eleventh Annual V.M. Goldschmidt Conference, May 20-24, Hot Springs, Virginia, USA (oral presentation, no abstract given)

Kathren, R. L., 1984. Radioactivity in the Environment, Philadelphia, Harwood Academy Publications

Krauskopf, K. B., 1967. Introduction to Geochemistry, New York: McGraw-Hill

Langmuir, D., 1978. Uranium solution-minral equilibria at low temperatures with applications to sedimentary ore deposits, Geochimica et Cosmochimica Acta, v. 42 p. 547-569.

Langmuir, D., 1997. Aqueous Environmental Geochemistry, Upper Saddle River, New Jersey, Prentice-Hall Inc.600 p.

Leslie, B. W., Pearcy, E. C., Prikryl J. D., 1993, Oxidative alteration of uraninite at the Nopal I deposit, Mexico Possible contaminant transport and source term constraints for the proposed repository at Yucca Mountain, in Scientific Basis for Nuclear Waste Management XVI. Interrante CG, Pablan RT (Eds) Materials Research Symposium Proceedings v. 294, p. 505-512

Levenspiel, O., 1972. Chemical Reaction Engineering (2^{nd} edition) Wiley, Chichester, 1972

Lindsay, W. L., 1979, Chemical Equilibria in Soils, Wiley, New York, 449pp.

Lofvendahl, R. and Holm, E., 1981, Radioactive disequilibria and apparent ages of secondary uranium minerals from Sweden, Lithos, v. 14 pp. 189 - 201

Marline Uranium Corporation, 1983, An evaluation of uranium development in Pittsylvania County Virginia: report submitted jointly by Marline Uranium Corporation and Union Carbide Corporation to the Virginia Uranium Administrative Group to the Virginia Uranium Administrative Group Pursuant to Section 45.1-285.1et seq of the Code of Virginia (1983) (Senate Bill 155), October, 15, 1983,

Menard, H. W., Jr., 1961. Some rates of regional erosion, Journal of Geology, 69, 154-161

Muto T., 1965. Thermochemical stability of ningyoite. Mineralogical Journal 4 245-274

Murakami, T., Ohnuki, T., Sato, T., Yanase, N., Kimura, H., 1994, Significance of the effect of mineral alteration on nuclide migration, Material Research Society Symposium Proceedings Vol. 333 pp. 645 – 652

Murakami, T., Ohnuki, T., Isobe, H., Sato, T., 1997, Mobility of uranium during weathering, American Mineralogist, Vol. 82 pp. 888 – 899

Nesbitt, H. W., and Wilson, R. E., 1992. Recent chemical weathering of basalts, American Journal of Science, 292, 740-777

Nesbitt, H. W., and Markovics, G., 1992. Weathering of granodioritic crust, long-term storage of elements in weathering profiles, and petrogenesis of siliciclastic sediments, Geochimica et Cosmochimica Acta, 61, 1653-1670

Ngyuyen, S. N., Silva, R. J., Weed, H.C., and Andrews, J. E., Jr. 1991. Standard Gibbs free energies of formation at the temperature 303.15 K of four uranyl silicates: soddyite, uranophane, sodium boltwoodite and sodium weeksite. Journal of Chemical Thermodynamics, 24 359-376

Pavich, M. J., Brown, L., Valette-Silver, N., Klein, J., Middleton, R., 1985, ^{10}Be analysis of a Quaternary weathering profile in the Virginia Piedmont, Geology, 13, 39-41

Pavich, M. J., 1986, Processes and rates of saprolite production and erosion on a foliated granitic rock of the Virginia Piedmont, In Colman, S. M. and Dethier, D. P. (eds), Rates of Chemical Weathering of Rocks and Minerals, Academic Press, New York, pp. 552-590

Pavich, M. J., 1989, Regolith residence time and the concept of surface age of the Piedmont "peneplain", Geomorphology, V. 2, p. 181-196

Pearcy, E. C., Prikryl, J. D., Murphy, W. M., Leslie, B. W., 1994, Alteration of uraninite from the Nopal I deposit, Pena Blanca District, Chihuahua, Mexico compared to degradation of spent nuclear fuel in the proposed U.S. high-level nuclear waste repository at Yucca Mountain, Nevada, Applied Geochemistry, V. 9 p. 713-732

Romero, L., Neretnieks, I., and Moreno, L., 1992. Movement of the redox front at the Osamu Utsumi uranium mine, Pocos de Caldas, Brazil, Journal of Geochemical Exploration, 45, 471-502

Sato, T., Murakami, T., Yanase, N., Isobe, H., Payne, T. E., and Airey, P. L., 1997, Iron nodules scavenging uranium from groundwater, Environmental Science and Technology, Vol. 31 pp. 2854 – 2858

Shoesmith, D. W., Sunder, S., 1992, The prediciton of nuclear fuel (UO_2) dissolution rates under waste disposal conditions, Journal of Nuclear Materials, v. 190 p. 20-35

Suzuki, Y., Murakami, T., Kogure, T., Isobe, H., Sato, T., 1998, Crystal chemistry and microstructures of uranyl phosphates, Material Research Society Symposium Proceedings Vol. 506 pp. 839 – 846

Thomas, M. F., 1994, Ages and Geomorphic relationships of saprolite mantles, in Rock Weathering and Landform Evolution, Robinson, D. A. and Williams, R. B. G., (Eds.) John Wiely and Sons Ltd, New York

Vochten, R. F., Van Haverbeke, L., and Van Springel, K., 1992. Transformation of chernikovite into meta-uranocircite II, $Ba(UO_2)(PO_4)_2 \bullet 6H_2O$ and study of its solubility

Warber, N., Schorscer, H. D., and Peters, Tj., 1992. Hydrothermal and supergene uranium mineralization at the Osamu Utsumi uranium mine, Pocos de Caldas, Minas Gerais, Brazil, Journal of Geochemical Exploration, 45, 53-112

Weast, R. C., Astle W. J., and Beyer, W. H. (Eds.), 1986, Handbook of Chemistry and Physics. CRC Press, Boca Raton, FL.

Woods, T. L., and Garrels R. M., 1987, Thermodynamic Values at low temperature for natural inorganic materials: an uncritical summary, Oxford University Press, New York, 242 pp.

Wronkiewicz, D. J., Bates J. K., Gerding T. J., Veleckis, E., Tani B. S., 1992, Uranium release and secondary phase formation during unsaturated testing of UO2 at 90oC, Journal of Nuclear Materials, v. 190, p. 107-127

Wronkiewicz, D. J., Bates J. K., Wolfe, S. F., Buck E. C., 1996, Ten-year results from unsaturated drip tests with UO2 at 90oC,: Implications for the corrosion of spent nuclear fuel, Journal of Nuclear Materials, v. 238, p. 78-95

Wronkiewicz, D. J., and Buck E. C., 1999, Uranium mineralogy and the geologic disposal of spent nuclear fuel, Reviews in Mineralogy, Volume 38: Uranium: Mineralogy, Geochemistry and the Environment, Burns, P. C., and Finch, R. (Eds)

Table 3-1. Chemical analyses (electron microprobe) of meta-autunite minerals from the saturated saprolite zone.

	(1)	(2)	(3)	(4)	(5)	(6)	(7)	(8)
UO_3	58.0	59.7	59.6	60.8	62.7	62.4	62.9	62.7
P_2O_5	14.4	15.6	15.0	15.1	16.2	15.8	15.2	15.5
BaO	15.5	11.1	11.6	5.6	0.8	1.8	2.4	1.7
CaO	< 0.1	1.6	1.3	3.2	5.3	3.7	3.6	3.9
SrO	< 0.1	< 0.1	0.4	< 0.1	< 0.1	1.2	0.9	1.2
PbO	< 0.1	< 0.1	< 0.1	0.3	< 0.1	0.1	< 0.1	< 0.1
Total*	87.8	88.0	87.9	85.0	85.0	85.0	84.9	84.9
P_2O_5/BaO	0.9	1.4	1.3	2.7	19.9	8.8	6.3	9.3
Ions based on 12 oxygen equivalents, ignoring interlayer H_2O								
U	2.0	2.0	2.0	2.0	2.0	2.0	2.1	2.0
P	2.0	2.1	2.0	2.0	2.1	2.0	2.0	2.0
Ba	1.0	0.7	0.7	0.3	0.0	0.1	0.1	0.1
Ca	----	0.3	0.2	0.5	0.9	0.6	0.6	0.6
Sr	----	----	0.0	----	----	0.1	0.1	0.1
Pb	----	----	----	0.0	----	----	----	----

*Total of data normalized to ideal H_2O. Totals of raw data are not representative due to apparent dehydration of crystals in microprobe vacuum. Oxides MgO, Na2O, and K2O are below detection limit of approximately 0.1 weight percent. (1) = Type II meta-uranocircite from oxidized ore bearing bedrock. (2) -(5) = U(VI) phosphates from saturated saprolite zone in drill hole DH1; (6)-(8) = U(VI) phosphates from saturated saprolite zone in drill hole DH2. Relative standard deviations of raw data (calculated from counting statistics) are: 1% or less for UO_3 and 2% or less for P_2O_5, BaO, and 2% to 3% for SrO.

Table 3-2. Chemical analyses (electron microprobe) of crandallite group mineral intergrown with Mn-oxide and kaolinite.

	(1)	(2)	(3)	(4)	(5)	(6)	(7)	(8)	(9)	(10)	(11)	(12)	(13)	(14)	(15)	(16)	(17)
Al_2O_3	31.2	31.2	31.1	30.8	30.6	30.5	30.4	30.2	29.8	29.2	27.9	27.7	27.2	7.9	21.7	20.8	23.7
P_2O_5	22.8	26.5	26.1	26.0	26.0	26.5	25.6	25.9	16.4	16.6	23.3	23.0	22.8	5.1	17.5	16.6	20.3
MnO	0.0	0.0	0.1	0.1	0.4	0.0	0.0	0.4	0.0	0.0	2.2	2.8	4.2	19.9	12.7	11.8	9.1
SiO_2	9.8	5.1	5.8	5.4	5.1	5.2	5.2	5.3	18.2	16.6	3.9	3.5	3.4	38.9	3.5	2.4	3.3
CaO	2.1	2.3	2.3	2.3	2.3	2.4	2.2	2.3	1.6	1.6	2.3	2.3	1.9	0.6	1.6	1.3	1.9
Fe_2O_3	0.9	1.0	1.0	0.8	1.0	1.0	1.0	0.9	1.1	1.3	1.0	1.3	1.6	4.7	3.3	3.5	2.2
SrO	3.3	2.5	2.4	2.5	2.3	2.6	2.5	2.4	2.6	2.5	3.0	2.9	2.7	0.2	2.3	1.6	2.8
BaO	12.2	15.8	15.4	15.1	16.0	15.9	15.7	15.3	7.6	8.0	13.3	13.9	13.0	6.9	11.6	11.6	12.8
UO_3	1.0	1.4	1.3	1.3	1.3	1.2	1.2	1.2	0.7	0.7	1.1	1.3	1.0	0.1	0.8	0.7	1.0
Total	83.3	85.8	85.5	84.4	84.8	85.3	83.9	83.9	77.9	76.5	77.9	78.6	77.7	84.2	75.0	70.3	77.0

PbO, K2O are below detection limit of approximately 0.1 weight percent. Totals do not equal 100% due to H_2O in mineral structure (crandallite may contain up to 20 Wt.% H_2O; Nriagu, 1984). SiO_2 values and high Al_2O_3 values are from kaolinite contamination of analyses. (1) - (5) are from DH1, 0.8 meters depth; (5) - (10) are from DH1, 2 meters depth, (11) - (13) are from DH1, 0.8 meters depth; (14) - (17) are from DH1, 2 meters depth. Relative standard deviations of raw data (calculated from counting statistics) are: 1% or less for Al_2O_3 and SiO_2; 2% or less for P2O5, BaO, CaO and SrO; 4% to 5% for other elements.

Table 3-3. Electron microprobe analyses of (U, P) bearing iron oxide mineral coating.

	(1)	(2)	(3)	(4)	(5)	(6)	(7)	(8)	(9)
Al_2O_3	18.44	12.59	6.53	4.22	2.90	4.77	4.50	6.73	4.21
P_2O_5	0.55	2.12	4.60	4.79	4.20	6.07	7.69	5.74	5.00
SiO_2	34.36	32.78	16.26	13.17	33.02	20.47	10.24	16.33	10.54
BaO	0.24	0.25	0.27	0.29	0.38	0.42	0.41	0.32	0.25
Fe_2O_3	10.91	29.49	35.56	35.88	26.52	31.88	42.31	36.10	43.75
UO_3	0.00	0.32	2.37	2.47	5.44	7.55	6.22	3.26	2.56
Total	64.51	77.55	65.59	60.82	72.45	71.15	71.36	68.47	66.31
P_2O_5/BaO	2.36	8.60	16.97	16.80	11.09	14.48	18.84	17.94	20.01

SrO, CaO, PbO, K_2O are below detection limit of approximately 0.1 weight percent. Totals do not equal 100% due to H_2O in mineral structure. (1) - (9) are from auger hole DH1, 2 meters depth. Relative standard deviations of raw data (calculated from counting statistics) are: 1% or less for Al_2O_3 and SiO_2; 2% or less Fe2O3 and CaO; 4% to 5% for other elements.

Table 3-4. Bulk geochemical analyses of saprolites and soils from the DH1 auger hole (see Fig.3-1 & 3-2 for location).

depth (m)	0.2	0.4	0.6	1.2	1.5	2.1	3.7	4.3	4.6	4.9	5.5	7.3	7.9	8.5	9.5	10.4	11.0	11.3	13.1	16.8	18.3
Oxides in Wt.%																					
Na_2O	0.2	0.1	0.1	0.1	0.1	0.1	0.0	0.1	0.1	0.1	0.7	1.6	3.1	4.6	6.2	6.5	7.2	7.1	6.4	7.3	7.2
MgO	0.3	0.3	0.4	0.4	0.4	0.4	0.4	0.4	0.4	0.4	0.4	0.4	0.4	0.5	0.4	0.5	0.4	0.4	0.5	0.6	0.5
Al_2O_3	16.6	17.9	23.5	26.6	24.7	26.0	26.0	26.8	25.4	22.9	20.2	19.8	20.2	20.4	19.8	19.1	18.7	18.7	17.2	17.2	16.3
SiO_2	68.6	66.2	50.4	52.1	55.0	54.7	57.4	54.0	56.0	59.9	64.6	64.5	63.8	61.5	63.9	64.0	65.3	65.5	67.1	64.9	68.2
P_2O_5	0.2	0.2	0.7	0.3	0.4	0.5	0.2	0.2	0.2	0.2	0.2	0.2	0.1	0.2	0.1	0.2	0.2	0.1	0.2	0.9	0.7
K_2O	0.4	0.4	0.4	0.3	0.2	0.1	0.4	0.2	0.3	0.2	0.4	0.4	0.3	0.3	0.2	0.3	0.3	0.3	0.3	0.3	0.2
CaO	0.1	0.1	0.1	0.1	0.1	0.1	0.1	0.0	0.0	0.0	0.1	0.1	0.1	0.2	0.2	0.2	0.2	0.2	0.3	1.2	1.0
TiO_2	0.7	0.6	0.7	0.7	0.7	0.7	0.8	0.8	0.7	0.6	0.6	0.5	0.5	0.6	0.6	0.6	0.6	0.5	0.6	0.5	0.5
MnO	0.0	0.0	0.0	0.0	0.0	0.0	0.1	0.0	0.0	0.1	0.0	0.1	0.1	0.1	0.0	0.0	0.0	0.0	0.1	0.1	0.0
Fe_2O_3	4.7	5.3	8.0	6.6	5.1	5.5	3.7	4.6	4.0	3.6	3.6	3.5	3.3	3.3	3.2	3.3	2.9	3.5	3.0	3.5	2.5
LOI	8.7	9.1	14.6	12.7	13.4	12.2	11.6	12.2	11.8	10.8	9.1	8.1	7.5	6.9	5.3	4.7	4.0	4.5	4.0	4.2	3.0
Total	100.5	100.2	99.0	99.8	100.1	100.3	100.5	99.3	98.9	98.8	99.9	99.2	99.7	98.6	99.9	99.3	99.7	100.8	99.5	100.6	100.2
Parts per million																					
Sr	98.7	119.0	596.1	190.8	205.4	291.9	54.5	56.1	28.2	112.6	81.2	82.0	30.9	83.0	46.8	44.0	36.4	38.0	67.0	126.0	103.6
Zr	247.3	223.0	158.6	290.9	297.4	320.7	371.8	387.7	402.6	323.5	297.3	335.0	304.0	332.0	253.8	300.0	234.4	418.0	263.3	486.0	235.0
Ba	446.8	502.7	2240.0	765.7	808.8	1050	393.1	354.5	344.5	652.2	458.2	492.6	370.2	561.5	308.4	456.9	413.1	542.0	737.7	812.0	579.1
Ce	99.4	111.9	430.4	200.5	194.9	315.2	130.7	117.0	90.9	144.5	130.9	132.1	68.5	147.6	91.4	88.5	77.9	71.4	103.2	90.5	87.1
U	48.1	61.5	237.3	146.8	217.2	337.5	162.7	213.2	192.0	207.5	242.5	247.1	268.2	338.4	272.9	862.6	772.4	901.0	1390.0	1260.0	1060.0

Table 3-5. Bulk geochemical analyses of saprolites and soils from the DH2 auger hole (see Fig.3-1 & 3-2 for location).

depth (m)	0.6	1.5	3.0	3.4	3.7	4.6	5.2	5.5	6.1	6.7	8.8	9.5	10.1
Oxides in Wt.%													
Na_2O	0.04	0.08	1.01	0.07	4.28	5.95	6.67	6.70	7.23	7.17	7.36	7.53	7.39
MgO	0.44	0.37	0.35	0.31	0.38	0.46	0.39	0.42	0.41	0.44	0.47	0.49	0.51
Al_2O_3	25.57	26.20	22.25	23.03	19.11	17.23	17.91	17.52	17.08	16.79	16.80	15.98	15.93
SiO_2	50.09	53.90	61.43	59.26	65.28	67.50	66.99	66.91	66.83	67.29	66.72	67.16	66.69
P_2O_5	0.15	0.19	0.19	0.56	0.22	0.16	0.27	0.17	0.75	0.84	0.73	0.94	1.17
K_2O	0.34	0.19	0.12	0.23	0.15	0.11	0.12	0.09	0.11	0.11	0.14	0.13	0.12
CaO	0.07	0.03	0.03	0.09	0.07	0.15	0.37	0.25	1.12	1.15	1.08	1.41	1.76
TiO_2	0.72	0.58	0.61	0.60	0.53	0.46	0.46	0.46	0.49	0.46	0.49	0.50	0.48
MnO	0.01	0.01	0.02	1.07	0.06	0.07	0.05	0.04	0.05	0.04	0.04	0.06	0.05
Fe_2O_3	6.48	4.82	4.13	3.94	3.41	3.05	2.73	2.86	2.65	2.59	2.94	2.82	3.02
LOI	15.74	12.73	9.98	10.96	6.42	4.57	4.25	4.38	3.40	3.54	3.51	3.09	3.27
Total	99.65	99.10	100.11	100.12	99.91	99.71	100.21	99.80	100.12	100.42	100.28	100.10	100.39
Parts per million													
Sr	81.17	92.11	83.26	401.25	93.43	68.18	86.19	66.00	109.49	103.99	109.74	137.65	157.30
Zr	317.75	271.92	261.78	304.20	249.22	244.17	244.54	214.00	227.36	220.69	240.11	285.97	310.17
Ba	436.75	437.80	441.17	2560.00	554.73	630.15	425.40	366.00	287.74	255.12	397.43	322.99	342.51
Ce	116.23	164.58	148.65	446.67	163.86	95.51	110.13	76.00	103.15	95.92	84.35	119.19	147.08
U	69.40	127.09	202.00	301.08	705.98	1230.00	945.00	953.00	407.53	627.99	515.05	166.00	216.82

Table 3-6. Percent gain/loss of major, minor and trace elements relative to unweathered uranium ore bearing bedrock in the DH1 auger hole (assuming constnat Ti; for calculation method see Langmuir, 1997).

depth (m)	0.2	0.4	0.6	1.2	1.5	2.1	3.7	4.3	4.6	4.9	5.5	7.3	7.9	8.5	9.5	10.4	11.0	11.3	13.1	16.8	18.3
Na	-98.6	-98.5	-98.8	-98.8	-98.9	-98.7	-99.8	-99.5	-99.3	-99.1	-92.4	-81.1	-61.5	-51.3	-33.1	-26.6	-16.3	-12.0	-26.4	-10.8	-7.1
Mg	-75.0	-70.3	-70.1	-67.6	-68.3	-66.8	-74.4	-77.2	-71.5	-68.9	-65.4	-59.7	-56.3	-57.3	-63.4	-57.6	-57.4	-54.7	-50.6	-42.1	-48.3
Al	-23.5	-5.4	1.6	24.4	8.0	27.6	8.9	2.5	15.5	23.4	8.9	17.7	24.9	7.8	7.1	9.3	10.0	17.0	-1.2	6.0	6.4
Si	-32.8	-25.4	-53.6	-48.1	-48.9	-42.9	-48.8	-56.0	-45.9	-31.3	-26.1	-18.3	-16.2	-30.8	-26.4	-22.3	-18.4	-13.1	-17.8	-15.0	-5.3
P	-90.3	-87.4	-61.2	-79.0	-78.1	-67.6	-90.6	-89.9	-89.2	-82.9	-84.4	-83.5	-88.6	-87.5	-90.0	-87.2	-88.4	-88.5	-87.1	-31.0	-39.7
K	90.7	103.3	70.3	26.1	-4.9	-33.9	52.2	-12.6	50.7	17.3	111.9	153.0	79.0	36.9	-4.6	95.4	64.5	61.7	79.2	85.1	48.9
Ca	-97.6	-97.0	-97.3	-98.8	-98.4	-98.0	-98.3	-99.4	-99.3	-98.9	-98.6	-97.2	-95.9	-95.1	-95.3	-94.4	-94.3	-94.2	-92.3	-62.0	-65.7
Ti	0.0	0.0	0.0	0.0	0.0	0.0	0.0	0.0	0.0	0.0	0.0	0.0	0.0	0.0	0.0	0.0	0.0	0.0	0.0	0.0	0.0
Mn	-85.8	-83.6	-86.6	-79.8	-67.6	-51.5	-8.0	-78.7	-39.7	99.7	-46.8	43.4	153.3	92.5	-21.4	-48.9	-40.1	-22.9	42.3	14.1	-9.3
Fe	15.2	49.3	84.8	63.5	17.6	43.2	-16.8	-5.5	-4.1	2.6	4.1	10.1	8.2	-8.2	-8.2	-0.4	-9.4	14.8	-9.0	13.2	-12.5
LOI	182.0	241.1	346.9	319.1	314.0	324.1	243.9	231.8	278.8	311.2	245.4	243.1	228.4	157.3	103.2	89.6	66.4	97.0	63.2	82.6	40.5
Sr	-64.1	-50.2	103.4	-29.5	-29.2	13.1	-82.0	-83.0	-89.9	-52.1	-65.5	-61.5	-85.0	-65.4	-80.0	-80.2	-83.1	-81.3	-69.5	-38.8	-46.6
Zr	-25.0	-22.1	-54.8	-10.2	-14.3	3.7	2.8	-2.0	20.6	14.9	5.4	31.5	23.6	15.7	-9.4	13.0	-9.2	72.0	0.0	97.3	1.1
Ba	-62.3	-51.1	77.7	-34.2	-35.1	-5.5	-69.7	-75.1	-71.3	-35.5	-54.8	-46.2	-58.1	-45.6	-69.4	-52.1	-55.5	-37.9	-22.0	-8.3	-30.6
Ce	-28.0	-6.6	193.2	47.9	34.2	143.7	-13.6	-29.4	-35.0	22.7	11.0	23.9	-33.4	22.9	-22.0	-20.3	-27.8	-29.8	-6.3	-12.2	-10.4
U	-96.9	-95.4	-85.5	-90.3	-86.6	-76.7	-90.4	-88.5	-87.7	-84.2	-81.6	-79.3	-76.7	-74.8	-79.2	-30.6	-36.0	-20.8	12.9	9.3	-2.5

Table 3-7. Selected ground water analyses from the weathered zone overlying the Coles Hill north orebody.

	(1)	(2)
Field pH	5.90	6.00
Field DO (ppm)	8.00	3.00
Major Constituents (ppm)		
Na	10.17	12.20
Mg	0.73	4.22
Si	16.28	16.10
K	0.26	0.12
Ca	3.00	17.10
HCO_3	25.00	23.00
SO_4	4.88	4.90
Cl	3.13	34.00
Selected Minor & Trace Constituents (ppb)		
Al	26.56	< 2.0
Mn	11.99	4.20
Fe	30.25	64.00
Cu	1.01	120.00
Sr	28.84	83.60
Ba	331.72	683.00
Pb	0.11	< 5.0
U	4.95	13.90
NO_3 (as N)	210.00	2300.00
F	170.00	170.00
PO_4 (as P)	100.00	300.00
VO_4 (as V)	0.81	< 5.00

(1) = Representative ground water from saprolite aquifer (sampled from auger hole DH2).
(2) = Representative ground water from the oxidized bedrock underlying the saprolite zone.

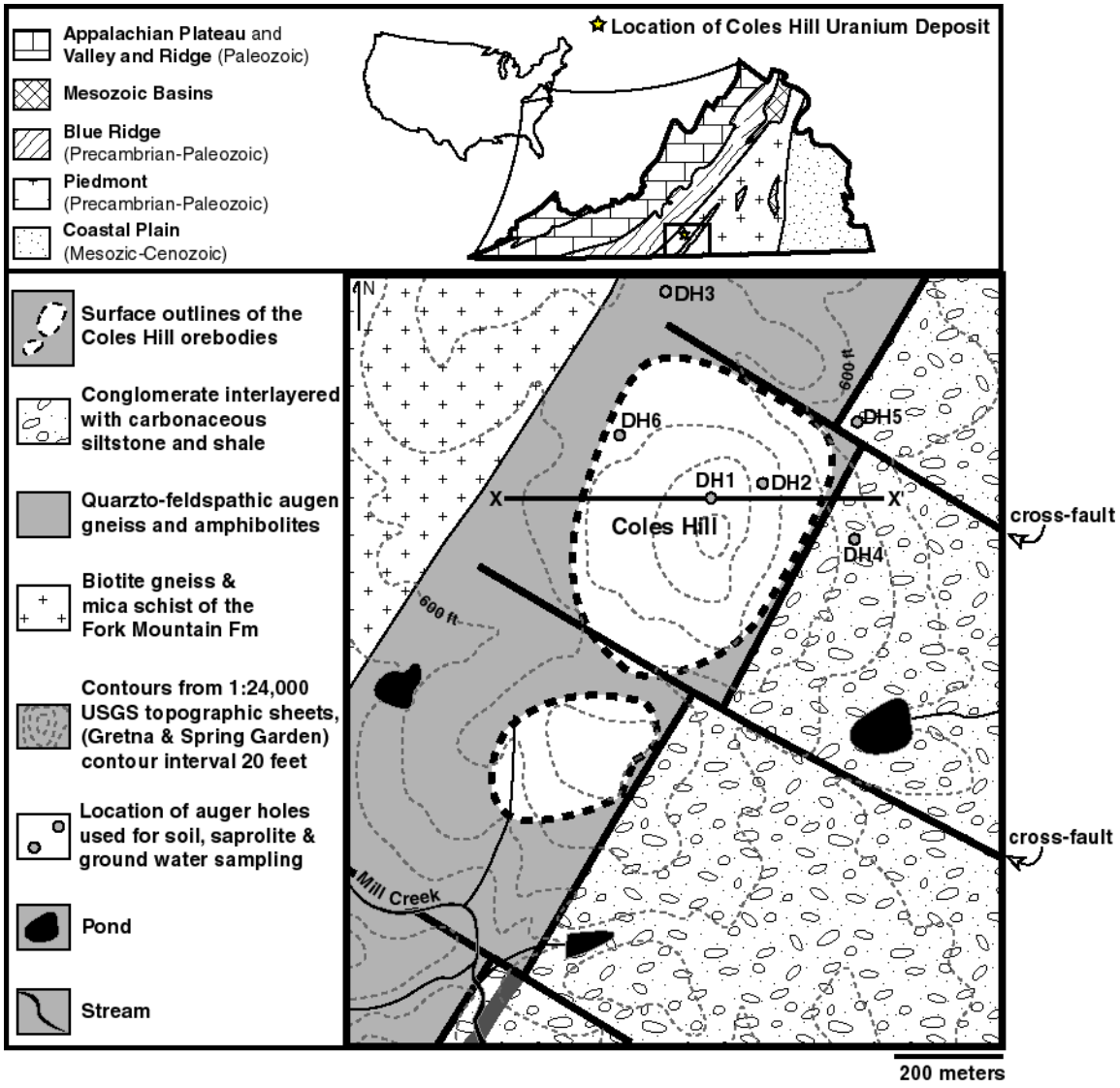

Figure 3-1. Location and geologic setting of the Coles Hill uranium deposit. The auger holes from which saprolite, soil and ground waters were sampled are also shown.

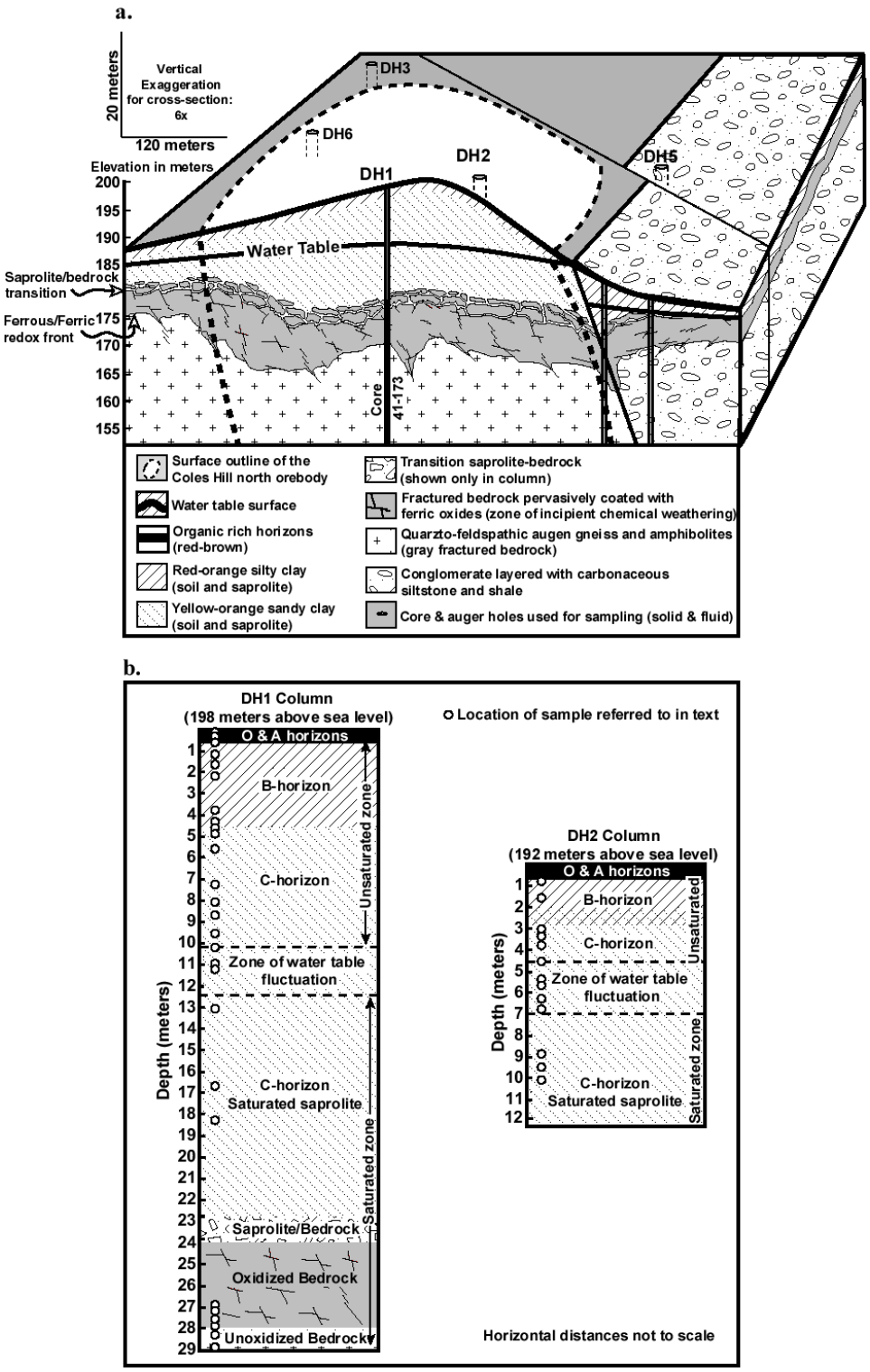

Figure 3-2. Geologic cross-section and representative columns through weathered zone overlying the Coles Hill uranium deposit. (a) Cross-section plotted using exploration drill hole logs (see Chapter 2) and data from auger drilling performed as part of this study. The auger holes from which saprolite, soil and ground waters were sampled are also shown. (b) Representative columns through the weathered zone showing locations of samples that were characterized mineralogically and geochemically.

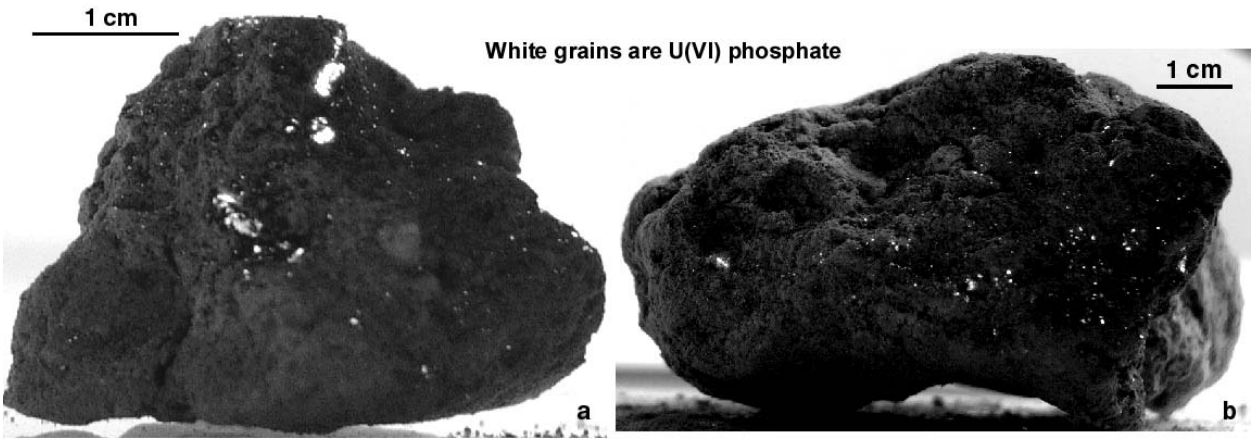

Figure 3-3. Hand samples of saprolite from below the water table (approximately 13 meters below the surface) from auger hole DH1. U(VI) phosphate minerals are white in these images: (a) aggregate of uranium phosphate grains associated with a zone enriched in manganese oxide (not visible), (b) uranium phosphate disseminated through out a weathered matrix consisting mostly of relict quartz and feldspars partially weathered to kaolinite.

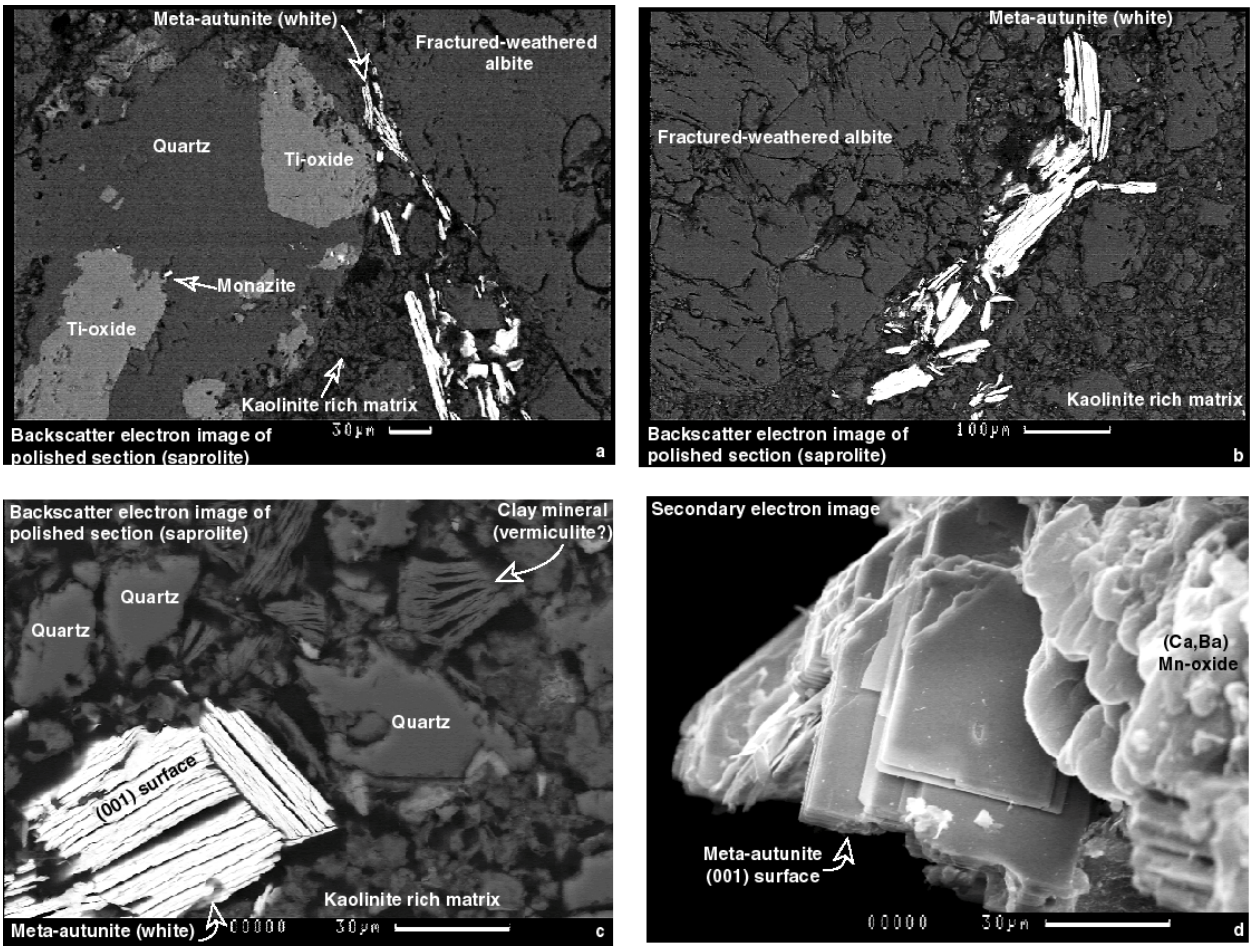

Figure 3-4. Electron images of U(VI) phosphate from the saturated saprolite zone: (a) typical textural relations between meta-autunite and other saprolite minerals (sample from DH1, 11.3 meters depth), (b) textural relationship between relatively large meta-autunite aggregate (300 microns) and weathered feldspar within a kaolinite rich saprolite matrix (sample from DH2, 5.5 meters depth), (c) textural relationship between meta-autunite, relict quartz and clay minerals within the saprolite matrix (sample from DH1, 16.8 meters depth), (d) surface of meta-autunite grain associated with (Ba, Ca) manganese oxide.

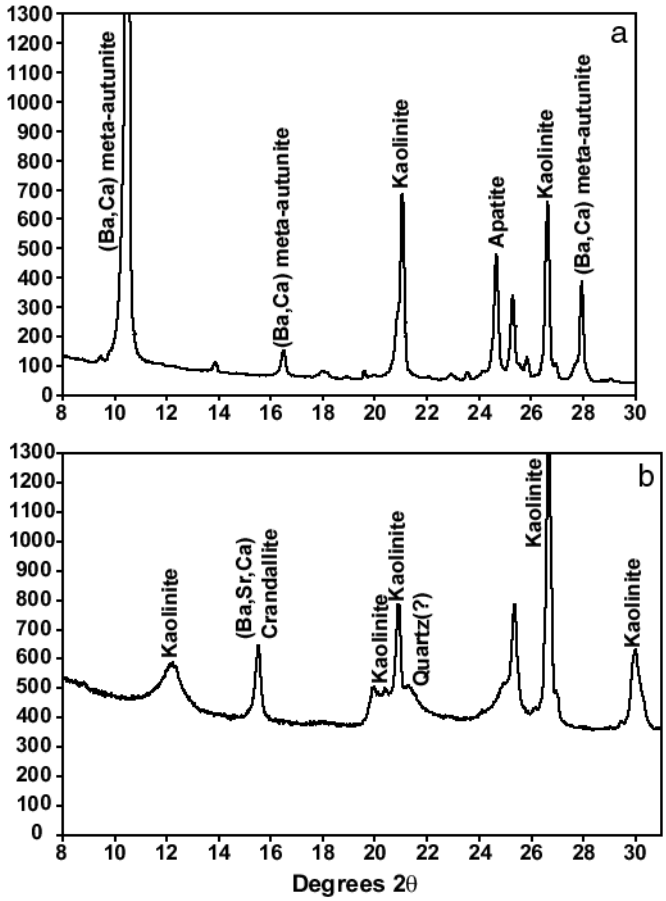

Figure 3-5. X-ray diffraction patterns of a representative heavy mineral separates (SG > 2.9) (data from R. Finch, 2001, personal communication): (a) is from the saturated saprolite zone (DH1, 11.3 meters depth). This pattern is similar to that measured for the underlying oxidized bedrock zone due to the abundance of Ba meta-autunite (the presence of kaolinite is due to impure mineral separation); (b) is from the unsaturated zone (DH1, 2.1 meters depth). This pattern is unlike that from the saturated saprolite due to the lack of meta-autunite and the abundance of a crandallite group mineral (the presence of kaolinite is due to impure mineral separation).

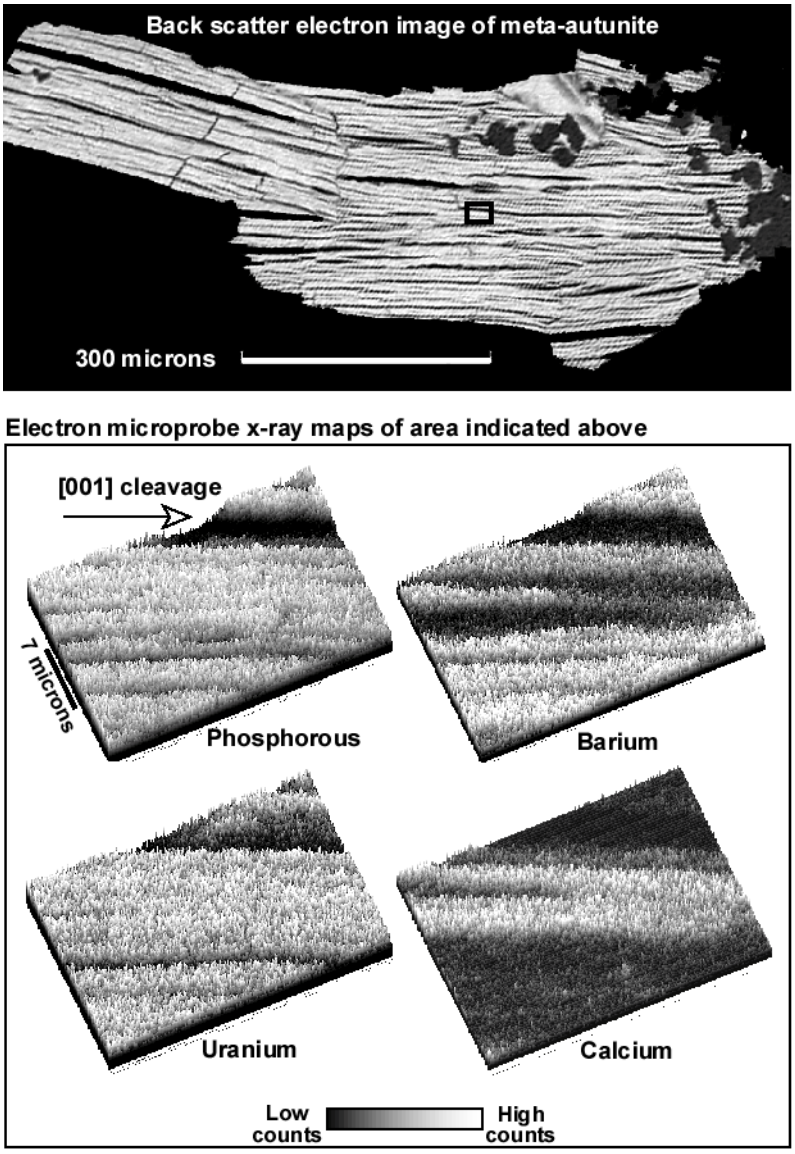

Figure 3-6. Backscatter electron image and electron microprobe x-ray maps (shown as x-ray intensity surface plots) of a (Ca,Ba)-autunite grain from the saturated saprolite zone (DH1, 11 meters depth). Note compositional heterogeneity (micron scale layering of Ba and Ca rich zones) is parallel to the (001) plane of the mineral suggesting that it may be the result of ion exchange of Ca for Ba within the meta-autunite inter-layer site.

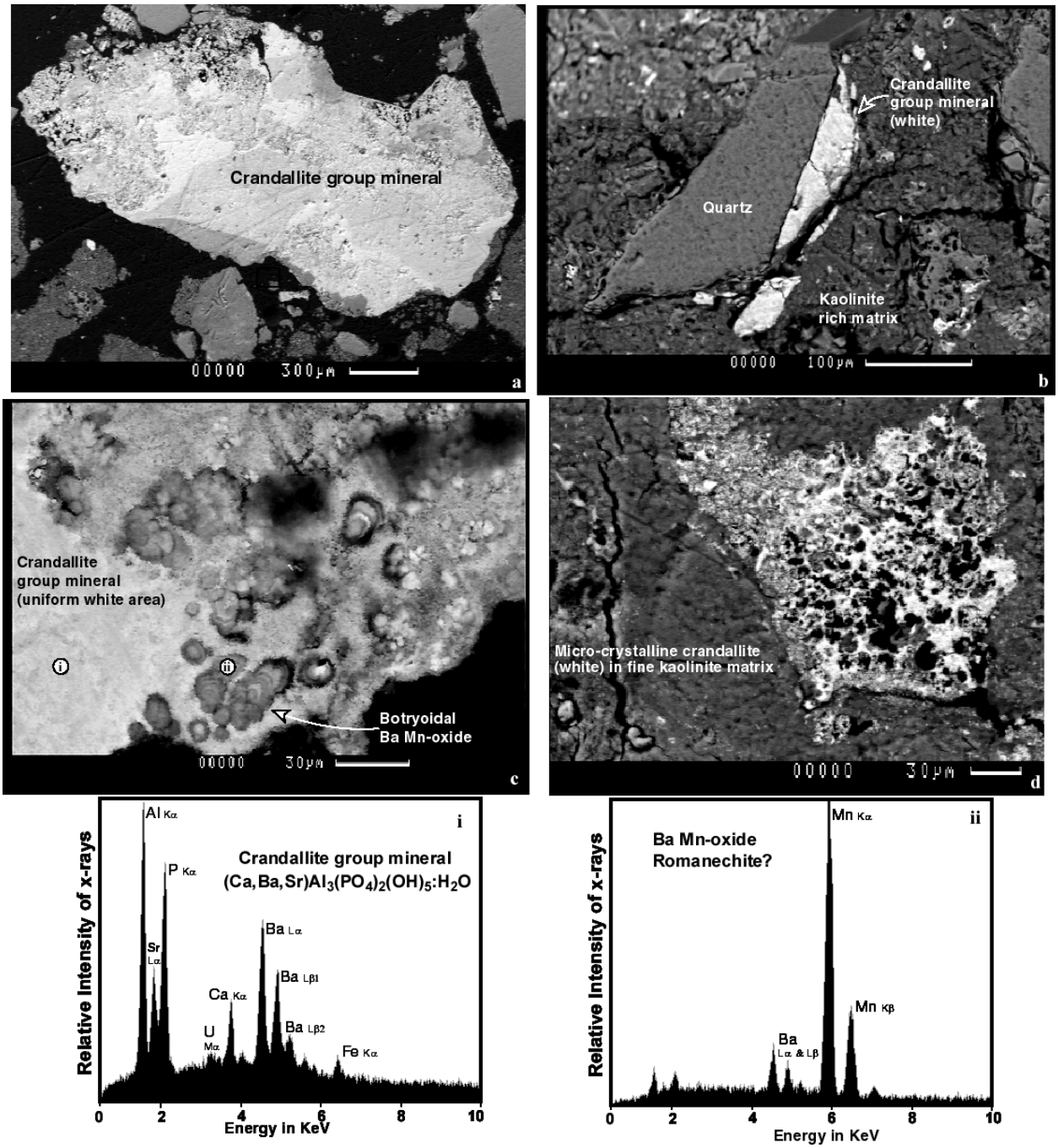

Figure 3-7. Backscatter electron images and energy dispersive x-ray spectra (EDS) of soil samples from the unsaturated zone overlying the Coles Hill north orebody. (a) Sample from DH1, 2.1 meters depth, showing a uranium bearing (Ba,Ca,Sr) Al-phosphate (white) identified as a crandallite group mineral by XRD, EDS and EMP, (b) sample from DH1, 0.6 meters depth, showing crandallite mineral growing adjacent to a relict quartz grain and within the kaolinite-rich matrix. (c) Expanded view of area indicated by black box on image (a) showing inclusions or intergrowths of a botryoidal Ba Mn-oxide (romanechite?) within the relatively large (> 400 micron) crandallite grain (note location of EDS spectra (x) and (y)), (d) Expanded view of micro-crystalline crandallite filling pore spaces and surrounding other soil minerals (e.g. relict quartz, and clays).

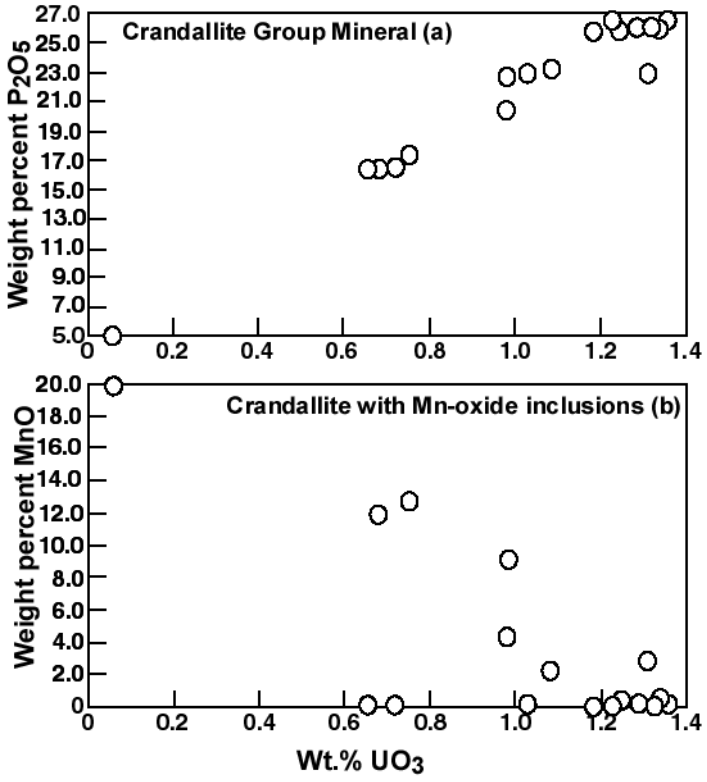

Figure 3-8. Electron microprobe data from the Crandallite group minerals shown on Fig. 3-7. The positive correlation between P and U and negative correlation between Mn and U suggests that in this area U is partitioned into the Al-phosphate phase rather than Mn-oxide minerals.

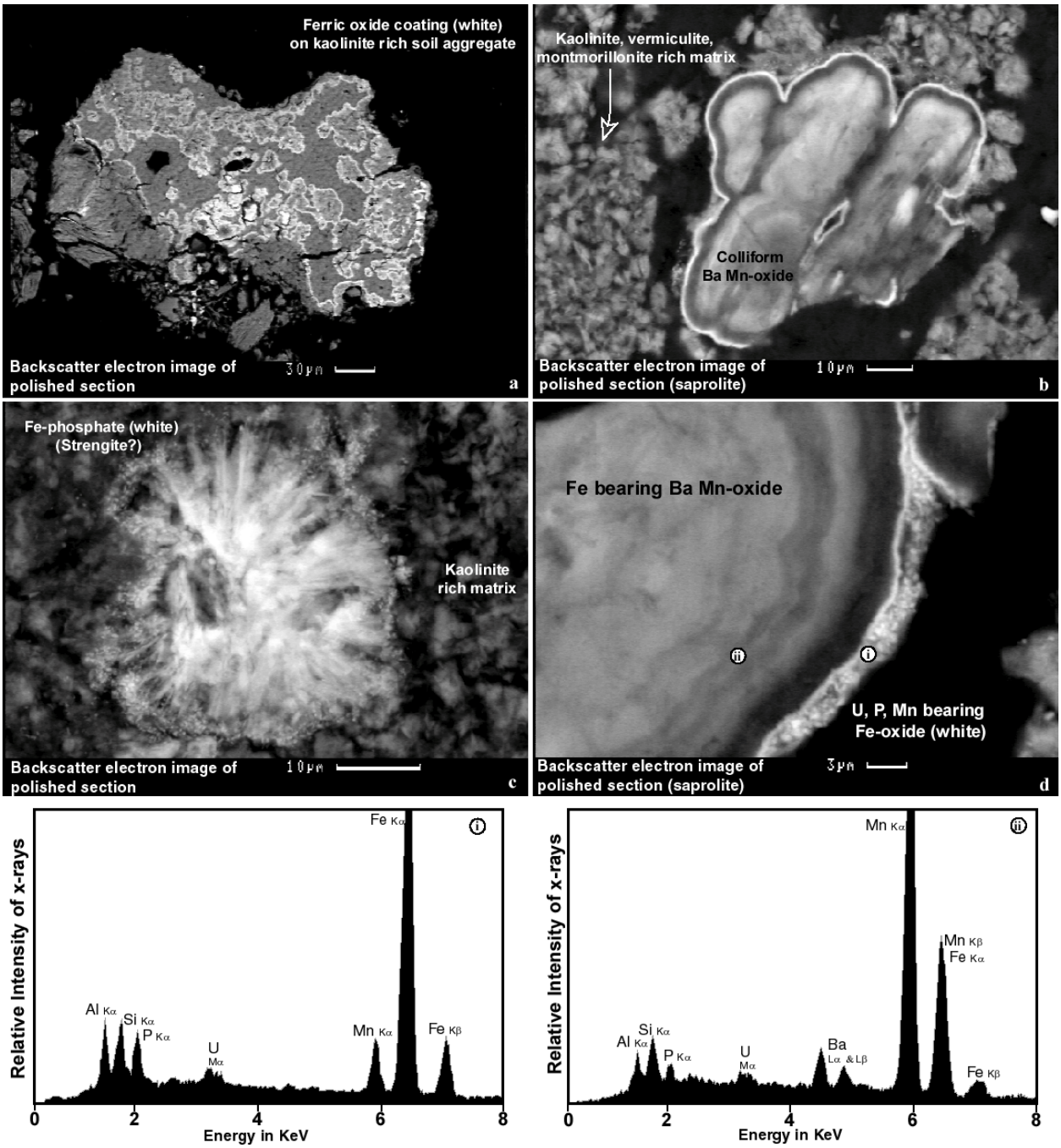

Figure 3-9. Backscatter electron images of iron and manganese minerals from the unsaturated zone overlying the Coles Hill north orebody: (a) polished section of a kaolinite-rich soil aggregate showing iron oxide rich mineral coating (white) (sample from DH1, 8 meters depth), (b) Ba Mn-oxide with rim of iron rich material (white) within a clay rich soil matrix (sample from DH1, 1.2 meters depth), (c) fibrous, radial growth of iron phosphate (strengite) within kaolinte rich soil matrix (sample from DH1, 2.1 meters depth), (d) enlarged view of iron oxide rich surface coating on a Ba Mn-oxide grain (sample from DH1, 1.2 meters depth). Note U peaks associated with these minerals in EDS spectra (Si and Al peaks due to kaolinite).

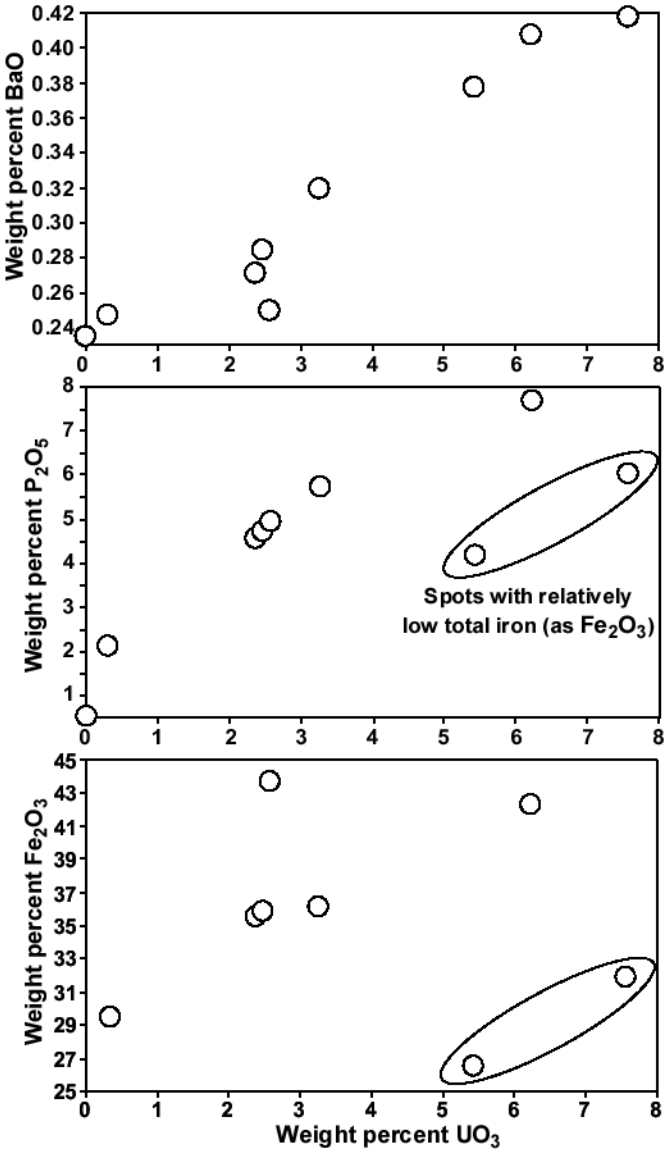

Figure 3-10. Electron microprobe data from iron oxide coating similar to the one shown in Fig.3-9c. Note positive correlation between P_2O_5 vs UO_3 and BaO vs UO_3.

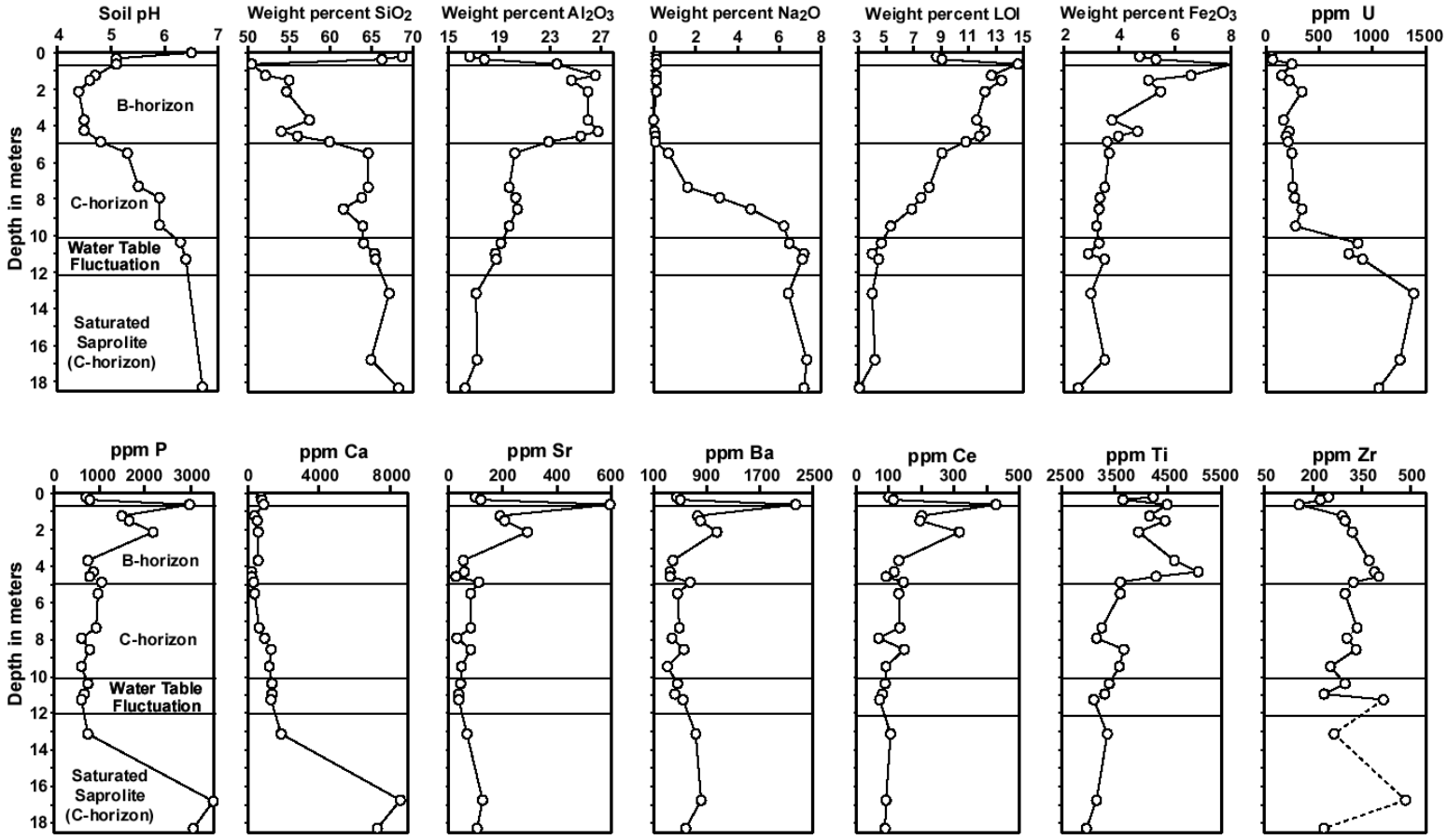

Figure 3-11. Soil pH and bulk concentration depth profiles for major elements and selected minor and trace elements in auger hole DH1. The present day water table is around 10.5 meters depth.

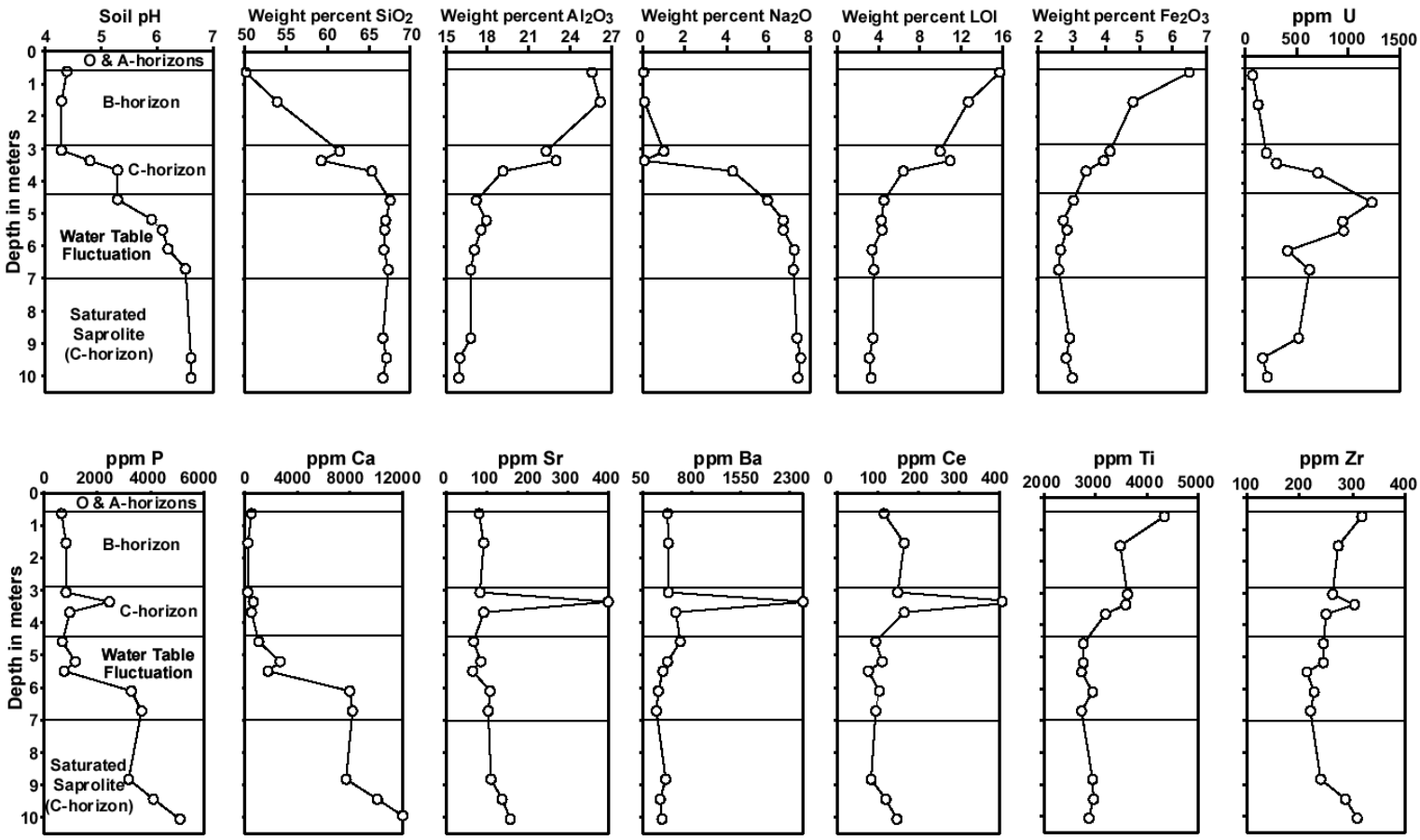

Figure 3-12. Soil pH and bulk concentration depth profiles for major elements and selected minor and trace elements in auger hole DH2. The present day water table is around 4.5 meters depth.

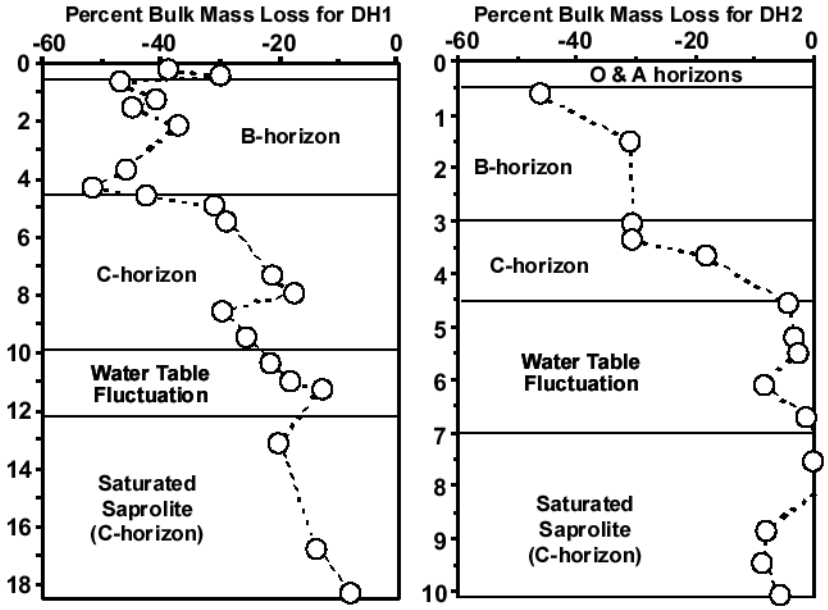

Figure 3-13. Bulk mass-loss profiles for the DH1 and DH2 profiles (calculated assuming that Ti is conserved).

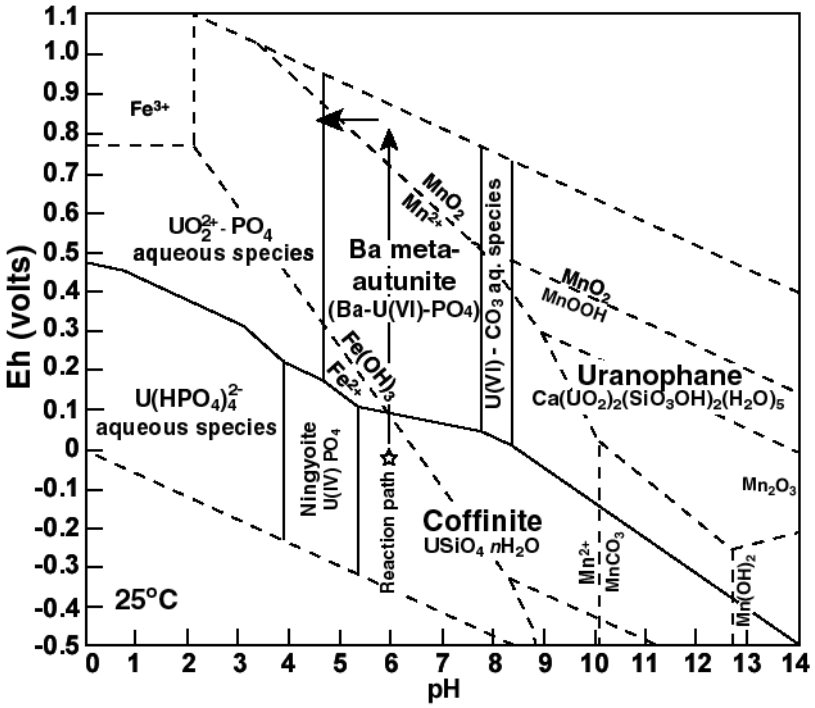

Figure 3-14. Eh-pH diagram plotted using activities calculated from the Coles Hill saprolite aquifer ground water. Diagram is for activities $10^{-3.4}$ Na^{+}, $10^{-4.6}$ Mg^{2+}, $10^{-3.2}$ $SiO_2(aq)$, $10^{-5.2}$ K^{+}, $10^{-4.2}$ Ca^{2+}, $10^{-5.7}$ Ba^{2+}, $10^{-7.7}$ UO_2^{2+}, $10^{-3.4}$ HCO_3^{-}, $10^{-5.6}$ $H_2PO_4^{-}$, $10^{-4.4}$ SO_4^{-} (source of solubility data discussed in text). Reaction path is estimated based on soil pH measurements as well as textural and mineralogical data such as the presence of Mn oxides and the observation that the Fe(II)/Fe(III) conversion closely corresponds with coffinite-Ba meta-autunite reaction.

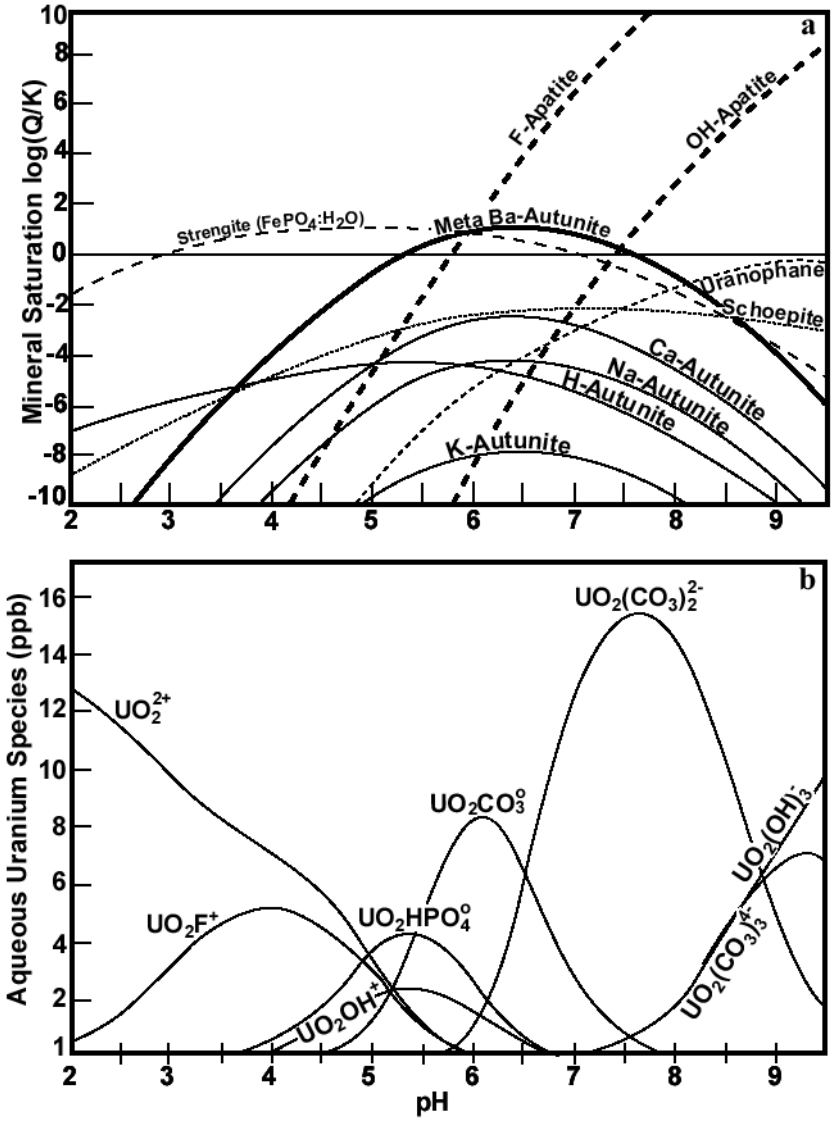

Figure 3-15. Solid and aqueous speciaiton diagram calculated using the same saprolite ground water composition that was used for calculating the Eh-pH diagram (Table 3-5). The sources of solubility data used are discussed in the text.

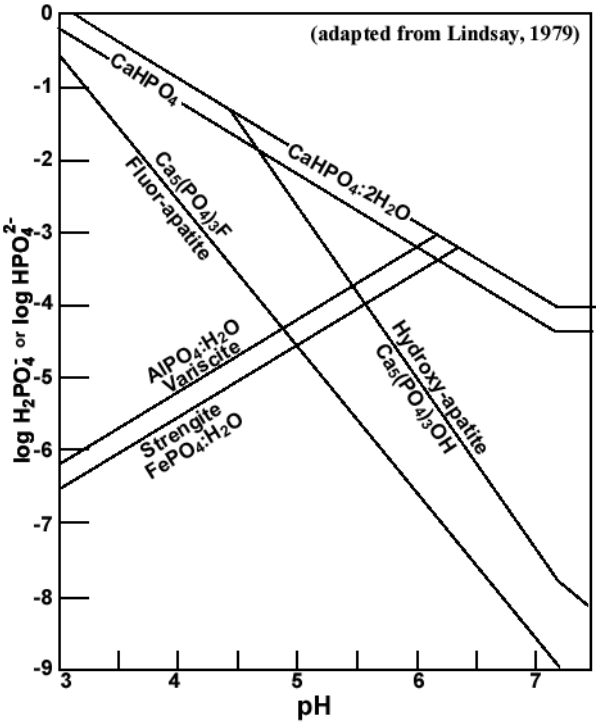

Figure 3-16. Phosphate solubility diagram for soils (adapted from Lindsay, 1979).

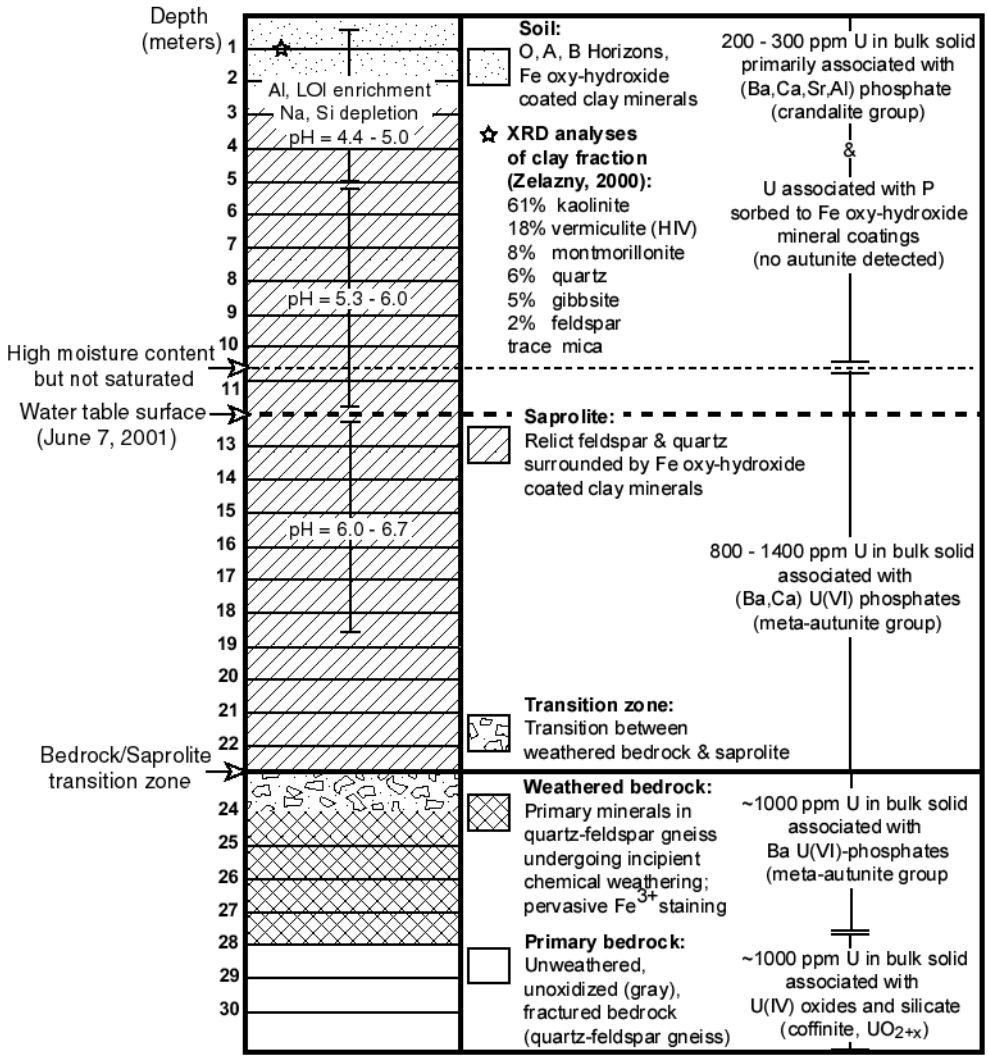

Figure 3-17. Summary of bulk geochemical and mineralogical data for the representative DH1 profile.

Summary and Project Conclusions

The study of the geochemistry and mineralogy of the Coles Hill uranium deposit and overlying weathering profile has shown that the natural attenuation of uranium within oxidizing, fluid rich environments may occur if certain geologic and geochemical criteria are met. Understanding these criteria requires characterization and modeling of key phenomena on a variety of scales ranging from the size of the deposit (hundreds of meters) to the mineral-grain scale (microns to nanometers).

The primary U(IV) bearing mineral assemblages formed during hydrothermal activity associated with Mesozoic faulting and are contained within cross-cutting fractures and cataclastic zones. The most abundant ore assemblage consists of coffinite, apatite, albite and chlorite, but uraninite-zeolite and uraninite-calcite assemblages are also present. A well defined ferrous/ferric redox front is present near the saprolite/bedrock interface. This front occurs within centimeters of the uranium redox transition where U(IV) mineral alteration is leading to the precipitation of U(VI) phases. One of the key findings of this study is that the volume of bedrock containing the ferrous/ferric redox front and uranous/uranyl transition zone at the Coles Hill uranium deposit has acted as a closed system with respect to uranium mass transport during oxidation. The primary mechanism of uranium fixation within the oxidizing zone is the precipitation of secondary U(VI)-bearing mineral assemblages dominated by Ba-uranyl phosphates (meta-autunite mineral group). Speciation and mineral stability calculations indicate that ground waters from the Coles Hill weathered zone are saturated with respect to this mineral and that it is capable of buffering dissolved uranium concentrations to values lower than 20 parts per billion.

Within overlying soil horizons uranium mobilized within the relatively low pH (<5.0) unsaturated environment is being reprecipitated below the water table as low solubility U(VI) phosphates also of the meta-autunite mineral group. This process is reflected in the bulk geochemistry of the weathering profile by the observation that samples from below the water table contain over 1000 ppm uranium while samples from the unsaturated zone contain 200 – 300 ppm uranium. The precipitation of U(VI) phosphates below the water table occurs due to relatively higher pH conditions in this zone (around 6.0) and a relatively high activity ratios of dissolved phosphate to carbonate (e.g. log $[H_2PO_4^-/HCO_3^-] > -3$). In the unsaturated zone

uranium is associated with a Ba, Ca, Sr aluminum phosphate of the crandallite group as well as with phosphate sorbed to iron oxy-hydroxide mineral coatings.

Estimates of the rate of saprolite production within the Virginia Piedmont (e.g. Pavich, 1986) suggest that the U(VI) phosphates responsible for the natural attenuation of uranium within the saturated saprolite zone overlying the Coles Hill uranium deposit may persist for hundreds of thousands of years. This has important implications for understanding the long term behavior of uranium within near surface environments typical of the eastern US.

Many other studies of uranium transport in natural systems have been performed (Miller et al, 1997). For example, investigations of the Koongara uranium deposit (studied as part of the Alligator Rivers Natural Analogue Project) located in northern Australia also revealed secondary phosphate mineralization as an important process by which uranium may be fixed within oxidizing, fluid rich environments. However, studies at the Koongara deposit as well as other uranium deposits in similar environments (e.g. Osamu Utsumi deposit in Brazil, studied as part of the Pocos de Caldas natural analogue project) show evidence for relatively high concentrations of uranium in ground waters (over 100 ppb) due to uranium minerals currently dissolving within the near surface horizons.

The Coles Hill site is therefore unique in that uranium concentrations in ground waters are being buffered to values below 20 ppb by the present-day precipitation of low solubility U(VI) phosphates. The Coles Hill uranium deposit thus represents an environmental system in which the natural attenuation of uranium transport is being achieved within an oxidizing environment. The phenomena involved in this process makes this site a unique natural laboratory for the study of uranium attenuation with potential applications for the design, performance assessments and implementation of cost effective uranium remediation and containment strategies, such as soil amendments techniques and in-situ reactive barriers technologies.